ANL/NE-12/4

The SAS4A/SASSYS-1 Safety Analysis Code System

Nuclear Engineering Division

ANL/NE-12/4

The SAS4A/SASSYS-1 Safety Analysis Code System

Chapter 12:
Sodium Voiding Model

F. E. Dunn
Nuclear Engineering Division
Argonne National Laboratory

January 31, 2012

TABLE OF CONTENTS

LIST OF FIGURES

LIST OF TABLES

NOMENCLATURE

Symbol	Definition	Units
$A_c(z,t)$	Coolant flow area	m^3
A_{fr}	User-input quantity in the friction factor expression	--
AA_0	Coefficient in the liquid slug momentum equation	Pa
b_{fr}	User-input quantity in the friction factor expression	--
BB_0	Coefficient in the liquid slug momentum equation	m^{-1}-s^{-1}
C_ℓ	Specific heat of liquid sodium	J/kg-K
$D_h(z,t)$	Hydraulic diameter	m
E_i	Heat flow to the vapor through the liquid-vapor Interfaces	J
E_t	Total heat energy added to a vapor bubble in a time step	J
E_{es}	Heat flow to the vapor from the cladding and structure	J
$F_c(z,t)$	Condensation momentum loss term	Pa/m
$f_v(z,t)$	Friction factor	--
$F_{ce}(z,t)$	Condensation momentum loss term to cladding film	Pa/m
$F_{cs}(z,t)$	Condensation momentum loss term to structure film	Pa/m
f_{rwb}, f_{rwt}	Liquid film rewetting factors.	--
g	Gravitational acceleration	m/s^2
$h_{ec}(z)$	Heat-transfer coefficient from the cladding surface to the sodium vapor	W/m^2-K
$h_{sc}(z)$	Heat-transfer coefficient from the structure surface to the sodium vapor	W/m^2-K
h_{cond}	User-supplied condensation heat-transfer coefficient	W/m^2-K
I_1, I_2, I_3, I_4, I_5	Coefficients in the liquid slug momentum equation	--
K	Bubble number	--
K_{vn}	Number of bubbles	--
$k_e(z)$	Cladding thermal conductivity	W/m-K
$k_\ell(z)$	Thermal conductivity of liquid sodium at temperature T(z)	W/m-K
$k_{or}(z,t)$	Orifice pressure drop term	--
p(z,t)	Vapor pressure	Pa

$P_e(z)$	Perimeter of cladding - $2\pi r_e$	m
$Q(z,t)$	Total heat flux per unit volume = $Q_e + Q_s$	W/m^3
$\tilde{Q}(t)$	Total heat flow rate into the sodium vapor	W
$q(z,t)$	Surface heat flow rate per unit area	W/m^2
$Q_c(z)$	Volume source due to direct heating by neutrons and gamma rays	W/m^3
$Q_e(z,t)$	Heat flow rate per unit volume through the cladding	W/m^3
$q_e(z,t)$	Cladding-to-vapor heat flux	W/m^2
$Q_s(z,t)$	Heat flow rate per unit volume through the structure	W/m^3
$q_s(z,t)$	Structure-to-vapor heat flux	W/m^2
$Q_{es}(t)$	Heat flow rate from cladding and structure	W
$r_e(z)$	Nominal radius of cladding	m
$R_{ec}(z,t)$	Thermal resistance between the cladding and the coolant	m^2-K/W
$R_{sc}(z,t)$	Thermal resistance between the structure and the coolant	m^2-K/W
s	Vapor heat transfer surface area	m^2
$T(z,t)$	Coolant temperature	K
t	Time	s
$T(z,t)$	Cladding temperature	K
$T_\ell(t)$	Liquid sodium temperature at liquid-vapor interface	K
$T_s(z,t)$	Structure temperature	K
$T_v(t)$	Sodium vapor temperature at liquid-vapor interface	K
$v(z,t)$	Velocity	m/s
v_{fe}	Velocity of liquid film on the cladding (currently fixed at zero)	m/s
v_{fs}	Velocity of liquid film on the structure (currently fixed at zero)	m/s
$W(z,t)$	Mass flow rate	kg/s
$w_{fe}(z,t)$	Thickness of liquid film on the cladding	m
$w_{fs}(z,t)$	Thickness of liquid film on the structure	m
z	Axial height	m
$z_i(1,t,K)$	Height of lower liquid-vapor interface in bubble K.	m
$z_i(2,t,K)$	Height of upper liquid-vapor interface in bubble K	m

α	Thermal diffusivity of liquid sodium = $k_\ell \rho_\ell C_\ell$	m^2/s
$\gamma(z,t)$	Ratio of cladding surface area to coolant volume	m-1
$\gamma_2(z,t)$	Ratio of surface area of structure to surface area of cladding	--
ΔI_j	Coefficients in the liquid slug momentum equation	--
Δr_e	Nominal cladding thickness	m
Δt	Time step	s
$\theta_1 \theta_2$	Coefficients which set the degree of implicitness of the liquid slug calculations	--
$\lambda(z,t)$	Heat of vaporization	J/kg
$\mu(z,t)$	Sodium vapor viscosity	Pa-s
$\rho_t(z)$	Density of liquid sodium	kg/m^3
$\rho_v(z)$	Density of sodium vapor	kg/m^3

Subscripts and Superscripts

b	Bottom
c	Coolant
e	Cladding
I	Interface quantity
J	Global node number of the node under consideration
J1	Global node number of the lower interface of the bubble under consideration
J2	Global node number of the upper interface of the bubble under consideration
ℓ	Liquid
L	Lower interface
s	Structure
t	Top
u	Upper interface
v	Vapor
1,2	Beginning and end of current time step

SODIUM VOIDING MODEL

12.1 Introduction

The sodium voiding model in SASSYS-1 and SAS4A is a multiple-bubble slug ejection boiling model similar to that used in SAS2A [12-1], SAS3A [12-2], and SAS3D [12-3], except that in SASSYS-1 and in SAS4A changes have been made in the finite differencing to handle flow area changes and non-uniform axial nodes more consistently and accurately. Another difference is that in addition to voiding due to boiling, SASSYS-1 and SAS4A will also calculate voiding due to plenum gas release from failed fuel pins. The main purposes of this model are to predict the rate and extent of voiding for the voiding reactivity calculations and to predict the heat removal from the cladding surface, after the onset of voiding, for the fuel and cladding temperature calculations.

Figure 12.1-1 illustrates the voiding model. Each channel in SASSYS-1 represents a fuel pin and its associated coolant and structure. Voiding is assumed to result in the formation of bubbles that fill the whole cross section of the coolant channel except for a film of liquid sodium that is left on the cladding and on the structure. Up to nine bubbles, separated by liquid slugs, are allowed in the channel at any time.

Currently, the film is treated as a static film of a thickness that changes due to vaporization or condensation. A dynamic film treatment in which film motion is determined by the combined effects of gravity and the shear force of streaming vapor will be added to a future version of the code.

The extent of voiding is determined mainly by liquid slug motion. The bubble pressures at the bubble-slug interfaces drive the liquid slugs. Therefore, the voiding calculation couples vapor or gas pressure calculations for the bubbles with momentum equations for the liquid slugs. If a bubble is small, it is assumed that the vapor or gas pressure within the bubble is constant throughout the bubble, and the bubble pressure is computed using the uniform vapor pressure model described in Section 12.5. For larger bubbles, the vapor pressure is calculated from the pressure gradient model explained in Section 12.6. Section 12.7 describes the gas voiding model.

The voiding model portrayed in Fig. 12.1-1 has been developed and extensively tested throughout the evolution of the SAS family of codes. A considerable body of experimental information dictated the choice of a multi-bubble slug ejection model. The justification for using a one-dimensional, slug flow model first came from stimulant material experiments by Grolmes and Fauske [12-4]. These tests indicated that voiding took place under slug flow conditions, with a small liquid film left on the cladding and structure. The multiple bubble, slug flow model has been compared with results from a variety of out-of-pile and in-pile experiments, including tests at Argonne with the OPERA, TREAT, and SLSF facilities, experiments conduced at KFK [12-5]. And the ORNL Sodium Boiling Tests [12-6]. These comparisons have consistently shown that the SASSYS-1 and SAS4A voiding model agrees well with experimental data that are prototypic of reactor conditions.

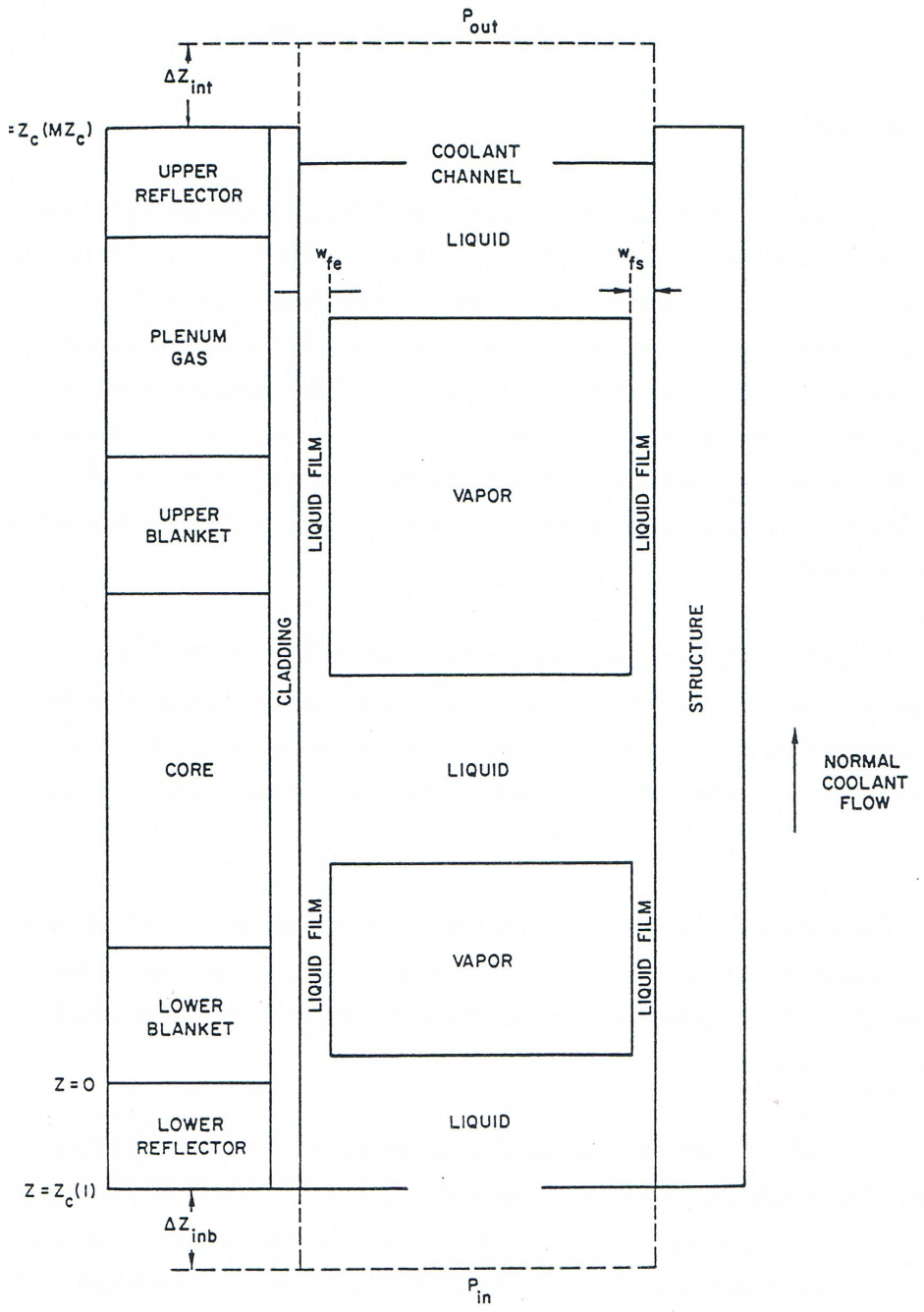

Figure 12.1-1. Voiding Model Geometry

When the voiding model is translated into a computer code, the result is a rather lengthy series of subroutines, which, at first glance, appears to be intimidatingly complex. However, this appearance is somewhat misleading. The voiding model coding seems less intricate if attention is focused initially on just those subroutines that perform the major calculations needed by the model. There are three such major calculations; in order, they are

1) a preliminary liquid slug flow calculation that neglects the effect of changes in the vapor bubble pressures over the time step (performed in subroutine TSC2),
2) the calculation of the advanced time pressures and mass flow rates in the vapor bubbles (performed in subroutine T4A3D), and
3) a liquid slug flow calculation that accounts for the updated bubble conditions (performed in subroutines TSC5, TSC6, and TSC7).

The remaining voiding model subroutines perform computations that either directly or indirectly support the three major calculations just listed (i.e., initialization of the calculation in TSCSET, determination of new time-step size in TSC9, etc.). A detailed description of all subroutines and the overall flow of the coding will be given in Section 12.10.

The relationship of the voiding model to other major modules in SASSYS-1 is diagrammed in Fig. 12.1-2. This drawing shows that the voiding model picks up its initial information from the transient heat-transfer modules, supplies information to the point kinetics module (which, in turn, feeds data to the transient heat-transfer module), and provides clad surface heat fluxes to the transient heat transfer module. Thus, the voiding model has a direct impact on most of the major modules in SASSYS-1. Further details of the interaction of the voiding model with other modes in the code will be presented in Section 12.9.

The remainder of the chapter is divided into five major categories: calculation of mass flow rates in the liquid slugs, calculation of vapor pressures in small bubbles through the uniform vapor pressure model, calculation of vapor pressures and mass flow rates in larger bubbles by the vapor pressure gradient model, the gas voiding model, and discussion of the coding itself. Sections 12.2 and 12.3 cover the first category of liquid slug calculations, Section 12.4 introduces the topic of vapor bubble calculations, Section 12.5 discusses the uniform vapor pressure model, Section 12.6 explains the pressure gradient model, Section 12.7 describes the gas voiding model and Sections 12.8 through 12.13 discuss various aspects of the voiding model coding, including physical properties correlations.

12.2 Liquid Slug Flow Rates

The mass flow rate in each of the individual slugs pictured in Fig. 12.1-1 is computed from the momentum equation similarly to the calculation of the prevoiding mass flow rate described in Chapter 3. Because of this similarity, the discussion here will be brief and will emphasize the additions that must be made to the model of Chapter 3 to accommodate the fact that there are several separate liquid slugs in the channel rather than one slug which fills the channel as in the prevoiding case. In particular, the model must now be able to handle the fact that the liquid slugs are continually changing length and must account properly for the effect of the bubble vapor pressures in driving the liquid slug flow rates.

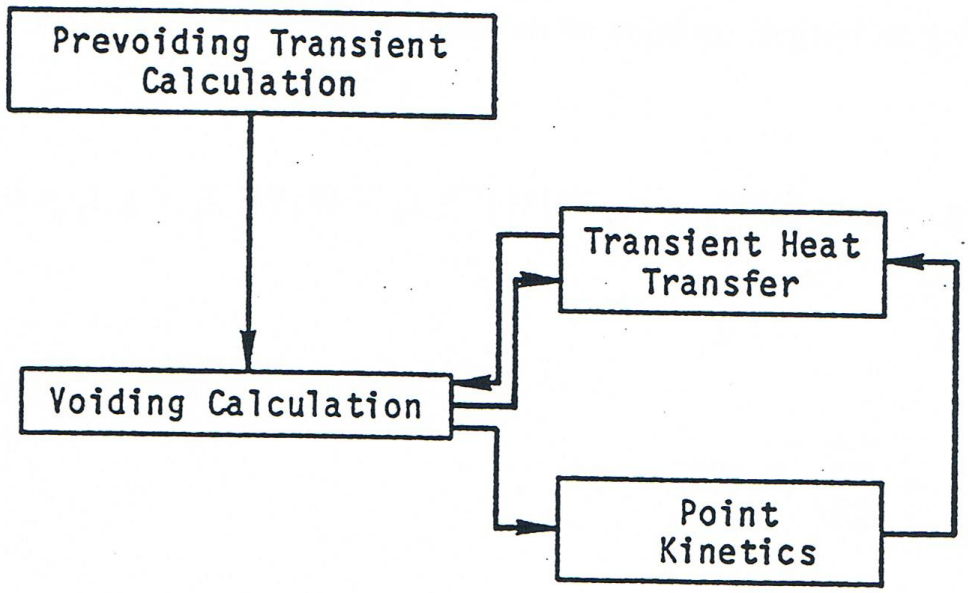

Figure 12.2-1. Schematic Drawing of the Relationship of the Voiding Model to Other SASSYS-1 Models

The foundation of the model is again the liquid momentum equation, Eq. 3.9-1:

$$\frac{1}{A_c}\frac{\partial W}{\partial t}+\frac{\partial p}{\partial z}+\frac{1}{A_c}\frac{\partial (Wv)}{\partial z}=-\left(\frac{\partial p}{\partial z}\right)_{fr}-\left(\frac{\partial p}{\partial z}\right)_{K}-\rho_c g \qquad (12.2\text{-}1)$$

with the terms as defined in Chapter 3. Now, however, the momentum equation is applied to each slug individually and is integrated over the length of each slug rather than over the length of the channel, giving an integral equation of the form of Eq. 3.9-5:

$$I_1\frac{\partial W}{\partial t}+p_t-p_b+W^2 I_2+A_{fr}\,W|W|^{1+b_{fr}}I_3+W|W|I_4+g\,I_5=0 \qquad (12.2\text{-}2)$$

where

$$I_1=\int\frac{dz}{A_c}=\sum_{JC=JST}^{JEND}X_{I1}(JC) \qquad (12.2\text{-}3)$$

$$X_{I1}(JC) = \frac{\Delta z(JC)}{A_c(JC)} \tag{12.2-4}$$

$$I_2 = \sum_{JC=JST}^{JEND} X_{I2}(JC) \tag{12.2-5}$$

$$X_{I2}(JC) = \frac{1}{A_c(JC)^2}\left[\frac{1}{\rho_c(JC+1)} - \frac{1}{\rho_c(JC)}\right] \tag{12.2-6}$$

$$I_3 = \int \frac{1}{2\rho_c A_c^2 D_h}\left[\frac{D_h}{\mu A_c}\right]^{b_{fr}} dz = \sum_{JC=JST}^{JEND} X_{I3}(JC) \tag{12.2-7}$$

$$X_{I3}(JC) = \frac{\Delta z(JC)}{\left[\rho_c(JC) + \rho_c(JC+1)\right] A_c(JC)^2 D_h(JC)}\left[\frac{D_h(JC)}{\bar{\mu}(JC) A_c(JC)}\right]^{b_{fr}} \tag{12.2-8}$$

$$I_4 = \sum_{JC=JST}^{JEND} K_{or}(JC) \tag{12.2-9}$$

$$I_5 = \int \rho_c\, dx = \sum_{JC=JST}^{JEND} X_{I5}(JC) \tag{12.2-10}$$

$$X_{I5}(JC) = .5\left[\rho_c(JC) + \rho_c(JC+1)\right]\Delta z(JC) \tag{12.2-11}$$

P_b = the pressure at the bottom of the slug,

and

P_t = the pressure at the top of the slug.

The variable JST is the number of the mesh segment in which the bottom of the liquid slug is located, while JEND is the number of the segment in which the top is contained. The liquid slug configuration in the SASSYS-1 axial mesh is shown in Fig. 12.2.1. Note that mesh segments JST and JEND are part liquid and part vapor. Since the integration is over only the liquid portions of these segments, the axial length terms $\Delta z(JC)$ in the expressions for X_{I1}, X_{I3}, and X_{I5} must be altered for segments JST and AJEND from being the mesh segment height to being the length of the portion of the segment which is filled with liquid. This is represented by the term $\Delta z'$ as follows:

$$\text{If } K>1, \Delta z'(JST)=z_c(JST+1)-z_i(L=1,t,\ K-1) \tag{12.2-12a}$$

$$\text{If } K=1, \Delta z'(JST)=\Delta z(JST) \tag{12.2-12b}$$

$$\text{If } K\le K_{vn}, \Delta z'(JEND)=z_i(L=1,t,K)-z_c(JEND) \tag{12.2-13a}$$

$$\text{If } K>K_{vn}, \Delta z'(JEND)=\Delta z(JEND) \tag{12.2-13b}$$

The notation z_i (L,t,K) for the interface position is derived from the coding and is to be interpreted as follows. The quantity L takes the value 1 or 2, with L=1 denoting the lower interface of bubble K and L=1 the upper interface. The variable t is simply time, and K is just the bubble number, with the numbering going from 1 for the lowest bubble in the channel to K_{vn} for the highest bubble.

Two other modifications must be made to accommodate the partial segments at the ends of the slug. First, the density p_c (JST) in the expressions for X_{I2} (JST) and X_{I3} (JST) must be replaced by the liquid density at the bubble interface; similarly, ρ_c (JEND+1) must be replaced by the interface value in X_{I2} (JEND) and X_{I3} (JEND). Second, the terms for JST and JEND in the computation of I_4 must be multiplied by the fraction $\Delta z'/\Delta z$.

If JST = 1, the effective inertial term $\left[\frac{\Delta z_i}{A}\right]_b$, must be added to I_1, and if JEND = MZC, the term $\left[\frac{\Delta z_i}{A}\right]_t$ must be included in I_1, just as in Chapter 3, Eq. 3.9-6.

In the special case of a small liquid slug entirely contained within one mesh segment, JST = JEND. Then,

$$\Delta z'(JST)=z_i(L=1,t,K)-z_i(L=2,t,K-1) \tag{12.2-14}$$

and there is only one term in each of the summations for I_1 through I_5.

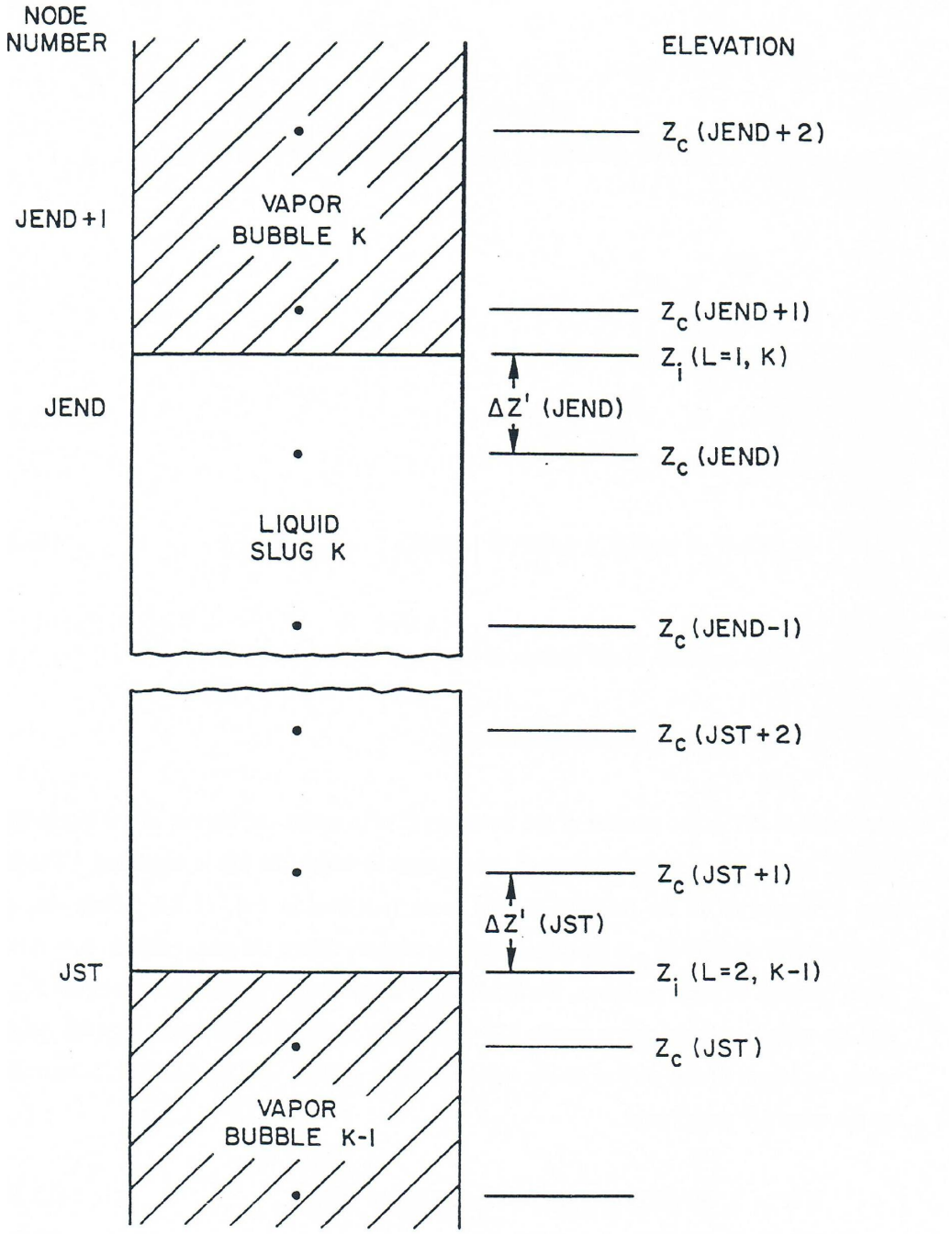

Figure 12.2-2. Placement of a Liquid Slug in the SASSYS-1 Axial Coolant Mesh

Equation 12.2-2 must now be finite differenced and solved for the liquid mass flow rate in the slug. The advanced time mass flow rate W is forward differenced in time, and functions of W in Eq. 12.2-2 are expressed using first-order Taylor series; see Eqs. 3.9-15 through 3.9-22 for the detailed expressions. However, the differenced form of Eq. 12.2-2 is more complex than the corresponding equation in the prevoiding model, Eq. 3.9-23, because now the coefficients I_1 through I_5 are functions of time due to motion of the liquid-vapor interfaces, and, therefore, the time level at which these coefficients are evaluated must be specified. To allow flexibility in the level of implicitness of the calculation, the variable explicit/implicit scheme used in Eq. 3.9-15 is applied to the coefficients in Eq. 12.2-2. The differenced equation is then

$$\begin{aligned}
&(\theta_1 I_1|_t + \theta_2 I_1|_{t+\Delta t})\frac{\Delta W}{\Delta t} + \theta_1\left(p_{t_1} - p_{b_1}\right) + \theta_2\left(p_{t_2} - p_{b_2}\right) \\
&\quad + (\theta_1 I_2|_t + \theta_2 I_2|_{t+\Delta t})(W_1^2 + 2\theta_2 W_1 \Delta W) \\
&\quad + A_{fr}(\theta_1 I_3|_t + \theta_2 I_3|_{t+\Delta t})\left[W_1|W_1|^{1+b_{fr}}\right. \\
&\quad \left. + \theta_2\left(2 + b_{fr}\right)|W_1|^{1+b_{fr}}\Delta W\right] \\
&\quad + (\theta_1 I_4|_t + \theta_2 I_4|_{t+\Delta t})(W_1|W_1| + 2\theta_2|W_1|\Delta W) \\
&\quad + (\theta_1 I_4|_t + \theta_2 I_4|_{t+\Delta t})g = 0\,.
\end{aligned} \tag{12.2-15}$$

The change in the coefficient I_2 over a time step is a function only of the change in interface liquid density, which is a very small effect and can be neglected. Therefore, I_2 is considered constant over the time step. In addition, the orifice coefficient I_4 is also assumed constant over the time step. The advanced time values of the other three coefficients are expressed using forward differencing in time. To illustrate, take the gravity coefficient I_5; at time t,

$$I_5(t) = \int_{Z_{JST}(t)}^{Z_{JEND}(t)} \rho_\ell(z)\,dz \tag{12.2-16}$$

and at time $t + \Delta t$,

$$I_5(t+\Delta t) = \int_{Z_{JEND}(t+\Delta t)}^{Z_{JEND}(t+\Delta t)} \rho_\ell(z)\,dz. \tag{12.2-17}$$

These two integrals are identical except in segments JST and JEND, where the bubble interface positions are changing with time. Taking the difference gives

$$I_5(t+\Delta t) - I_5(t) = \int_{Z_{JEND}(t)}^{Z_{JEND}(t+\Delta t)} \rho_\ell(z)\,dt - \int_{Z_{JST}(t)}^{Z_{JST}(t+\Delta t)} \rho_\ell(z)\,dz. \tag{12.2-18}$$

The interface position z_i can be written as a linear function of the interface velocity v_i, so that

$$dz = v_i\,dt. \tag{12.2-19}$$

Therefore, $I_5(t + \Delta t)$ is

$$\begin{aligned} I_5(t+\Delta t) = I_5(t) &+ \rho_{\ell i}(JEND)\int_t^{t+\Delta t} v_i(L=1,t',K)\,dt' \\ &- \rho_{\ell i}(JST)\int_t^{t+\Delta t} v_i(L=2,t',K-1)\,dt'. \end{aligned} \tag{12.2-20}$$

If the velocity is assumed to vary linearly over the time step, the time integrals in Eq. 12.2-20 become

$$\begin{aligned} \int_t^{t+\Delta t} v_i(t')\,dt' &= \bar{v}\,\Delta t \\ &= \left[v_i(t) + \frac{\Delta v}{2v_i}\right]\Delta t \\ &= v_i(t)\left[1 + \frac{\Delta v}{2v_i(t)}\right]\Delta t \\ &= v_i(t)\left[1 + \frac{\Delta W}{2W_1}\right]\Delta t \end{aligned} \tag{12.2-21}$$

where $\Delta v = v_i$ (t+Δt) – $v_i(t)$. Therefore, $I_5(t+\Delta t)$ is

$$\begin{aligned} I_5(t+\Delta t) = I_5(t) &+ \rho_{\ell i}(JEND)\,v_i(L=1,t,K)\left[1 + \frac{\Delta W}{2W_1}\right]\Delta t \\ &- \rho_{\ell i}(JST)\,v_i(L=2,t,K-1)\left[1 + \frac{\Delta W}{2W_1}\right]\Delta t. \end{aligned} \tag{12.2-22}$$

This expression is valid for a liquid slug that is bounded at both ends by vapor bubbles. However, slugs that extend out the top of the subassembly do not have a moving upper interface, and so the integral over the upper interface in Eq. 12.2-18 is zero. Similarly, the integral over the lower interface is zero for slugs extending out the bottom of the subassembly. To preserve the ease of using one expression for $I_5(t+\Delta t)$ for all types of liquid slugs, Eq. 3.2-22 is rewritten as

$$I_5(t+\Delta t) = I_5(t) + \Delta I_5 + \Delta W\ I_5' \tag{12.2-23}$$

where

$$\Delta I_5 = \Delta t\, v_i(L=1,t,K)\, \rho_{\ell_i}(JEND)\, x_u - \Delta t\, v_i(L=2,t,K-1)\, \rho_{\ell_i}(JST)\, x_L \tag{12.2-24}$$

$$I_5' = \frac{\Delta I_5}{2W_1} \tag{12.2-25}$$

$$x_L = 1, \text{for slug types 2 or 3} \tag{12.2-26a}$$

$$x_L = 0, \text{otherwise} \tag{12.2-26b}$$

$$x_u = 1, \text{for slug types 1 or 2} \tag{12.2-27a}$$

$$x_u = 0, \text{otherwise.} \tag{12.2-27b}$$

Slug type 1 refers to a slug that extends below the subassembly inlet, type 2 to a slug that is bounded top and bottom by bubbles, and type 3 to a slug that extends out the subassembly Table 12.2-1 defines all slug-type numbers used in the code, as well as listing the bubble-type numbers that are part of the coding. Not that the increment ΔI_5 represents the change in I_5 if the change in the mass flow rate of the slug is ignored, while the I'_5 term accounts for the change due to acceleration of the slug.

The expressions for I_1 $(t+\Delta t)$ and $I_3(t+\Delta t)$ are derived in the same way as was Eq. 12.2-23. The resulting equations are

$$I_1(t+\Delta t) = I_1(t) + \Delta I_1 \tag{12.2-28}$$

where

$$\Delta I_1 = \frac{\Delta t\, v_i(L=1,t,K) x_u}{A_c(JEND)} - \frac{\Delta t\, v_i(L=2,t,K-1) x_L}{A_c(JST)} \tag{12.2-29}$$

Table 12.2-1. Liquid Slug Types and Bubble Types Used in Coolant Dynamics Model

1. Bubble Types

The FORTRAN variable IBUB1 and IBUB2 refer to bubble types.

IBUB	Bubble Type
1	Bubble within the subassembly; uniform vapor pressure bubble.
2	Bubble within the subassembly; pressure gradient model.
3	Bubble extends out the top of the subassembly; uniform vapor pressure bubble.
4	Bubble extends out the top of the subassembly; pressure gradient model.
5	Bubble extends out both the top and bottom of the subassembly.
6	Bubble extends out the bottom of the subassembly.

2. Liquid Slug Types

The FORTRAN variables ILIQ1 and ILIQ2 refer to liquid slug type.

ILIQ	Liquid Slug Type
1	Lower liquid slug, below the lowest bubble.
2	Intermediate liquid slug, with bubbles above and below.
3	Upper liquid slug, above the highest bubble.
4	Liquid slug fills whole subassembly; no voiding.
5	Lower liquid slug below the subassembly inlet, below a type-5 or -6 bubble.
6	Upper liquid slug above the subassembly outlet, above a tpe-3, -4, or -5 bubble.

and

$$I_3(t+\Delta t) = I_3(t) + \Delta I_3 + \Delta W I_3' \tag{12.2-30}$$

with

$$\Delta I_3 = \frac{\Delta t\, v_i\left(L=1,t,K\right)x_u}{2\,A_c\left(JEND\right)^2\,\rho_{\ell t}\left(K\right)D_h\left(JEND\right)}\left[\frac{D_h\left(JEND\right)}{A_c\left(JEND\right)\bar{\mu}\left(JEND\right)}\right]^{b_{fr}} - \frac{\Delta t\, v_i\left(L=2,t,K-1\right)x_L}{2\,A_c\left(JST\right)^2\,\rho_{\ell b}\left(K\right)D_h\left(JST\right)}\left[\frac{D_h\left(JST\right)}{A_c\left(JST\right)\bar{\mu}\left(JST\right)}\right]^{b_{fr}} \tag{12.2-31}$$

and

$$I_3' = \frac{\Delta I_3}{2W_1}\,. \tag{12.2-32}$$

The effect of slug acceleration is omitted in $I_1(t+\Delta t)$.

Substituting the above expressions for the advanced time coefficients into Eq. 12.2-15 and neglecting second-order terms produces the differenced momentum equation

$$\begin{aligned}\left(I_1+\theta_2\,\Delta I_1\right)\frac{\Delta W}{\Delta t}=&\theta_1\left(p_{b1}-p_{t1}\right)+\theta_2\left(p_{b2}-p_{t2}\right)-I_2\,W_1^2\\&-2\theta_2\,\Delta W W_1 I_2-A_{fr}\left(I_3+\theta_2\Delta I_3\right)W_1\left|W_1\right|^{1+b_{fr}}\\&-\left(2+b_{fr}\right)\theta_2 A_{fr} I_3\left|W_1\right|^{1+b_{fr}}\Delta W\\&-\theta_2\,A_{fr}\,W_1\,I_3'\left|W_1\right|^{1+b_{fr}}\Delta W-I_4(W_1\,|\,W_1\,|+2\theta_2 W_1\Delta W)\\&-g\left(I_5+\theta_2\,\Delta I_5\right)-gI_5'\,\theta_2\,\Delta W\end{aligned}\tag{12.2-33}$$

which gives

$$\Delta W=\frac{\Delta t\left[AA_0+\left(\Delta p_b-\Delta p_t\right)\theta_2\right]}{I_1+\theta_2\,\Delta I_1+\theta_2\,BB_0\,\Delta t}\tag{12.2-34}$$

where

$$\begin{aligned}AA_0=&\,p_{b1}-p_{t1}-I_2\,W_1^2-A_{fr}\left(I_3+\theta_2\,\Delta I_3\right)W_1\left|W_1\right|^{1+b_{fr}}\\&-I_4\,W_1\left|W_1\right|-g\left(I_5+\theta_2\,\Delta I_5\right)\end{aligned}\tag{12.2-35}$$

and

$$\begin{aligned}BB_0=&\,2W_1\,I_2+\left(2+b_{fr}\right)A_{fr}\,I_3\,\left|W_1\right|^{1+b_{fr}}+2I_4\left|W_1\right|\\&+A_{fr}\left|W_1\right|^{1+b_{fr}}W_1\,I_3'+gI_5'\end{aligned}\tag{12.2-36}$$

Thus the change in flow rate for a liquid slug is related to the changes in vapor pressures in the bubbles above and below the liquid slug, or to the changes in inlet and outlet coolant pressures.

12.3 Interface Velocities

The average velocity in a liquid slug is

$$v_\ell=\frac{W}{\rho_\ell A_c}\tag{12.3-1}$$

but the presence of films on the cladding and structure causes the liquid-vapor interface to move at a somewhat different velocity. Figure 12.3-1 shows an interface moving at a velocity v_i for a time interval Δ_t. A film of liquid sodium is present in the vapor region

on both the cladding and structure. The cladding film is of thickness w_{fe}, while that on the structure has thickness w_{fa}. The film on the cladding can move with velocity w_{fe}, and the structure film can have a velocity of v_{fs}. In later versions of SASSYS-1, film motion modeling will be available, and so v_{fe} and v_{fa} are included in the equations below for completeness; currently, however, film motion is neglected, and v_{fe} and v_{fs} are set to zero.

If the coolant channel volume between z_i (t) and z_i (t+Δt) is taken as a control volume, then the liquid volume V_ℓ in the control volume at time t is

$$V_l(t) = P_e v_i \Delta t (w_{fe} + \gamma_2 w_{fs}) \tag{12.3-2}$$

where P_e is the outer perimeter of the cladding and γ_2 is the ratio of the surface area of the structure to the surface area of the cladding. At t+Δt the liquid volume in the control volume is

$$V_\ell(t+\Delta t) = A_c\, v_i\, \Delta t \tag{12.3-3}$$

Accounting for the liquid added to and subtracted from the control volume during Δt gives

$$V_\ell(t+\Delta t) = V_\ell(t) + v_\ell\, A_c \Delta t - P_e\left(w_{fe}\, v_{fe} + \gamma_2\, w_{fs}\, v_{fs}\right)\Delta t \tag{12.3-4}$$

Substituting Eqs. 12.3-2 and 12.3-3 into 12.3-4 gives

$$\begin{aligned} A_c\, v_i\, \Delta t = {} & P_e\, v_i\, \Delta t\left(w_{fe} + \gamma_2\, w_{fs}\right) + v_\ell\, A_c\, \Delta t \\ & - P_e\, \Delta t\left(w_{fe}\, v_{fe} + \gamma_2\, w_{fs}\, v_{fs}\right) \end{aligned} \tag{12.3-5}$$

or

$$vi = \frac{v_\ell - P_e\left(w_{fe}\, v_{ve} + \gamma_2\, w_{fs}\, v_{vs}\right)/A_c}{1 - P_e\left(w_{fe} + \gamma_2\, w_{fs}\right)/A_c} \tag{12.3-6}$$

which is the equation used for computing interface velocities. Note that this equation is applicable whether the interface is moving in the positive or the negative axial direction and holds whether the interface is moving towards the liquid side or the vapor side.

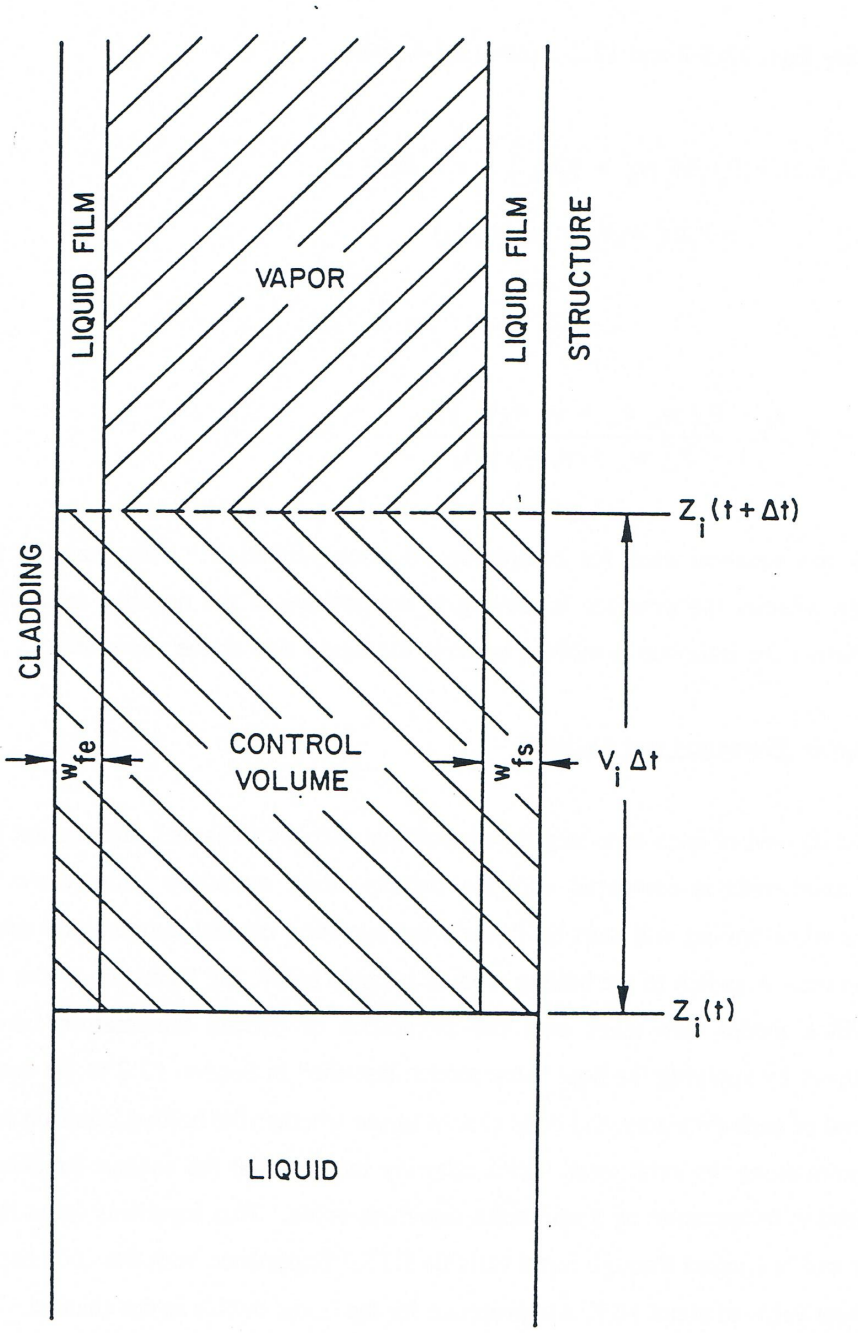

Figure 12.3-1. Geometry Associated with the Liquid-Vapor Interface Velocity Calculation

12.4 Bubble Formation and Collapse

At the end of each time step before voiding starts in a channel, the coolant temperature at each axial node is compared with the corresponding saturation temperature. The code estimates when boiling will start by linearly extrapolating coolant temperatures and saturation temperatures. A switch to the boiling module is made before the formation of the first bubble. The voiding model then takes over the calculation of coolant temperatures and saturation temperatures by applying the liquid slug model described in Section 12.2 to the entire channel. At the end of each time step, the code checks to see whether the boiling criterion has been met at any point along the axial mesh. This criterion requires that the coolant temperature exceed the saturation temperature by a minimum superheat value. This superheat value is selected by the user and is entered through input variable DTS. Experience with the code has shown that a superheat value of about 10 K is appropriate for the initial bubble in the channel. This amount of superheat prevents the bubble from collapsing immediately after formation and appears to produce results that agree well with the experimental results discussed in the introduction to the chapter.

Once the code predicts that the coolant temperature has exceeded the saturation temperature plus the superheat, it begins an iterative process to determine within a small tolerance the time at which the superheat criterion is satisfied exactly. This is done by checking to see by how much the coolant temperature exceeds the sum of the saturation temperature plus the superheat. This temperature excess is used in a linear interpolation to reduce the time step to a value at which the superheat criterion will be met more closely. The code then goes back to the beginning of the time step and repeats the coolant and saturation temperature calculations and again checks the superheat criterion. If the criterion is met to within a built-in tolerance (0.001 K), the code fixes that time as the time of voiding initiation for the channel and forms a vapor bubble at that point in the channel. If the criterion is not met, the code repeats the calculation of the temperature excess beyond the superheat criterion, calculates a new reduced time step, and again goes back to the beginning of the time step and repeats the temperature calculations. This iterative procedure continues until the superheat criterion is met satisfactorily. Normally, the procedure converges with three or four iterations.

After voiding has started in a channel, the voiding model calculation tests at the end of each coolant time step for the formation of new bubbles within the liquid slugs. The formation of new bubbles after voiding has started is subject to the following limitations and modifications.

a. If the maximum number of bubbles (nine bubbles) already exist in the channel, then new bubbles will not be formed.

b. No new bubbles will be formed within a minimum distance, s_{Lmin} (minimum slug length) of a bubble-liquid interface, so nodes within s_{Lmin} of an interface are not checked for bubble formation. Interpolated coolant temperatures and saturation temperatures at a distance s_{Lmin} from each interface are checked, and a bubble is formed at this position if the superheat criterion is exceeded. The minimum

distance s_{Lmin} is an input variable SLMIN; experience with the code indicates that a value of about 2 cm is reasonable for most situations.

c. No more than one new bubble will be formed in a channel in any time step.

d. After the first bubble is formed, time steps are not repeated so as to match exactly the superheat criterion for later bubbles; when the superheat criterion is exceeded, a new bubble is formed with whatever superheat happens to exist. The superheat used in the superheat criterion for bubbles after the first one should be somewhat less than the value used at the start of boiling, generally 3 K or 4 K. This is also a user-input quantity and is read into input variable DTINT. At the end of each time step, linear extrapolation of coolant and saturation temperatures is used to predict when the next bubble will form. This prediction is used to limit the size of future time steps, so that the saturation criterion is normally exceeded only slightly when a new bubble is formed.

Bubbles are assumed to fill the whole cross section of the coolant channel, except for a liquid film left on the cladding and structure. A bubble starts with zero length and with the initial temperature equal to the coolant liquid temperature at the time of bubble formation.

Pressures are continuous across the liquid-vapor interfaces; but sharp temperature gradients can occur in the liquid temperature a short distance from the interface can be significantly different from the vapor temperature at the interface. For each bubble interface, the code calculates one pressure, a vapor temperature, and a liquid temperature at a position far enough from the interface that it is unaffected by the vapor temperature. Also, the bubble interface position and velocity are calculated. In addition to bubble interface values, coolant temperatures, pressures, densities, and flow rate are calculated at the mesh segment interfaces. The liquid film thickness in a voided region is calculated as the average for the segment. Flow areas and hydraulic diameters are treated as constant within a segment although they can vary from segment to segment.

The vapor bubble pressure is assumed to be always equal to the saturation pressure corresponding to its temperature. Thus, the formation of a vapor bubble with a nonzero amount of superheat leads to an immediate jump in pressure at the bubble location.

The initial bubble growth is due mainly to two effects: (1) the initial jump in pressure corresponding to the superheat, drives the liquid slugs apart, forming a larger bubble; and (2) heat flow through the liquid-vapor interface produces vapor to fill the bubble and sustain the pressure. When the bubble gets larger, vaporization of the liquid film on the cladding becomes the main source of vapor. The vapor pressure and temperature are assumed to be spatially uniform during the initial bubble growth. This model for the initial bubble growth is similar to the mode of Fauske and Cronenberg [12-7, 12-8] and also similar to that of Schelechtendahl [12-9].

After the bubble length exceeds a user-specified minimum length (usually 3-10 cm), the vapor bubble calculation is switched to a different model. Heat flow through the liquid-vapor interfaces is ignored, but axial variations in vapor pressure within the

bubble are accounted for. Vaporization of the liquid films in the hot part of the core, and condensation in cooler regions, can lead to high vapor velocities and corresponding appreciable pressure gradients within a vapor bubble. The numerical scheme that is used to calculate the time and space variations in the vapor pressure is an implicit scheme that can handle moderately large (a few milliseconds) time steps. Wave effects tend to be suppressed by the numerical scheme.

Condensation in cooler regions can cause a vapor bubble to shrink. If the bubble size decreased to below the minimum length for the pressure variation model, then the initial uniform pressure model is used again. If the bubble size decreases to less than a minimum bubble size, and if at the same time the rate of decrease of the bubble size exceeds a minimum value, then the bubble is assumed to collapse and the bubble is eliminated from the calculation. When a bubble collapse, the liquid slugs above and below the bubble are combined into one slug, and the flow rate of the combined slug is determined by conserving the combined momentum of the two slugs.

12.5 Uniform Vapor Pressure Model: Small Vapor Bubbles

In this model, the bubble growth is determined by coupling the momentum equations for the liquid slugs, as described in Section 12.2, with an energy balance in the vapor bubble, assuming saturation conditions and spatially uniform pressure and temperature within a bubble. The rate of formation and condensation of vapor is determined by the heat flow through the liquid films on the cladding and structure and through the liquid-vapor interfaces.

Figure 12.5-1 shows the control volume considered in the uniform vapor pressure model. The control volume extends from the lower liquid-vapor interface to the upper one, and from the outer surface of the cladding to the inner surface of the structure. This means that the liquid film remaining on the structure and cladding is included in the control volume. The dots in the figure indicate the locations of the fixed axial mesh points. The piecewise constant representation of the outer cladding radius is consistent with the ability of the code to handle variable flow area.

The primary focus of this model is to obtain the temperature within the vapor bubble. Once the temperature is known, it can be used to calculate the vapor pressure, since saturation conditions have been assumed. The vapor pressure is the driving force for motion of the liquid slugs, so finding the vapor pressures in all bubbles provides the link between conditions in the liquid slugs and conditions in the bubbles and therefore leads to a complete description of conditions throughout the channel.

The vapor temperature is found by taking an energy balance within the control volume described above. The energy balance can be stated qualitatively as

Net energy transferred to the volume =Net change in energy within the volume.

The energy transferred to the control volume can be divided into two sources:

Energy transferred = (Heat flow from the cladding and the structure)
+ (Heat flow through the vapor-liquid interfaces).

Also, the net change in energy is divided between temperature change and phase change.

Change in energy = (Energy change due to temperature change of vapor present at time t) + (energy change due to vaporization or condensation during the time step).

The remainder of this section will formulate equations that model each portion of the energy balance and that, when combined, will reduce to a set of linear equations that give the vapor temperatures of the bubbles in the channel in terms of known quantities. Subsection 12.5.1 will discuss heat flow from the cladding and structure, Subsection 12.5.2 will analyze heat flow through the liquid-vapor interface, Subsection 12.5.3 will detail the change in vapor energy due to temperature and phase changes, and Subsection 12.5.4 will produce the final energy balance and the equations governing the bubble temperatures. Subsection 12.5.5 will then discuss the solution of the bubble temperature equations.

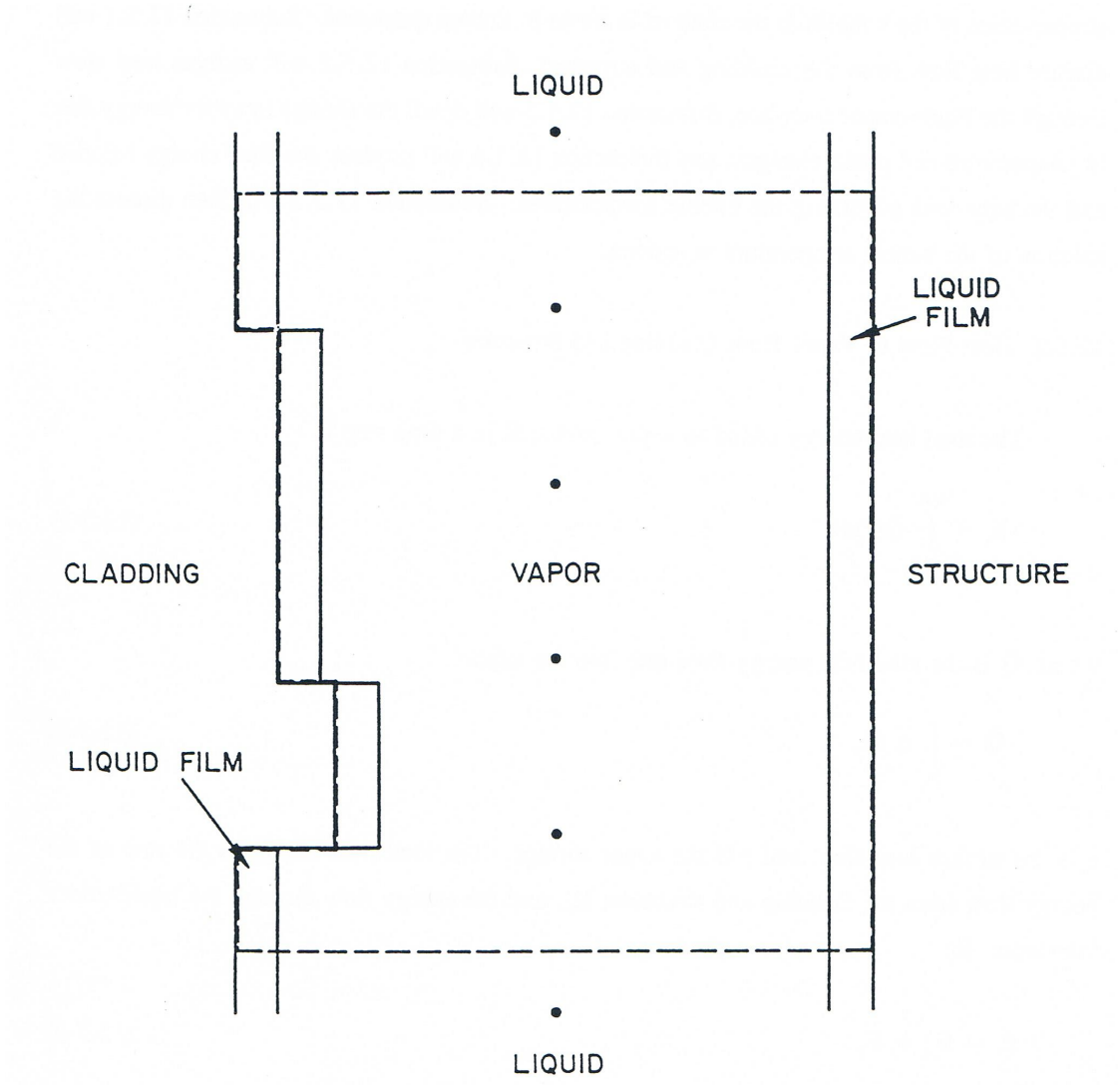

Figure 12.5-1. Control volume for the Uniform Vapor Pressure Model (control volume is outlines by the dashed line)

12.5.1 Heat Flow to Vapor from Cladding and Structure

The total heat energy added to vapor bubble K in a time step is

$$E_t = \int_t^{t+\Delta t} \tilde{Q}(\tau)\, d\tau \qquad (12.5\text{-}1)$$

where $\tilde{Q}$ is the total heat energy flow rate into the vapor:

$$\tilde{Q} = \int_s q\, ds, \tag{12.5-2}$$

q is the surface heat flux, and s is the vapor surface. The total heat energy is the sum of the energy flow from the cladding and structure, E_{es}, and the energy flow through the liquid-vapor interfaces, E_i:

$$E_t = E_{es} + E_i \tag{12.5-3}$$

The cladding and structure term, E_{es} is approximated by

$$E_{es} = \frac{\Delta t}{2}\left[Q_{es}(K,t) + Q_{es}(K,t+\Delta t)\right] \tag{12.5-4}$$

where Q_{es} is the heat flow from the cladding and structure,

$$Q_{es}(K,t) = P_e \int_{z_i(L=1,t,K)}^{z_2(L=2,t,K)} \left[q_e(z,t) + \gamma_2\, q_s(z,t)\right] dz \tag{12.5-5}$$

with

$z_i(2,t,K)$ = height of upper liquid-vapor interface

$z_i(1,t,K)$ = height of lower liquid-vapor interface

P_e =perimeter of cladding = $2\pi r_e$

r_e =nominal radius of cladding

γ_2 =ratio of surface area of structure to surface area of cladding

q_e =cladding-to-vapor heat flux

and

q_s =structure-to-vapor heat flux.

The heat fluxes are calculated from Newton's law of cooling as

$$q_e(z,t) = \frac{T_e(z,t) - T(K,t)}{R_{ec}(z,t)} \tag{12.5-6a}$$

and

$$q_s(z,t) = \frac{T_s(z,t) - T(K,t)}{R_{sc}(z,t)} \qquad (12.5\text{-}6b)$$

where $T(K,t)$ is the uniform temperatures within bubble K at time t and R_{ec} and R_{sc} are the thermal resistances between the cladding and vapor and he structure and vapor, respectively.

The form of the thermal resistances is best discussed in terms of a thermal network. Focusing first on the cladding-vapor resistance, Fig. 12.5-2 shows the thermal network formed by the cladding, liquid film on the cladding, and vapor and gives the thermal resistances associated with each region. Because of the high thermal conductivity of liquid metals, the resistance of the liquid sodium film can be taken to be just the conductive resistance. The total thermal resistance is then the sum of the individual resistances, or

$$R_{ec} = \frac{1}{h_{ec}} + R_{ehf} \qquad (12.5\text{-}7)$$

where R_{ehf} is the resistance of the cladding, as discussed in Chapter 3 (see Section 3.5.1, Eq. 3.5-7) and h_{ec} is the heat-transfer coefficient which models the combined resistances of the liquid film and the vapor. The coefficient h_{ec} is just $1/\left(\frac{1}{h_c} + \frac{w_{fe}}{k_\ell}\right)$; however, this is not as simple an expression as it appears, since the convective heat-transfer coefficient h_c is not a constant or a simple function of temperature. To circumvent this difficulty, a temperature correlation based on physical data was developed for h_{ec} and used in SASSYS-1. This correlation is based on the temperature difference between the cladding and the vapor and is structured as follows. If the cladding is more than 100 K hotter than the vapor, the liquid film is assumed to be at the same temperature as the vapor, which amounts to neglecting the thermal resistance of the vapor. The coefficient h_{ec} then takes the form

$$h_{ec}(z) = \frac{k_l(z)}{w_{fe}(z)} \text{ if } T_e(z) > T(K) + 100 \qquad (12.5\text{-}8)$$

where

$k\ell(z)$= thermal conductivity of liquid sodium at temperature T(K)

and

$w_{fe}(z)$=thickness of liquid film on the cladding

and $T(K)$ represents an extrapolated vapor temperature for advanced time values of h_{ec}. If the cladding is more than 100 K colder than the vapor, the liquid film is assumed to be at the same temperature as the cladding, and so the resistance of the film is neglected. The heat-transfer coefficient from the vapor to the film is a condensation coefficient

h_{cond} which is supplied by the user through the input variable HCOND. A reasonable value for HCOND is around $6x10^4$ W/m^2-K. The coefficient h_{ec} then becomes

$$h_{ec}(z) = h_{cond} \text{ if } T_e(z) < T(K) - 100 \tag{12.5-9}$$

For $T(K) - 100 \le T_e(z) \le T(K) + 100$, h_{ec} is calculated as an interpolation of the condensation coefficient and the conductive film resistance according to the formula

$$h_{ec}(z) = h_{cond} + \frac{\frac{k_\ell(z)}{w_{fe}(z)} - h_{cond}}{1 + \exp\left(\frac{T(K) - T_e(z)}{2}\right)}, \quad T(K) - 100 \le T_e(z) \le T(K) + 100 \tag{12.5-10}$$

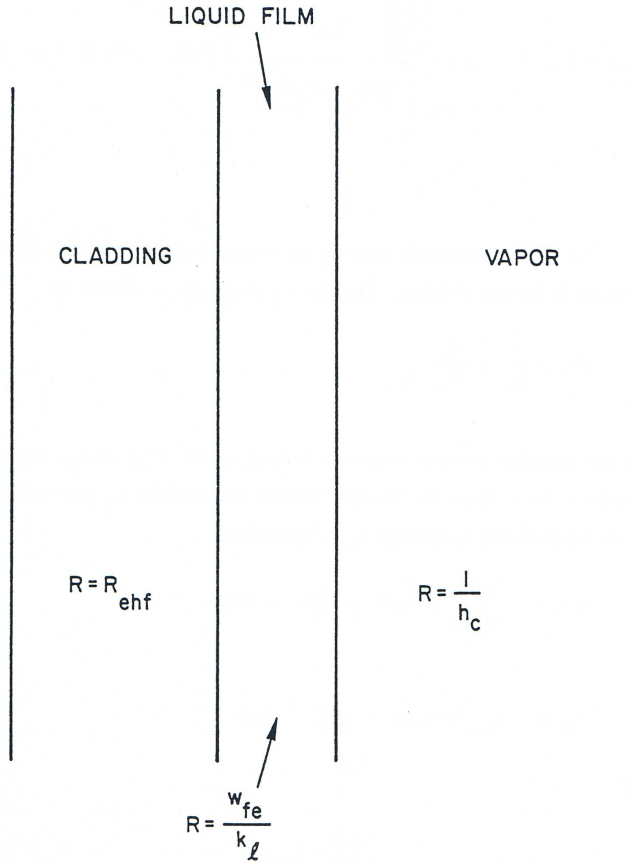

Figure 12.5-2. Thermal Network Formed by the Cladding, Cladding Film, and Vapor

The thermal resistance between the structure and he vapor is calculated using the same procedure as for the cladding. The thermal resistance is defined as

$$R_{sc} = \frac{1}{h_{sc}} + \frac{d_{sti}}{2k_{sti}} \qquad (12.5\text{-}11)$$

with the structure thermal resistance defined as the ratio of d_{sti}, the thickness of the inner structure node, to twice the structure thermal conductivity k_{sti} (see Section 3.5.2, Eq. 3.5-18), and the heat-transfer coefficient h_{sc} computed as

$$h_{sc}(z) = \frac{k_{\ell}(z)}{w_{fs}(z)} \text{ if } T_s(z) > T(K) - 100 \qquad (12.5\text{-}12)$$

$$h_{sc}(z) = h_{cond} \text{ if } T_s(z) < T(K) - 100 \qquad (12.5\text{-}13)$$

and

$$h_{sc}(z) = h_{cond} + \frac{\frac{k_{\ell}(z)}{w_{fe}(z)} - h_{cond}}{1 + \exp\frac{T(K) - T_e(z)}{2}}, \quad T(K) - 100 \le T_s(z) \le T(K) + 100 \qquad (12.5\text{-}14)$$

where $w_{fs}(z)$ is the thickness of liquid film on the structure.

With the cladding-to-vapor and structure-to-vapor heat fluxes now defined, Eq. 12.5-5 can be solved for $Q_{es}(K,t)$ in terms of known quantities. The problem how is to use Eq. 12.5-5 to express $Q_{es}(K,t + \Delta t)$ as a linear function of the change in vapor temperatures over the time step Δt. The difficulty comes from the fact that the advanced time interface positions z_i (which are the limits of integration in the expression for $Q_{es}(K,t + \Delta t)$ are dependent on the advanced time vapor pressures and, therefore, on the advanced time temperatures. However, $Q_{es}(K,t + \Delta t)$ can be written as a linear function of the temperature changes if the interface positions are written as the sum of two functions, one which contains only known quantities and one which is a linear function of the change in vapor temperature. To this end, the interface position at $t + \Delta t$ can be written as a linear function

$$z_i(L, t + \Delta t, K) = z_i(L, t, K) + \Delta z_i(K, L) \qquad (12.5\text{-}15)$$

with the change in position Δ_{zi} given by

$$\Delta z_i(K, L) = \frac{\Delta t}{2}\left(v_i(L, t, K) + v_i(L, t + \Delta t, K)\right). \qquad (12.5\text{-}16)$$

The advanced time interface velocity can also be expressed as a linear function

$$v_i(L, t + \Delta t, K) = v_i(L, t, K) + \Delta v_i(K, L) \qquad (12.5\text{-}17)$$

with the change in interface velocity computed from the change in liquid slug mass flow rate

$$\Delta v_i(K,L) = \frac{\Delta W(K')}{(\rho_\ell A_c)_{K',L}} \tag{12.5-18}$$

where

$$K' = K \; if \; L = 1, \tag{12.5-19a}$$

$$K' = K + 1 \; if \; L = 2, \tag{12.5-19b}$$

and $(\rho_\ell A_c)_{K',L}$ is the product of the liquid density and channel flow area at the bubble interface. It is assumed in Eq. 12.5-18 that the change in interface velocity can be expressed as the change in the average slug velocity (see Eq. 12.3-1), with the correction for film thickness ignored. If now the expression for the change in liquid slug mass flow rate, eq. 12.2-34 derived in Section 3.2, is combined with Eq. 12.5-18 and inserted into Eq. 12.5-17, the advanced time interface velocity becomes

$$v_i(L,t+\Delta t,K) = v_i(L,t,K) + \frac{1}{(\rho_\ell A_c)_{K',L}} \frac{\Delta t\left[AA_0(K') + (\Delta p_{K'-1} - \Delta p_{K'})\theta_2\right]}{I_1(K') + \theta_2 \Delta I_1(K') + \theta_2 BB_0(K')\Delta t} \tag{12.5-20}$$

where Δp_K is the change in pressure in bubble K during the time step and K' is defined as above. Substituting Eqs. 12.5-16 and 12.5-20 into Eq. 12.5-15 gives the advanced time interface position as

$$z_i(L,t+\Delta t,K) = z_i(L,t,K) + v_i(L,t,K)\Delta t + \frac{\Delta t}{2} \frac{1}{(\rho_\ell A_c)_{K',L}} \frac{\Delta t\left[AA_0(K') + (\Delta p_{K'-1} - \Delta p_{K'})\theta_2\right]}{I_1(K') + \theta_2 \Delta I_1(K') + \theta_2 BB_0(K')\Delta t} \tag{12.5-21}$$

which can be rewritten as

$$z_i(L,t+\Delta t,K) = z_{i0}(K,L) + \Delta z'(K,L) \tag{12.5-22}$$

where $z_{i0}(K,L)$ is the function

$$z_{i0}(K,L) = z_i(L,t,K) + \Delta z_0(K,L) \tag{12.5-23}$$

with

$$\Delta z_{i0}(K,L) = v_i(L,t,K) + \frac{1}{2} \frac{\Delta W_0(K')\Delta t}{(\rho_\ell A_c)_{K',L}} \tag{12.5-24}$$

and

$$\Delta W_0(K') = \frac{AA_0(K')\Delta t}{I_1(K') + \theta_2 \Delta I_1(K') + BB_0(K')\theta_2 \Delta t} \tag{12.5-25}$$

and $\Delta z'(K,L)$ is

$$\Delta z'(K,L) = \frac{dz_i(K,L)}{dp}\left(\Delta p_{K'-1} - \Delta p_{K'}\right) \tag{12.5-26}$$

with

$$\frac{dz_i(K,L)}{dp} = \frac{\theta_2 \Delta t^2}{2(\rho_\ell A_c)_{K',L}\left[I_1(K') + \theta_2 \Delta I_1(K') + BB_0(K')\theta_2 \Delta t\right]} \tag{12.5-27}$$

The expression for $\frac{dz_i}{dp}$ is obtained by taking the derivative with respect to pressure of Eq. 12.5-16, using Eq. 12.5-20. The function z_{i0} is a function only of known quantities and is the approximate position to which the interface would move at $t+\Delta$ if the bubble pressures did not change over the time step. The additional change in interface position due to bubble pressure changes is accounted for by $\Delta z'$, which is a linear function of the pressure changes.

Using Eq. 12.5-22 for the interface position, the integral for the cladding and structure heat flow $Q_{es}(K,t+\Delta t)$ can be expressed as the sum of three integrals:

$$\begin{aligned} Q_{es}(K,t+\Delta t) = P_e &\int_{z_{i0}(K,1)}^{z_{i0}(K,2)} \left[q_e(z,t+\Delta t) + \gamma_2 q_s(z,t\Delta t)\right]dz \\ + P_e &\int_{z_{i0}(K,2)}^{z_{i0}(K,2)+\Delta z'(K,1)} \left[q_e(z,t+\Delta t) + \gamma_2 q_s(z,t\Delta t)\right]dz \\ + P_e &\int_{z_{i0}(K,1)+\Delta z'(K,1)}^{z_{i0}(K,1)} \left[q_e(z,t+\Delta t) + \gamma_2 q_s(z,t\Delta t)\right]dz \end{aligned} \tag{12.5-28}$$

If the vapor temperature $T(K,t+\Delta t)$ is linearized to be $T(K,t) + \Delta T(K)$, the first integral is a function only of $\Delta T(K)$ and known quantities, since the advanced time cladding and structure temperatures are determined by extrapolation from values calculated in the transient heat-transfer module at the previous two heat-transfer time steps and, therefore, are considered known. Using Eqs. 3-5-6 for the heat fluxes, the first integral can be written as the sum $I_{e1}(K) + I_{e2}(K)\Delta T(K)$, where

$$I_{e1}(K)=P_e\int_{z_{i0}(K,1)}^{z_{i0}(K,2)}\left\{\frac{T_e(z,t+\Delta T)-T(K,t)}{R_{ec}(z,t+\Delta t)}+\frac{\gamma_2\left[T_s(z,t+\Delta T)-T(K,t)\right]}{R_{sc}(z,t+\Delta t)}\right\}dz \tag{12.5-29a}$$

and

$$I_{e2}(K)=-P_e\int_{z_{i0}(K,1)}^{z_{i0}(K,2)}\left[\frac{1}{R_{ec}(z,t+\Delta t)}+\frac{\gamma_2}{R_{sc}(z,t+\Delta t)}\right]dz \tag{12.5-29b}$$

The second and third integrals are evaluated by assuming that the heat fluxes are constant in space over the domain of integration; this is a reasonable assumption, since $\Delta z'$ is a small quantity. If second-order terms proportional to $\Delta T\Delta z'$ are dropped, the second integral is just $I_{e3}(K)\Delta z'(K,2)$, with

$$I_{e3}(K)=P_e\left\{\frac{T_e\left[z_{i0}(K,2),t+\Delta t\right]-T(K,t)}{R_{ec}\left[z_{i0}(K,2),t+\Delta t\right]}+\gamma_2\left[\frac{T_s\left[z_{i0}(K,2),\,t+\Delta t\right]-T(K,t)}{R_{sc}\left[z_{i0}(K,2),t+\Delta t\right]}\right]\right\} \tag{12.5-29c}$$

and the third integral is $I_{e3}(K)\Delta z'(K,1)$, where

$$I_{e4}(K)=-P_e\left\{\frac{T_e\left[z_{i0}(K,1),t+\Delta t\right]-T(K,t)}{R_{ec}\left[z_{i0}(K,1),t+\Delta t\right]}+\gamma_2\left[\frac{T_s\left[z_{i0}(K,1),\,t+\Delta t\right]-T(K,t)}{R_{sc}\left[z_{i0}(K,1),t+\Delta t\right]}\right]\right\} \tag{12.5-29d}$$

This gives for $Q_{es}(K,\,t+\Delta t)$

$$Q_{es}(K,\,t+\Delta t)=I_{e1}(K)+I_{e2}(K)\Delta T(K)+I_{e3}(K)\Delta z'(K,2)+I_{e4}(K)\Delta z'(K,1) \tag{12.5-30}$$

which, by the definition of $\Delta z'$ and the assumption of saturation conditions, is a function only of known quantities and the changes in bubble temperatures.

Note that Eq. 12.5-30 is valid regardless of the direction of motion of either interface. The sign of $\Delta z'$ will be positive for upward interface motion and negative for downward motion, giving the correct sign to the last two terms in Eq. 12.5-30.

The energy flow in E_{es} is therefore given by the linear equation

$$E_{es} = \frac{\Delta t}{2}\Big[Q_{es}(K,t) + I_{e1}(K) + \Big(I_{e2}(K) + I_{e3}(K)\frac{dz_i(K,2)}{dp} - I_{e4}(K)\frac{dz_i(K,1)}{dp}\Big)\Delta p_K - I_{e3}(K)\frac{dz_i(K,1)}{dp}\Delta p_{K+1} + I_{e4}(K)\frac{dz_i(K,1)}{dp}\Delta p_{K-1}\Big] \quad (12.5\text{-}31)$$

where the definition of $\Delta z'$ in terms of Δp has been used.

12.5.2 Heat Flow through Liquid-Vapor Interface

The SASSYS-1 calculation of the heat flow through the liquid-vapor interface is based on the work by Cronenberg [12-7]. In the method, the total heat flow through the liquid-vapor interfaces is the sum of an upper interface term I_{iu} and a lower interface term $I_{i\ell}$.

$$E_i = \Delta t\left(I_{iu} + I_{i\ell}\right) \quad (12.5\text{-}32)$$

where

$$I_{ix} = k_\ell A_{cx}\left.\frac{\overline{\partial T_{\ell_x}}}{\partial \xi}\right|_{\xi=0} \quad (12.5\text{-}33)$$

with

x = u or ℓ

A_{cx} = area of coolant channel

$T_{\ell x}$ = liquid temperature near interface

k_ℓ = liquid thermal conductivity near interface

ξ = axial distance from interface

ξ = $z - z_i$ for upper interface

ξ = $-(z - z_i)$ for lower interface

and

$\overline{\frac{\partial T_{\ell_x}}{\partial \xi}}$ is the time average of the spatial derivative for the time step

An expression for the coolant temperature derivative $\overline{\frac{\partial T_{\ell_x}}{\partial \xi}}$ can be derived from the general heat conduction equation written for the liquid slug as

$$\alpha \frac{\partial^2 T_\ell(\xi,t')}{\partial \xi^2} + \frac{Q(\xi,t')}{\rho_\ell C_\ell} = \frac{\partial^2 T_\ell(\xi,t')}{\partial t'} \tag{12.5-34}$$

where

α = $k_\ell/\rho_\ell C_\ell$, the thermal diffusivity of liquid sodium

k_ℓ = thermal conductivity of the liquid

C_ℓ = liquid heat capacity

ρ_ℓ = liquid density

Q = heat input per unit volume in the liquid

T_ℓ = temperature in liquid slug

ξ = distance into liquid slug form liquid-vapor interface

and

t' = time since the vapor bubble started to form

The heat input Q includes both the direct heating Q_c and the heat flow $Q_{ec} + Q_{sc}$ from the cladding and structure to the liquid slug:

$$Q = Q_c + Q_{ec} + Q_{sc} \tag{12.5-35}$$

where the functional form of Q_c is given in Chapter 3, Eq. 3.3-6, and Q_{ec} and Q_{sc} are calculated form Newton's law of cooling in the form of Eqs. 3.3-7 and 3.3-8 in Chapter 3.

The boundary conditions for the problem are

$$T_\ell(\xi = 0, t') = T(t'), \text{the vapor temperature at the liquid - vapor interface,} \tag{12.5-36a}$$

and

$$T_\ell(\xi = \infty, t') < \infty, \tag{12.5-36b}$$

and the initial condition is

$$T_\ell(\xi, t' = 0)\text{known.} \tag{12.5-36c}$$

The heat conduction equation, together with the initial and boundary conditions, can be solved for T_ℓ through the use of the Laplace transform method. The details of this approach are presented in Appendix 12.1; here, just the main points will be listed. The procedure involves four main stages:

1) Take the Laplace transform of the heat conduction equation, Eq. 12.5-34. This produces a second-order ordinary differential equation in space.
2) Solve the differential equation produced in stage 1 for the Laplace transform of T_ℓ as a function of ξ.
3) Take the spatial derivative of the Laplace transform of T_ℓ and evaluate it at $\xi = 0$.
4) Take the inverse Laplace transform of the derivative from stage 3, producing $\left.\frac{\partial T_\ell}{\partial \xi}\right|_{\xi=0}$.

This procedure results in the following expression for $\left.\frac{\partial T_\ell}{\partial \xi}\right|_{\xi=0}$:

$$\begin{aligned}\frac{\partial T_\ell(\xi=0,t')}{\partial \xi} = {} & \frac{-1}{\sqrt{\pi\alpha}}\int_0^{t'}\frac{\partial T_\ell(\xi=0,\tau)}{\partial \tau}\frac{1}{\sqrt{t'-\tau}}d\tau \\ & - \frac{T_\ell(\xi=0,t'=0)}{\sqrt{\alpha\pi t'}} + \int_0^\infty d\xi \int_0^{t'} \frac{\xi Q(\xi,\tau)\exp\left[-\frac{\xi^2}{4\alpha(t'-\tau)}\right]}{2k_\ell\sqrt{\pi\alpha(t'-\tau)^3}}d\tau \\ & + \int_0^\infty \frac{T_\ell(\xi,t'=0)\xi\exp\left[-\frac{\xi^2}{4\alpha t'}\right]}{2\alpha\sqrt{\pi\alpha(t')^3}}d\xi\end{aligned} \tag{12.5-37}$$

To evaluate the terms in Eq. 12.5-37, first note that the exponential function in the third and fourth terms decays very rapidly with increasing ξ due to the small thermal diffusivity of liquid sodium. Therefore, for purposes of solving eq. 12.5-37, it is valid to assume that the initial temperature distribution ($t' = 0$) is uniform near the interface, or

$$T_\ell(\xi, t' = 0) = T_0 \tag{12.5-38}$$

Then the fourth term in Eq. 12.5-37 is easily integrated to give

$$\int_0^{\infty} \frac{T_0}{\alpha} \frac{\xi \exp\left(-\xi^2/4\alpha t'\right)}{2\sqrt{\pi\alpha\left(t'\right)^3}} d\xi = \frac{T_0}{\sqrt{\pi\alpha t'}}, \tag{12.5-39}$$

so the second and fourth terms cancel.

Similarly, $Q(\xi, \tau)$ can be approximated as the spatially constant function $Q_{Ox}(\tau)$ near the interface so the third term becomes

$$\int_0^{t'} d\tau \int_0^{\infty} d\xi \frac{\xi Q_{Ox} \exp\left[-\frac{\xi^2}{4\alpha\left(t'-\tau\right)}\right]}{2k_\ell \sqrt{\pi\alpha\left(t'-\tau\right)^3}} = \int_0^{t'} \frac{d\tau Q_{Ox}\left(\tau\right)}{k_\ell} \left(\frac{\alpha}{\pi\left(t'-\tau\right)}\right)^{1/2} \tag{12.5-40}$$

with $Q_{Ox}(\tau)$ defined as

$$Q_{Ox}\left(\tau\right) = \gamma\left[\frac{T_{e_x}\left(\tau\right) - T\left(\tau\right)}{R_{ecx}} + \gamma_2 \frac{T_{s_x}\left(\tau\right) - T\left(\tau\right)}{R_{scx}}\right] \tag{12.5-41}$$

where

γ = ratio of cladding surface area to coolant volume

γ_2 = ratio of surface area of structure to surface area of cladding

R_{ecx} = thermal resistance between the cladding and the coolant at the interface

R_{scx} = thermal resistance between the structure and the coolant at the interface

and

$$x = \begin{cases} U \text{ at the upper interface} \\ \ell \text{ at the lower interface} \end{cases}$$

Thus, Eq. 12.5-37 has the reduced form

$$\frac{\partial T_l}{\partial \xi}\left(\xi = 0, t'\right) = \frac{1}{\sqrt{\pi}} \int_0^{t'} \left[Q_{Ox}\left(\tau\right)\frac{\sqrt{a}}{k_\ell} - \frac{1}{\sqrt{a}}\frac{\partial T_\ell}{\partial \tau}\left(\xi = 0, \tau\right)\right] \frac{d\tau}{\sqrt{t'-r}} \tag{12.5-42}$$

which can be rewritten in terms of t, the time since initiation of the transient, through the variable transformation $t' = t - t_b$:

$$\left.\frac{\partial T_{\ell_x}(t)}{\partial \xi}\right|_{\xi=0} = \frac{1}{\sqrt{\pi}} \int_{t_b}^{t} \left[Q_{Ox}(\tau) \frac{\sqrt{a}}{k_\ell} - \frac{1}{\sqrt{a}} \frac{\partial T_{(\tau)}}{\partial \tau} \right] \frac{d\tau}{\sqrt{t-r}} \tag{12.5-43}$$

The boundary condition at $\xi = 0$ has been incorporated into this expression. Equation 12.5-43 will be somewhat easier to work with if the function

$$f_x(\tau) \equiv Q_{Ox}(\tau) \frac{\sqrt{a}}{k_\ell} - \frac{1}{\sqrt{a}} \frac{\partial T[\tau]}{\partial \tau} \tag{12.5-44}$$

is used to give the simpler equation

$$\left.\frac{\partial T_{\ell_x}(t)}{\partial \xi}\right|_{\xi=0} = \frac{1}{\sqrt{\pi}} \int_{t_b}^{t} \frac{d\tau}{\sqrt{t-\tau}} f_x(\tau) \tag{12.5-45}$$

Now, the time average over the time step Δt of $\left.\frac{\partial T_{\ell_x}}{\partial \xi}\right|_{\xi=0}$ needed to compute the interface heat flow from Eq. 12.5-53 can be written as

$$\left.\frac{\partial \overline{t}_{\ell_x}}{\partial \xi}\right|_{\xi=0} = \frac{1}{\Delta t} \int_0^{\Delta t} d\varepsilon \left.\frac{\partial T_{\ell_z}(t_k+\varepsilon)}{\partial \xi}\right|_{\xi=0} \tag{12.5-46}$$

with $\left.\frac{\partial T_{\ell_x}}{\partial \xi}\right|_{\xi=0}$ expressed as in Eq. 12.5-45 and $t = t_k$ the time at the beginning of the time step. To accomplish the goal of expressing the energy balance for the bubble as a linear function of the vapor temperatures, the integral in Eq. 12.5-46 must be written as a linear function of the vapor temperatures. This in turn means that the function $f_x(\tau)$ must be approximated so that Eq. 12.5-45 can b integrated and so that the resulting expression is linear in the vapor temperature. This can be done by writing $\left.\frac{\partial T_{\ell_x}}{\partial \xi}\right|_{\xi=0}$

$$\begin{aligned} \left.\frac{\partial T_{\ell_x}(t_k+\varepsilon)}{\partial \xi}\right|_{\xi=0} &= \frac{1}{\sqrt{\pi}} \int_{t_b}^{t_k+\varepsilon} \frac{d\tau}{\sqrt{t_k-\tau+\varepsilon}} f_x(\tau) \\ &= \frac{1}{\sqrt{\pi}} \int_{t_b}^{t_k} \frac{d\tau}{\sqrt{t_k-\tau+\varepsilon}} f_x(\tau) + \frac{1}{\sqrt{\pi}} \int_{b}^{t_k+\varepsilon} \frac{d\tau}{\sqrt{t_k-\tau+\varepsilon}} f_x(\tau) \end{aligned} \tag{12.5-47}$$

The first term in Eq. 12.5-47 is a function only of known quantities, since the range of integration extends only up to the beginning of the current time step. Therefore, the dependence on advanced time vapor temperatures is contained entirely in the second

term of Eq. 12.5-47. To integrate this term, define the quantity $\bar{f}_{x\Delta t}$ to be the simple average of $f_x(\tau)$ over the range of integration:

$$\begin{aligned}\bar{f}_{x\Delta t} &= \frac{1}{\Delta t}\int_{t_k}^{t_k+\Delta t} dt f_x(t) \\ &= \frac{1}{\Delta t}\int_{t_k}^{t_k+\Delta t} dt\left[Q_{Ox}(t)\frac{\sqrt{a}}{k_\ell} - \frac{1}{\sqrt{a}}\frac{\partial T(t)}{\partial t}\right]\end{aligned} \tag{12.5-48}$$

If the cladding, structure, and vapor temperatures in the expression given above for Q_{Ox} are assumed linear in time over Δt, $\bar{f}_{x\Delta t}$ becomes

$$\begin{aligned}\bar{f}_{x\Delta t} &= \frac{1}{\Delta t}\left[\frac{\sqrt{\alpha}}{k_\ell}\frac{\Delta t}{2}\left(Q_{Ox}(t_k)+Q_{Ox}(t_k+\Delta t)\right) - \frac{1}{\sqrt{\alpha}}\left(T(t_k+\Delta t)-T(t_k)\right)\right] \\ &= 1/2\left[Q_{Ox}(t_k)+Q_{Ox}(t_k+\Delta t)\right]\frac{\sqrt{\alpha}}{k_\ell} - \frac{1}{\sqrt{\alpha}}\frac{T(t_k+\Delta t)-T(t_k)}{\Delta t}\end{aligned} \tag{12.5-49}$$

Since Δt (and therefore ε) is small, it is reasonable to approximate $f_x(\tau)$ as $\bar{f}_{x\Delta t}$ from t_k to $t_k + \varepsilon$. Thus, the second term in Eq. 12.5-47 becomes

$$\frac{1}{\sqrt{\pi}}\int_{t_k}^{t_k+\varepsilon}\frac{d\tau}{\sqrt{t_k-\tau+\varepsilon}}f_x(\tau) = \frac{1}{\sqrt{\pi}}\int_{t_k}^{t_k+\varepsilon}\frac{d\tau}{\sqrt{t_k-\tau+\varepsilon}}\bar{f}_{x\Delta t} \tag{12.5-50}$$

This equation can be integrated easily by making the change of variable $\tau' = t_k - \tau + \varepsilon$ to give

$$\frac{1}{\sqrt{\pi}}\int_{t_k}^{t_k+\varepsilon}\frac{d\tau}{\sqrt{t_k-\tau+\varepsilon}}\bar{f}_{x\Delta t} = \bar{f}_{x\Delta t}\int_0^{\varepsilon}\frac{d\tau'}{\sqrt{\tau'}} = 2\sqrt{\varepsilon}\,\bar{f}_{x\Delta t} \tag{12.5-51}$$

which is linear in $T(t_k + \Delta t)$.

The interface heat flow has now been expressed as a linear function of the advanced time vapor temperature. However, one problem remains; namely, evaluation of the integral in the first term in Eq. 3.5-47. One simple way to handle this is to approximate $f_x(\tau)$ by some average value $\bar{f}_x$ over the range of integration, giving

$$\int_{t_b}^{t_k} \frac{d\tau}{\sqrt{t_k+\varepsilon-\tau}}\, f_x(\tau) = \bar{f}_x \int_{t_b}^{t_k} \frac{d\tau'}{\sqrt{\tau_k-\varepsilon-\tau}}$$
$$= \bar{f}_x \int_{\varepsilon}^{t_k+\varepsilon-t_b} \frac{d\tau'}{\sqrt{\tau'}} \qquad (12.5\text{-}52)$$
$$= 2\bar{f}_x\left(\sqrt{\tau_k+\varepsilon-\tau_b}-\sqrt{\varepsilon}\right)$$

where the integral has been evaluated using the change of variable $\tau' = t_k + \varepsilon - \tau$ as above. Now, the problem reduces to one of selecting an appropriate value for $\bar{f}_x$. The range of integration is too large to use the simple average as was done above. An alternative approach, is to examine the integral in the first term of Eq. 12.5-47 and try to develop an expression for $\bar{f}_x$ which is a function of t_k and which can be computed form values at earlier time steps through a recursion relation. To this end, use the fact that ε is mall to approximate the first integral in Eq. 12.5-47 as

$$\int_{t_b}^{t_k} \frac{d\tau}{\sqrt{t_k+\varepsilon-\tau}}\, f_x(\tau) \approx \int_{t_b}^{t_k} \frac{d\tau}{\sqrt{t_k-\tau}} f_x(\tau)$$
$$= \int_{0}^{t_k-t_b} \frac{d\tau'}{\sqrt{\tau'}} f_x(t_k-\tau') \qquad (12.5\text{-}53)$$

The transformation $\tau' = t_k - \tau$ was used in the last integral in Eq. 12.5-53. Now, define the function g,(τ′) as

$$g_x(\tau') = f_x(t_k-\tau') \qquad (12.5\text{-}54)$$

and the weighted average of g_x as

$$\bar{g}_x(t_k) = \frac{\int_0^{t_k-t_b} \frac{d\tau'}{\sqrt{\tau'}} g_x(\tau')}{\int_0^{t_k-t_b} \frac{d\tau'}{\sqrt{\tau'}}} \qquad (12.5\text{-}55)$$

As will be shown below, $\bar{g}_x(t_k)$ can be determined form a recursion relation.

Rearranging eq. 12.5-55 gives the integral in Eq. 12.5-53 the form

$$\int_0^{t_k-t_b} \frac{d\tau'}{\sqrt{\tau'}} f_x(t_k-\tau') = 2\sqrt{\tau_k-t_b}\,\bar{g}_x(t_k) \qquad (12.5\text{-}56)$$

The function $\bar{f}_x$ can now be expressed in terms of $\bar{g}_x(t_k)$ by combining Eqs. 12.5-52, 12.5-53, and 12.5-56 to give

$$\begin{aligned} 2\bar{f}_x\left(\sqrt{t_k+\varepsilon-\tau_b}-\sqrt{\varepsilon}\right) &= \int_{t_b}^{t_k} \frac{d\tau}{\sqrt{t_k+\varepsilon-\tau}} f_x(\tau) \\ &\approx \int_{t_b}^{t_k} \frac{d\tau}{\sqrt{t_k-\tau}} f_x(\tau) \\ &= 2\sqrt{t_k-t_b}\,\bar{g}_x(t_k) \end{aligned} \tag{12.5-57}$$

Since ε is small compared to $t_k - t_b$ for all but the times right after the bubble has formed, it is reasonable to approximate $\sqrt{\tau_k+\varepsilon-t_b}-\sqrt{\varepsilon}$ by $\sqrt{t_k-t_b}$ and therefore to choose

$$\bar{f}_x = \bar{g}_x(t_k) \tag{12.5-58}$$

as the approximation to $f_x(\tau)$ for $t_b \le \tau \le t_k$. This expression can be computed from a recursion relation by writing $\bar{g}_x(t_k+\Delta t)$ as

$$\begin{aligned} \bar{g}_x(t_k+\Delta t) &= \int_0^{t_k+\Delta t-t_b} \frac{d\tau'}{\sqrt{\tau'}} f_x(t_k+\Delta t-\tau') \Big/ \int_0^{t_k+\Delta t-t_b} \frac{d\tau'}{\sqrt{\tau'}} \\ &= \frac{1}{2\sqrt{t_k+\Delta t-t_b}}\left[\int_0^{\Delta t} \frac{d\tau'}{\sqrt{\tau'}} f_x(t_k+\Delta t-\tau') + \int_{\Delta t}^{t_k+\Delta t-t_b} \frac{d\tau'}{\sqrt{\tau'}} f_x(t_k+\Delta t-\tau')\right] \end{aligned} \tag{12.5-59}$$

Substituting the approximations $f_x(t_k+\Delta t-\tau') = \bar{f}_{x\Delta t}$ for $0 \le \tau' \le \Delta t$ and $f_x(t_k+\Delta t-\tau') = \bar{g}(t_k)$ for $\Delta t \le \tau' \le t_k+\Delta t-t_b$ as used above reduces the integrals in Eq. 12.5-59 to

$$\begin{aligned} \bar{g}_x(t_k+\Delta t) &= \frac{1}{2\sqrt{t_k+\Delta t-t_b}}\left[\int_0^{\Delta t} \frac{d\tau'}{\sqrt{\tau'}} \bar{f}_{x\Delta t} + \int_{\Delta t}^{t_k+\Delta t-t_b} \frac{d\tau'}{\sqrt{\tau'}} \bar{g}_x(t_k)\right] \\ &= \frac{1}{\sqrt{t_k+\Delta t-t_b}}\left[\bar{f}_{x\Delta t}\sqrt{\Delta t} + \bar{g}_x(t_k)\left(\sqrt{t_k+\Delta t-t_b}-\sqrt{\Delta t}\right)\right] \\ &= \bar{g}_x(t_k)\left[1-\frac{\sqrt{\Delta t}}{\sqrt{t_k+\Delta t-t_b}}\right] + \bar{f}_{x\Delta t}\frac{\sqrt{\Delta t}}{\sqrt{t_k+\Delta t-t_b}} \end{aligned} \tag{12.5-60}$$

so that once the advanced time vapor temperatures are computed, the value of $\bar{g}_x$ for the next time step can be calculated.

With a means now available for obtaining $\bar{g}_x(t_x)$, the expression for $\left.\frac{\partial T_{\ell_x}}{\alpha\xi}\right|_{\xi=0}$ in Eq. 12.5-47 can be considered fully determined, and Eq. 12.5-47 can be written

$$\left.\frac{\partial T_{\ell_x}(t_k+\varepsilon)}{\partial\xi}\right|_{\xi=0}=\frac{1}{\sqrt{\pi}}\left[2\bar{g}_x(t_k)\left(\sqrt{t_k+\varepsilon-t_b}-\sqrt{\varepsilon}\right)+2\bar{f}_{x\Delta t}\sqrt{\varepsilon}\right] \tag{12.5-61}$$

The time average of Eq. 12.5-61 is then

$$\begin{aligned}\left.\overline{\frac{\partial T_{\ell_x}}{\partial\xi}}\right|_{\xi=0}&=\frac{2}{\sqrt{\pi}}\frac{1}{\Delta t}\int_0^{\Delta t}d\varepsilon\ \left[\bar{g}_x(t_k)\left(\sqrt{t_k+\varepsilon-t_b}-\sqrt{\varepsilon}\right)+\bar{f}_{x\Delta t}\sqrt{\varepsilon}\right]\\&=\frac{4}{3\sqrt{\pi}}\frac{1}{\Delta t}\left[\bar{g}_x(t_k)\left(t_k+\Delta t-t_b\right)^{3/2}-\left(t_k-t_b\right)^{3/2}-\left(\Delta t\right)^{3/2}\right.\\&\quad\left.+\bar{f}_{x\Delta t}\left(\Delta t\right)^{3/2}\right]\end{aligned} \tag{12.5-62}$$

Thus, the interface heat flow I_{ix} is, from Eq. 12.5033 and substituting for $\bar{f}_{x\Delta t}$

$$\begin{aligned}I_{ix}=k_\ell A_{cx}\frac{4}{3\sqrt{\pi}}\ \frac{1}{\Delta t}&\left[\bar{g}_x(t)\left(\left(t+\Delta t-t_b\right)^{3/2}-\left(t-t_b\right)^{3/2}-\left(\Delta t\right)^{3/2}\right)\right.\\&+\left(\Delta t\right)^{3/2}\left(\frac{1}{2}\left[\ Q_{OX}(t)+Q_{Ox}(t+\Delta t)\right]\frac{\sqrt{\alpha}}{k_\ell}\right.\\&\left.\left.-\frac{1}{\sqrt{\alpha}}\ \frac{T(t+\Delta t)-T(t)}{\Delta t}\right]\right)\end{aligned} \tag{12.5-63}$$

which, substituting the definition of Q_{0x}, is

$$
\begin{aligned}
I_{ix} = \frac{k_\ell}{\sqrt{\pi}} A_{cx} \frac{4}{3} \Bigg[\; & \bar{g}_x(t) \left(\frac{\left(t+\Delta t-t_b\right)^{3/2} - \left(t-t_b\right)^{3/2}}{\Delta t} - \sqrt{\Delta t} \right) \\
& + \sqrt{\Delta t} \Bigg(\frac{\gamma}{2} \left[\frac{T_{ex}(t) + T_{ex}(t+\Delta t) - T(t) - T(t+\Delta t)}{R_{ecx}} \right] \\
& + \gamma_2 \frac{T_{sx}(t) + T_{sx}(t+\Delta t) - T(t) - T(t+\Delta t)}{R_{scx}} \Bigg] \frac{\sqrt{\alpha}}{k_\ell} \\
& - \frac{1}{\sqrt{\alpha}} \frac{T(t+\Delta t) - T(t)}{\Delta t} \Bigg] \Bigg) \\
= \frac{4}{3} \frac{k_\ell}{\sqrt{\pi}} & A_{cx} \bar{g}_x(t) \left(\frac{\left(t+\Delta t-t_b\right)^{3/2} - \left(t-t_b\right)^{3/2}}{\Delta t} - \sqrt{\Delta t} \right) \\
& + \frac{2}{3} \frac{\sqrt{\alpha}}{\sqrt{\pi}} \gamma \sqrt{\Delta t} A_{cx} \left[\frac{T_{ex}(t) + T_{ex}(t+\Delta t) - 2T(t)}{R_{ecx}} \right. \\
& \left. + \gamma_2 \frac{T_{sx}(t) + T_{sx}(t+\Delta t) - 2T(t)}{R_{scx}} \right] \\
& - \Delta T \left[\frac{2}{3} \frac{\sqrt{\alpha}}{\sqrt{\pi}} A_{cx} \gamma \sqrt{\Delta t} \left(\frac{1}{R_{ecx}} + \frac{\gamma_2}{R_{scx}} \right) + \frac{4}{3} \frac{k_\ell}{\sqrt{\pi}} \frac{A_{ex}}{\sqrt{\alpha}} \frac{1}{\sqrt{\Delta t}} \right]
\end{aligned}
\tag{12.5-64}
$$

where $T(t + \Delta t) = T(t) + \Delta T$. Using this expression in Eq. 12.5-32 for E_i, the total heat flow through the liquid-vapor interfaces, gives

$$
E_i = \left(I_{i0} + I_{i1} \Delta T\right) \Delta t \tag{12.5-65}
$$

where

$$
\begin{aligned}
I_{i0} = \frac{k_\ell}{\sqrt{\pi}} \Bigg\{ \sum_{x=u,\ell} & A_{cx} \left[\frac{2}{3} \frac{\sqrt{\alpha}}{k_\ell} \gamma \sqrt{\Delta t} \left[\frac{T_{ex}(t) + T_{ex}(t+\Delta t) - 2T(t)}{R_{ecx}} \right. \right. \\
& \left. + \gamma_2 \frac{T_{sx}(t) + T_{sx}(t+\Delta t) - 2T(t)}{R_{scx}} \right] \\
& \left. + \frac{4}{3} \bar{g}_x(t) \left[\frac{\left(t+\Delta t-t_b\right)^{3/2} - \left(t-t_b\right)^{3/2} - \sqrt{\Delta t}}{\Delta t} \right] \right] \Bigg\}
\end{aligned}
\tag{12.5-66}
$$

and

$$I_{ix} = \frac{k_\ell}{\sqrt{\pi}} \frac{4}{3} \sqrt{\Delta t} \left\{ - \frac{1}{\Delta t \sqrt{\alpha}} \left(A_{cu} + A_{c\ell} \right) - \frac{\gamma}{2k_\ell} \sqrt{\alpha} \left[\sum_{x=u,\ell} A_{cx} \left(\frac{1}{R_{ecx}} + \frac{\gamma_2}{R_{scx}} \right) \right] \right\}. \quad (12.5\text{-}67)$$

This completes the task of expressing the heat flow through the interface as a linear function of the advanced time vapor temperatures.

12.5.3 Change in Vapor Energy

The heat flow into the bubble control volume is used both to produce new vapor and to raise the temperature of already existing vapor. During a time interval Δt, the vapor temperature goes from T to $T + \Delta T$, the pressure goes from p_v to $p_v + \Delta p$, the density goes from ρ_v to $\rho_v + \Delta\rho_v$, the bubble volume goes from V_v to $V_v + \Delta V$, and the vapor energy changes by ΔE. The changes Δp and $\Delta\rho_v$ are related to ΔT by the requirement that saturation conditions prevail in the vapor.

Two processes contribute to the energy change ΔE. One is the heating of the quantity of vapor present at the beginning of the time step from temperature T to temperature $T + \Delta T$. The other is the vaporizing of some of the liquid film to form additional vapor, giving a total vapor mass of $(\rho + \Delta\rho_v)$ $(V_v + \Delta V)$ at the end of the time step. However, it is not straightforward to formulate an expression for the energy change by directly considering the heating of the vapor (because the volume and density changes which take place during the heating) and the vaporization of some of the liquid film (because the amount of film vaporized is unknown). Therefore a thermodynamically equivalent path is followed which does allow straightforward expression of the energy change. This path can be described in the following three steps:

Step 1: Condense the vapor in the bubble at time t to liquid at constant pressure and temperature:

$$\Delta E(1) = -(\rho_v V_v)\lambda \quad (12.5\text{-}68)$$

where λ is the heat of vaporization at time t and

$$V_v = \int A_c dz$$

$$= A_c(JST)\Delta z'(JST) + \sum_{Jc=JST+1}^{JEND-1} A_c(JC)\Delta z(JC) + \quad (12.5\text{-}69)$$

$$A_c(JEND)\Delta z'(JEND)$$

Refer to Fig. 12.2-1 for the notation.

Step 2: Heat the liquid from Step 1 to $T + \Delta T$:

$$\Delta E(2) = C_\ell (\rho_v V_v) \Delta T \tag{12.5-70}$$

where C_ℓ is the heat capacity of the liquid and the compressibility of the liquid is neglected.

Step 3: Vaporize the liquid form Step 2 plus enough liquid from the film to fill the volume $V_v + \Delta V$:

$$\Delta E(3) = (\rho_v + \Delta\rho_v)(V_v + \Delta V)(\lambda + \Delta\lambda). \tag{12.5-71}$$

If the vapor undergoes a net energy loss rather than a gain, the liquid in Step 2 shows a temperature drop of ΔT and part of the vapor in Step 3 condenses onto the cladding and/or structure.

The energy change is then

$$\Delta E = \Delta E(1) + \Delta E(2) + \Delta E(3) \tag{12.5-72}$$

or, neglecting second-order terms,

$$\Delta E = \rho_v V_v \Delta\lambda + \rho_v \lambda \Delta V + \lambda V_v \Delta\rho_v + \rho_v V_v C_\ell \Delta T. \tag{12.5-73}$$

Now, the energy change must be expressed as a linear function of the change in vapor temperature ΔT. To do this, first look at the volume change ΔV. This term is currently modeled as the change in volume at the liquid-vapor interfaces due to interface motion, neglecting any volume change due to flow area changes caused by cladding motion during the time step. Accordingly, using earlier notation, ΔV for bubble K is just

$$\Delta V = \left[A_{c\ell}(t+\Delta t)\, z_i(1, t+\Delta t, K) - A_{c\ell}(t)\, z_i(1, t, K)\right] + \left[A_{cu}(t+\Delta t)\, z_i(2, t+\Delta t, K\right. \\ \left. - A_{cu}(t)\, z_i(2, t, K)\right] \tag{12.5-74}$$

The flow area A_c at the interfaces is written as a time-dependent function to account for the possibility that an interface might cross from one mesh segment to another during the time step. Since the flow area can vary from mesh segment to mesh segment, this might result in a change in interface flow area from t to $t+\Delta t$.

To simplify the expression for ΔV, define an average interface area at the lower interface as

$$\bar{A}_c(K,1) = \frac{\int_{z_i(1,t,K)}^{z_i(1,t+\Delta t,K)} A_c(z)\,dz}{z_i(1,t+\Delta t,K) - z_i(1,t,K)} \tag{12.5-75}$$

A similar definition can be made at the upper interface. The ΔV becomes

$$\begin{aligned}\Delta V = {} & \bar{A}_c(K,2)\left[z_i(2,t+\Delta t,K) - z_i(2,t,K)\right] \\ & - \bar{A}_c(K,1)\left[z_i(1,t,+\Delta t,K) - z_i(1,t,K)\right]\end{aligned} \tag{12.5-76}$$

The advanced time interface positions $z_i(L,t+\Delta t,K)$ can be expressed in terms of the changes in pressure at the interfaces via Eq. 12.5-22 to give

$$\begin{aligned}\Delta V &= \Delta V_0 + \bar{A}_c(K,2)\Delta z'(K,2) - \bar{A}_c(K,1)\Delta z'(K,1) \\ &= \Delta V_0 + \bar{A}_c(K,2)\frac{dz_i(K,2)}{dp}\left(\Delta p_K - \Delta p_{K+1}\right) \\ &\quad - \bar{A}_c(K,1)\frac{dz_i(K,1)}{dp}\left(\Delta p_{K-1} - \Delta p_K\right)\end{aligned} \tag{12.5-77}$$

where

$$\Delta V_0 = \bar{A}_c(K,2)\Delta z_0(K,2) - \bar{A}_c(K,1)\Delta z_0(K,1) \tag{12.5-78}$$

Using Eq. 12.5-77 in Eq. 12.5-73 for the energy change ΔE produces an expression for ΔE in terms of the changes in λ, ρ_v, and p_v as well as T. To reduce this to a linear equation in ΔT, the changes in λ, ρ_v, and p_v are approximated by

$$\Delta\lambda = \Delta T\frac{d\lambda}{dT} \tag{12.5-79a}$$

$$\Delta\rho_v = \Delta T\frac{d\rho_v}{dT} \tag{12.5-79b}$$

and

$$\Delta p = \Delta T\frac{dp_v}{dT} \tag{12.5-79c}$$

where the temperature derivatives are evaluated along the saturation curve. Incorporating Eqs. 12.5-79 into Eq. 12.5-73 results in a formulation for the change in energy within the control volume which is a linear function of ΔT:

$$\Delta E = \Delta E_0 + \Delta E_1 \Delta T(K) + \Delta E_2 \Delta T(K+1) + \Delta E_3 \Delta T(K-1) \tag{12.5-80}$$

where

$$\Delta E_0 = \lambda \rho_v \Delta V_0 \tag{12.5-81}$$

$$\Delta E_1 = \lambda \left\{ \rho_v \frac{dp(K)}{dT} \left[\bar{A}_c(K,1) \frac{dz_i(K,1)}{dp} + \bar{A}_c(K,2) \frac{dz_i(K,2)}{dp} \right] + (V_v + \Delta V_0) \frac{d\rho_v}{dT} + \rho_v \Delta V_0 \frac{d\lambda}{dT} + \rho_v V_v C_\ell \right) \tag{12.5-82}$$

$$\Delta E_2 = 0 \text{ if } K = K_{vn} = \text{last bubble in channel} \tag{12.5-83a}$$

and otherwise,

$$\Delta E_2 = -\rho_v \lambda \bar{A}_c(K,2) \frac{dz_i(K,2)}{dp} \frac{dp(K+1)}{dT}; \tag{12.5-83b}$$

$$\Delta E_3 = 0 \; if \; K = 1 \tag{12.5-84a}$$

and otherwise,

$$\Delta E_2 = -\rho_v \lambda \bar{A}_c(K,1) \frac{dz_i(K,1)}{dp} \frac{dp(K-1)}{dT} \tag{12.5-84b}$$

12.5.4 Energy Balance

As discussed at the beginning of this section, an energy balance exists between the energy transferred to the control volume and the change in energy within the volume. The change in energy is given by Eq. 12.5-80, derived in the previous subsection. The energy transferred to the volume, E_t, is the sum of the energy flow from the cladding and structure, E_{es}, and the energy flow through the liquid-vapor interfaces, E_i; this was expressed in Eq. 12.5-3. Substituting Eqs. 12.5-31 and 12.5-65, the expressions for E_{es} and E_i derived in Subsections 12.5.1 and 12.5.2, respectively, into Eq. 12.5-3 gives the total energy transferred to the control volume as

$$E_t = E_{t0} + E_{t1}\,\Delta T(K) + E_{t2}\Delta T(K+1) + E_{t3}\Delta T(K-1) \tag{12.5-85}$$

where

$$E_{t0} = \Delta t\left[\frac{Q_{es}(K,t) + I_{e1}(K)}{2} + I_{i0}\right] \tag{12.5-86}$$

$$E_{t1} = \Delta t\left[\frac{I_{e2}(K)}{2} + I_{i1} + \frac{I_{e3}(K)}{2}\frac{dz_i(K,2)}{dp}\frac{dp(K)}{dT} - \frac{I_{e4}(K)}{2}\frac{dz_i(K,1)}{dp}\frac{dp(K)}{dT}\right] \tag{12.5-87}$$

$$E_{t2} = 0 \text{ if } K = K_{vn} \tag{12.5-88a}$$

and otherwise,

$$E_{t2} = -\frac{\Delta t}{2} I_{e3}(K)\frac{dz_i(K,2)}{dp}\frac{dp(K+1)}{dT} \tag{12.5-88b}$$

$$E_{t3} = 0 \text{ if } K = 1 \tag{12.5-89a}$$

and otherwise,

$$E_{t3} = \frac{\Delta t}{2} I_{e4}(K)\frac{dz_i(K,1)}{dp}\frac{dp(K-1)}{dT}. \tag{12.5-89b}$$

The overall energy balance is then

$$E_t = \Delta E \tag{12.5-90}$$

If the expression for E_t from Eq. 12.5-85 and that for ΔE from Eq. 12.5-80 are inserted into Eq. 12.5-90, the result is a linear equation in terms of the changes in the vapor temperatures of bubbles K-1, K, and K+1:

$$C_4(K) + C_1(K)\Delta T(K) + C_2(K)\Delta T(K+1) + C_3(K)\Delta T(K-1) = 0 \tag{12.5-91}$$

where

$$C_4(K) = \Delta E_0(K) - E_{t0}(K) \tag{12.5-92}$$

$$C_1(K) = \Delta E_1(K) - E_{t1}(K) \tag{12.5-93}$$

$$C_2(K) = \Delta E_2(K) - E_{t2}(K) \tag{12.5-94}$$

$$C_3(K) = \Delta E_3(K) - E_{t3}(K). \tag{12.5-95}$$

12.5.5 Vapor Temperatures

Equation 12.5-91 can be written for each uniform pressure bubble in the channel. The equations are then solved for the changes in vapor temperature for each bubble as follows. First, each bubble in the channel is checked in order from the bottom of the channel to the top to determine whether it is a uniform-pressure or variable-pressure bubble. This determines how the uniform-pressure bubbles are distributed throughout the channel and allows the temperature calculation to be carried out simultaneously for all bubbles that are in any one group of bubbles (e.g., if the lowest bubble in the channel is a large, pressure-gradient bubble with four small constant pressure bubbles above it, the temperatures in the four small bubbles will be computed simultaneously). In general, if a series of N bubbles of uniform vapor pressure extends from bubble K_b to bubble K_t, then the temperatures in the N bubbles are calculated by solving a set of linear equations consisting of Eq. 12.5-91 written for each of the N bubbles. These N equations will be written in terms of N unknowns if $\Delta T(K_b\text{-}1)$ and $\Delta T(K_t\text{+}1)$ are set to extrapolated values (or to zero, if K_b=1 or $K_t = K_{vN}$) and the coefficient C_4 is modified to be

$$C_4(K_b) \rightarrow C_4(K_b) + C_3(K_b)\Delta T(K_b - 1), \text{ if } K_b > 1 \tag{12.5-96}$$

$$C_4(K_t) \rightarrow C_4(K_t) + C_2(K_t)\Delta T(K_t + 1), \text{ if } K_t < K_{vN} \tag{12.5-97}$$

The N equations are then solved using Gaussian elimination. After the bubble temperatures are obtained, the saturation conditions are used to obtain the bubble pressures.

12.6 Vapor Pressure gradient Model: Large Vapor Bubbles

As mentioned above, whenever a bubble grows to a length greater than a user-specified value (usually 5-50 cm), the vapor bubble calculation is switched from the uniform-vapor-pressure model to a vapor-pressure-gradient model. Saturation conditions are assumed in this model, so the vapor energy equation can be combined with the mass continuity equation. The vapor continuity and momentum equations are

solved simultaneously for each node in a bubble using a fully implicit finite differencing scheme.

The equations described in this section are only for the vapor. Any liquid in a bubble region is assumed to be a film on the cladding and structure, and this film is treated separately, as described at the beginning of Section 12.1. The vapor calculation is influenced by the liquid film in only two ways: heat flow through the film provides the vapor source for the vapor calculations; and if a two-phase friction factor multiplier for the friction between the vapor and the film is used, then the film thickness determines the value of this multiplier.

12.6.1 Continuity and Momentum Equations

The vapor continuity equation can be written as

$$\frac{\partial W}{\partial z} + \frac{\partial \left(\rho_v A_c\right)}{\partial t} = \frac{Q}{\lambda} A_c , \tag{12.6-1}$$

while the vapor momentum equation is given by

$$\frac{\partial p}{\partial z} = -\frac{1}{A_c}\frac{\partial}{\partial z}\frac{W^2}{\rho_v A_c} - \frac{f_v W|W|}{2\rho_v D_h A_c^2} + F_c - \frac{1}{A_c}\frac{\partial W}{\partial t} - \frac{W|W|}{2\rho_v A_c^2}\frac{\partial k_{or}}{\partial z}. \tag{12.6-2}$$

The symbols used in Eqs. 12.6-1 and 12.6-2 are defined as follows:

W = vapor mass flow rate

z = axial height

ρ_v = sodium vapor density

A_c = coolant flow area

t = time

Q = heat flow rate per unit volume

λ = heat of vaporization

p = pressure

f_v = friction factor

D_h = hydraulic diameter

F_c = condensation momentum loss term

k_{or} = orifice pressure drop term

Note that, because the flow area A_c is included in the mass and momentum equations as a function of both space and time, the model is able to treat problems involving variable flow areas.

The heat flow rate per unit volume is given by

$$Q = \gamma \left[\frac{T_e - T}{R_{ec}} + \gamma_2 \frac{T_s - T}{R_{sc}} \right] \tag{12.6-3}$$

where

λ = ratio of cladding surface area to coolant volume

T_e = cladding temperature

T_s = structure temperature

T = vapor temperature

R_{ec} = thermal resistance between the cladding and the vapor

R_{sc} = thermal resistance between the structure and the vapor

γ_2 = ratio of structure surface are to cladding surface area

The thermal resistances R_{ec} and R_{sc} account for the resistance to heat flow of the cladding, liquid film, and vapor and are computed according to the expressions discussed in Subsection 12.5.1.

The expression for the heat flow rate Q can be rewritten as the sum of the heat flow rate through the cladding, Q_e, and the heat flow rate through the structure, Q_s, where

$$Q_e = \gamma \frac{T_e - T}{R_{ec}} \tag{12.6-4}$$

and

$$Q_s = \gamma\gamma_2 \frac{T_s - T}{R_{sc}}. \tag{12.6-5}$$

These two quantities are used to compute the condensation momentum loss term F_c. This term accounts for momentum lost from the system when flowing sodium vapor condenses on cladding or structure that is colder than the vapor. Only a momentum loss term is included, since it is assumed that the system does not gain momentum when vaporization occurs from cladding or structure that is hotter than the sodium film. The condensation momentum loss is simply the product of the rate of mass

condensing per unit volume, $\frac{Q}{\lambda}$, times the average velocity, $\frac{W}{2\rho_v A_c}$. Splitting the condensation momentum loss term into separate contributions from the cladding and structure then gives.

$$F_c = F_{ce} + F_{cs}, \tag{12.6-6}$$

where

$$F_{ce} = \begin{cases} 0, Q_e \geq 0, \\ \dfrac{Q_e W}{2\rho_v A_c \lambda}, Q_e < 0 \end{cases} \tag{12.6-7a, b}$$

and

$$F_{cs} = \begin{cases} 0, Q_s \geq 0, \\ \dfrac{Q_s W}{2\rho_v A_c \lambda}, Q_s < 0. \end{cases} \tag{12.6-8a, b}$$

These definitions reflect the assumption that momentum is lost when condensation of vapor occurs (Q_e, Q_s negative) but that no momentum change occurs when liquid is vaporized (Q_e, Q_s positive).

The friction factor, f_v is expressed as

$$f_v + A_{fr}\left(\frac{D_h|W|}{\mu A_c}\right)^{b_{fr}} f_{tp}, \tag{12.6-9}$$

where μ is the vapor viscosity and A_{fr} and b are input constants. The quantity in parentheses, $D_h|W|/(\mu A_c)$, is just the Reynolds number of the sodium vapor. The two-phase friction factor multiplier, f_{tp}, is based on a correlation by Wallis [12-10]:

$$f_{tp} = 1 + 300 f_{2\phi}\left(w_{fe} + \gamma_2 w_{fs}\right)/\left[(1+\gamma_2)D_h\right] \tag{12.6-10}$$

where $f_{2\phi}$ is set to 1.0 when the two-phase multiplier is used and is set to 0 by the user if a smooth tube friction factor is described.

Two approximations are made to Eqs. 12.6-1 and 12.6-2 before finite differencing. First, in the continuity equation, the term

$$\frac{\partial(\rho_v A_c)}{\partial t} = \rho_v \frac{\partial A_c}{\partial t} + A_c \frac{\partial \rho_v}{\partial t} \tag{12.6-11}$$

is taken to be

$$\frac{\partial(\rho_v A_c)}{\partial t} = A_c \frac{\partial \rho_v}{\partial t} \tag{12.6-12}$$

So that A_c is assumed constant in time (but not space) over the time step for purposes fo solving the mass and momentum equations for the vapor pressures and mass flow rates. This assumption is also made with the variables D_h, γ, and γ_2. This simplification is a reasonable one, since one of these four quantities changes rapidly with time. Second, in the momentum equations, the momentum convection term can be expanded as

$$\frac{\partial}{\partial z}\left(\frac{W^2}{\rho_v A_c}\right) = \frac{1}{A_c}\frac{\partial}{\partial z}\left(\frac{W^2}{\rho_v}\right) + \frac{W^2}{\rho_v}\frac{\partial}{\partial z}\left(\frac{1}{A_c}\right). \tag{12.6-13}$$

Any changes in area over a spatial node are incorporated into the orifice term, and so $\frac{W^2}{\rho_v}\frac{\partial}{\partial z}\left(\frac{1}{A_c}\right)$ is included in the $\frac{\partial k_{or}}{\partial z}$ term. Therefore,

$$\frac{\partial}{\partial z}\left(\frac{W^2}{\rho_v A_c}\right) = \frac{1}{A_c}\frac{\partial}{\partial z}\left(\frac{W^2}{\rho_v}\right) \tag{12.6-14}$$

so A_c appears piecewise constant in space. This is also true for D_h, γ, and γ_2.

Therefore, the continuity and momentum equations to be differenced are

$$\frac{\partial W}{\partial z} + A_c \frac{\partial \rho_v}{\partial t} = \frac{Q}{\lambda} A_c \tag{12.6-15}$$

and

$$\frac{\partial p}{\partial z} = -\frac{1}{A_c^2}\frac{\partial}{\partial z}\left(\frac{W^2}{\rho_v}\right) - A_{fr}\frac{W|W|^{1+b_{fr}}}{2\rho_v D_h^{1-b_{fr}} A_c^{2+b_{fr}}} + F_c - \frac{1}{A_c}\frac{\partial W}{\partial t} - \frac{W|W|}{2\rho_v A_c^2}\frac{\partial k_{or}}{\partial z} \tag{12.6-16}$$

12.6.2 Finite Differencing

The mass and momentum equations must now be reduced to algebraic equations that can be coded into SASSYS-1. This is accomplished in three steps: (1) the equations are discretized using finite differences, (2) the advanced time terms are linearized, and

(3) saturation conditions are imposed to limit the independent variables to the change in mass flow rate and the change in pressure. The details of these three steps are presented below. The result is the set of algebraic equations 12.6-45, 12.6-79, 12.6-87 (discretized form of the continuity equation at an interior node, lower interface, and upper interface of a bubble, respectively), 12.6-128, 12.6-143, and 12.6-149 (discretized form of the momentum equation in the interior, the lower interface, and the upper interface). These equations are then solved according to the procedure discussed in Section 12.6.3. As indicated in Fig. 12.6-1, some of the variables in the mass and momentum equations are calculated at node boundaries, whereas others are calculated at node mid-points. In general, midpoint quantities are used as if they were constant over the node. The quantities defined at node boundaries are z, T, p, W, ρ_v, μ, and the velocity V. At liquid-vapor interfaces, these quantities are defined at the interface, and the vapor velocity is set to the value of the interface velocity.

Midpoint quantities include T_e, T_s, R_{ec}, A_c, D_h, γ, γ_2, k_{or}, γ, Q, F_e, and the spatially averaged coolant temperature $\overline{T}$. With all variables, a subscript 1 indicates that the variable is evaluated at the beginning of the time step; a subscript 2 means the variable is taken to be at the end of the time step.

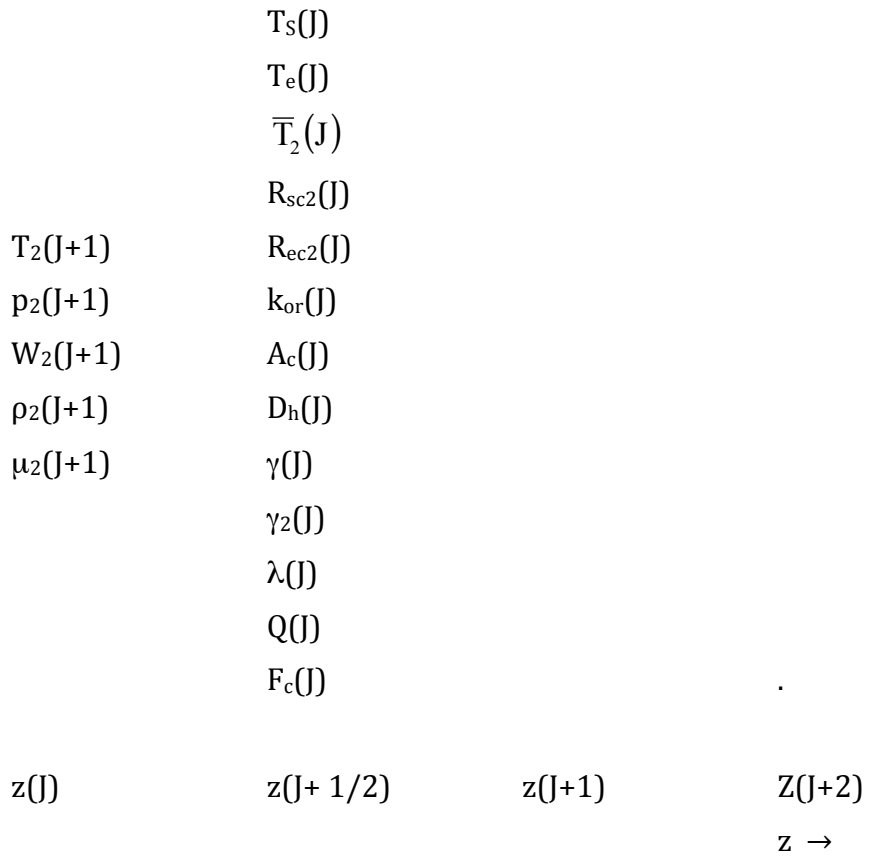

Figure 12.6-1. SASSYS-1 Voiding Model Axial Coolant Mesh Variable Placement

12.6.2.1 Finite Differencing of the Continuity Equation for a Mesh Segment Contained Entirely in One Bubble

This section gives a detailed explanation of how the continuity equation is expressed in finite difference form. The extra factors required to model bubble-liquid interfaces correctly are not included here; they will be discussed in Section 12.6.2.2. Therefore, the equations to be developed in this section apply as they stand only to axial mesh segments which are entirely contained within the bubble.

12.6.2.1.1 Differencing of the Continuity Equation

The terms making up the continuity equation are differenced as follows:

$$\frac{\partial W}{\partial z}\Big|_{J+1/2} = + \frac{W_2(J+1) - W_2(J)}{z(J+1) - z(J)} \tag{12.6-17}$$

and

$$A_c \frac{\partial \rho_v}{\partial t}\Big|_{J+1/2} = A_c(J) \frac{\rho_2(J) - \rho_1(J) + \rho_2(J+1) - \rho_1(J+1)}{2\Delta t}. \tag{12.6-18}$$

These differencing schemes are illustrated in Fig. 12.6-2. Also,

$$\begin{aligned} Q_2(J) &= \gamma(J)\left[\frac{T_{e_2}(J) - \overline{T}_2(J)}{R_{ec_2}(J)} + \gamma_2(J)\frac{T_{s_2}(J) - \overline{T}_2(J)}{R_{sc_2}(J)}\right] \\ &= Q_{e_2}(J) + Q_{s_2}(J) \end{aligned} \tag{12.6-19}$$

Therefore, the differenced continuity equation becomes

$$\begin{aligned} &\frac{W_2(J+1) - W_2(J)}{z(J+1) - z(J)} + A_c(J)\frac{\rho_2(J) - \rho_1(J) + \rho_2(J+1) - \rho_1(J+1)}{2\Delta t} \\ &\qquad = A_c(J)\frac{Q_2(J)}{\lambda_2(J)} \end{aligned} \tag{12.6-20}$$

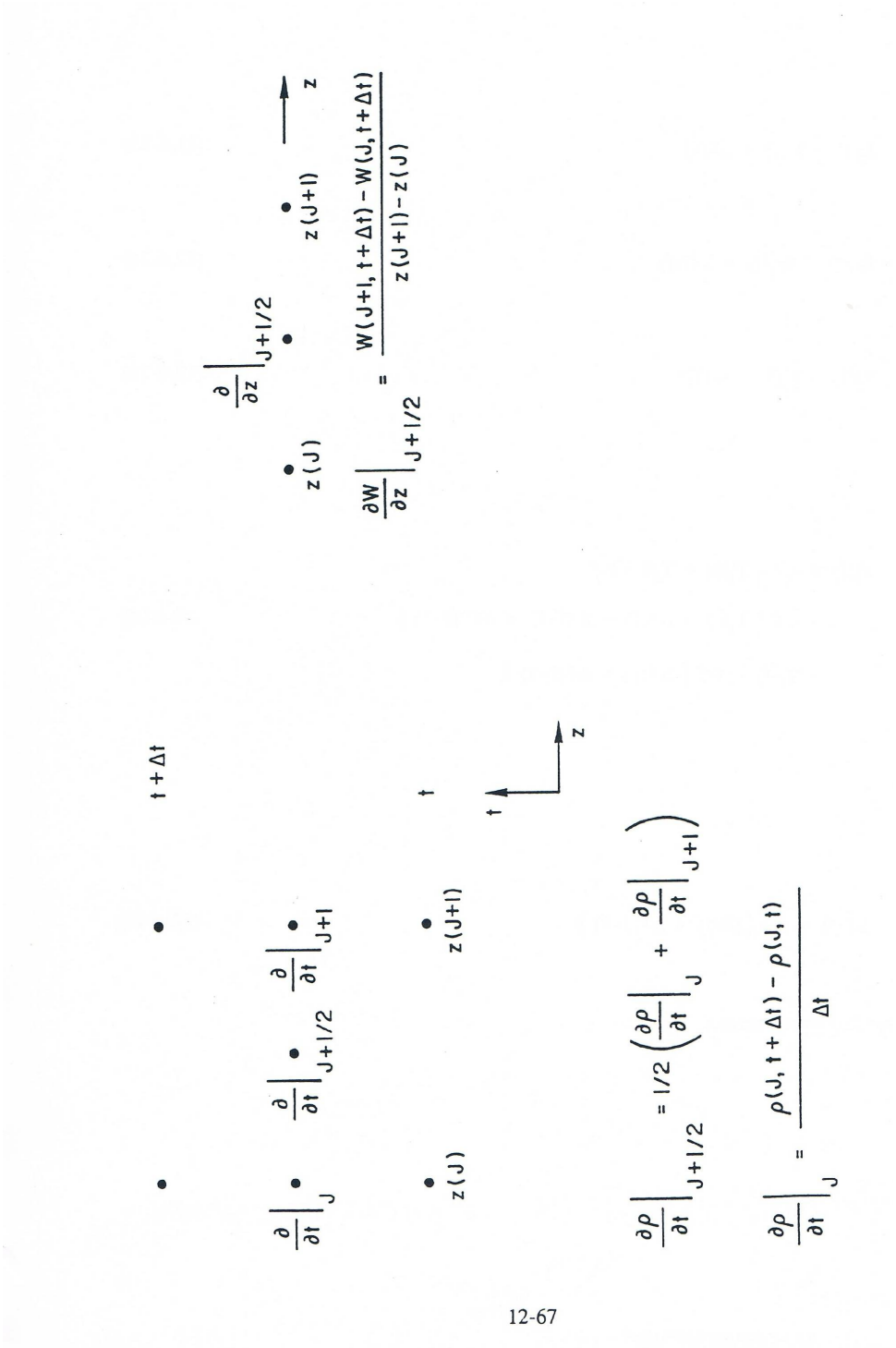

Figure 12.6-2. Evaluation of Derivatives at an Interior Node in the SASSYS-1 Voiding Model

12.6.2.1.2 Linearization of Advanced Time Terms

Equation 12.6-20 can be linearized by expressing the advanced time terms in the form

$$x_2(J) = x_1(J) + \Delta z(J) \tag{12.6-21}$$

where *x* is any quantity. This produces

$$\rho_2(J) = \rho_1(J) + \Delta\rho(J) \tag{12.6-22}$$

$$\lambda_2(J) = \lambda_1(J) + \Delta\lambda(J) \tag{12.6-23}$$

$$W_2(J) = W_1(J) + \Delta W(J) \tag{12.6-24}$$

$$T_2(J) = T_1(J) + \Delta T(J) \tag{12.6-25}$$

Since

$$\overline{T}_2(J) = \frac{1}{2}\left(T_2(J) + T_2(J+1)\right)$$

$$= \frac{1}{2}\left(T_1(J) + \Delta T(J) + T_1(J+1) + \Delta T(J+1)\right) \tag{12.6-26}$$

$$= \overline{T}_1(J) + \frac{1}{2}\left(\Delta T(J) + \Delta T(J+1)\right)$$

then

$$\Delta\overline{T}(J) = 1/2\left(\Delta T(J) + \Delta T(J+1)\right) \tag{12.6-27}$$

The heat flux then becomes

$$Q_2(J) = \gamma(J)\left[\frac{T_{e_2}(J) - \bar{T}_1(J) - \Delta\bar{T}(J)}{R_{ec_2}(J)} + \gamma_2(J)\frac{T_{s_2}(J) - \bar{T}_1(J) - \Delta\bar{T}(J)}{R_{sc_2}(J)}\right]$$
$$= \gamma(J)\left[\frac{T_{e_2}(J) - \bar{T}_1(J)}{R_{ec_2}(J)} + \gamma_2(J)\frac{T_{s_2}(J) - \bar{T}_1(J)}{R_{sc_2}(J)}\right. \tag{12.6-28}$$
$$\left. - \frac{(\Delta T(J) + \Delta T(J+1))}{2}\left[\frac{1}{R_{ec_2}(J)} + \frac{\gamma_2(J)}{R_{sc_2}(J)}\right]\right]$$

The heat flux expression can be written in a more compact form by defining the variable $Q_o(J)$

$$Q_o(J) = \gamma(J)\left[\frac{T_{e_2}(J) - \bar{T}(J)}{R_{ec_2}(J)} + \gamma_2(J)\frac{T_{s_2}(J) - \bar{T}_1(J)}{R_{sc_2}(J)}\right] \tag{12.6-29}$$

The derivative with respect to vapor temperature of Q_o is then

$$\frac{dQ_o}{dT_J} = -\gamma(J)\left[\frac{1}{R_{ec_2}(J)} + \frac{\gamma_2(J)}{R_{sc_2}(J)}\right] \tag{12.6-30}$$

These can be substituted into the above equation for $Q_2(J)$ to give

$$Q_2(J) = Q_o(J) + \frac{1}{2}\frac{dQ_o}{dT_J}(\Delta T(J) + \Delta T(J+1)). \tag{12.6-31}$$

Substituting Eqs. 12.6-22 through 12.6-25 and 12.6-31 for the advanced time terms in the differenced continuity equation, Eq. 12.6-20 gives

$$\frac{W_1(J+1) - W_1(J) + \Delta W(J+1) - \Delta W(J)}{z(J+1) - z(J)} + A_c(J)\frac{\Delta\rho(J) + \Delta\rho(J+1)}{2\Delta t}$$
$$= \frac{A_c(J)}{\lambda_1(J) + \Delta\lambda(J)}\left(Q_o(J) + 1/2\frac{dQ_o}{dT_J}(\Delta T(J) + \Delta T(J+1))\right) \tag{12.6-32}$$

If $\Delta\lambda(J) << \lambda_1(J)$.

$$\frac{1}{\lambda_1(J) + \Delta\lambda(J)} \approx \frac{1}{\lambda_1(J)}\left[1 - \frac{\Delta\lambda(J)}{\lambda_1(J)}\right] \tag{12.6-33}$$

which changes Eq. 12.6-32 to

$$\frac{W_1(J+1)-W_1(J)+\Delta W(J+1)-\Delta W(J)}{z(J+1)-z(J)}+A_c(J)\frac{\Delta\rho(J)+\Delta\rho(J+1)}{2\Delta t}$$
$$=A_c(J)\frac{Q_o(J)}{\lambda_1(J)}\left(1+\frac{\Delta T(J)+\Delta T(J+1)}{2Q_o(J)}\frac{dQ_o}{dT_J}\right)\left(1-\frac{\Delta\lambda(J)}{\lambda_1(J)}\right) \quad (12.6\text{-}34)$$

Eliminating second-order terms gives the linearized differenced continuity equation

$$\frac{W_1(J+1)-W_1(J)+\Delta W(J+1)-\Delta W(J)}{z(J+1)-z(J)}+A_c(J)\frac{\Delta\rho(J)+\Delta\rho(J+1)}{2\Delta t}$$
$$=A_c(J)\frac{Q_o(J)}{\lambda_1(J)}\left(1+\frac{\Delta T(J)+\Delta T(J+1)}{2Q_o(J)}\frac{dQ_o}{dT_J}-\frac{\Delta\lambda(J)}{\lambda_1(J)}\right) \quad (12.6\text{-}35)$$

12.6.2.1.3 Utilization of Saturation Conditions to Limit the Independent Variables to ΔW and Δp

Since saturation conditions are assumed, ρ, T, and λ are all functions of p only. Therefore, the difference terms can be expressed in terms of Δp as follows:

$$\Delta T(J)=\Delta p(J)\frac{dT}{dp_J} \quad (12.6\text{-}36)$$

$$\Delta\rho(J)=\Delta p(J)\frac{d\rho}{dp_J} \quad (12.6\text{-}37)$$

$$\Delta\lambda(J)=1/2\left(\Delta p(J)+\Delta p(J+1)\right)\frac{d\lambda}{dp_J} \quad (12.6\text{-}38)$$

with $\Delta p(J) = p_2(J) - p_1(J)$. All derivatives are evaluated at the start of the time step. When Eqs. 12.6-36 through 12.6-38 are inserted into Eq. 12.6-35 the result is a differenced continuity equation which is linear in ΔW and Δp:

$$\frac{W_1(J+1)-W_1(J)+\Delta W(J+1)-\Delta W(J)}{z(J+1)-z(J)}+A_c(J)\frac{1}{2\Delta t}\left(\Delta p(J)\frac{d\rho}{dp_J}+\Delta p(J+1)\frac{d\rho}{dp}(J+1)\right)$$
$$=A_c(J)\frac{Q_o(J)}{\lambda_1(J)}\left[1+\left(\Delta p(J)\frac{dT}{dp_J}+\Delta p(J+1)\frac{dT}{dp_{J+1}}\right)\frac{1}{2Q_o(J)}\frac{dQ_o}{dT_J}\right.$$
$$\left.-\left(\Delta p(J)+\Delta p(J+1)\right)\frac{1}{2\lambda_1(J)}\frac{d\lambda}{dp_J}\right] \quad (12.6\text{-}39)$$

Multiply through by $(z(J+1) - z(J))\,\Delta t$ and define the coefficients

$$c_{1,j} = \left(z(J+1) - z(J)\right) A_c(J) \left[\frac{1}{2} \frac{d\rho}{dp_J} - \frac{\Delta t}{2\lambda_1(J)} \frac{dT}{dp_J} \frac{dQ_o}{dT_J} + \frac{Q_o(J)\Delta t}{2\lambda_1^2(J)} \frac{d\lambda}{dp_J} \right] \tag{12.6-40}$$

$$c_{2,j} = -\Delta t \tag{12.6-41}$$

$$c_{3,j} = \left(z(J+1) - z(J)\right) A_c(J) \left[\frac{1}{2} \frac{d\rho}{dp_{J+1}} - \frac{\Delta t}{2\lambda_1(J)} \frac{dT}{dp_{J+1}} \frac{dQ_o}{dT_J} + \frac{Q_o(J)\Delta t}{2\lambda_1^2(J)} \frac{d\lambda}{dp_J} \right] \tag{12.6-42}$$

$$c_{4,J} = \Delta t \tag{12.6-43}$$

Also, define the source term

$$h_J = W_1(J) - W_1(J+1) + \left(z(J+1) - z(J)\right) A_c(J) \frac{Q_o(J)}{\lambda_1(J)} \Delta t \tag{12.6-44}$$

Then the differenced mass equation becomes

$$c_{1,J}\,\Delta p(J) + c_{2,J}\,\Delta W(J) + c_{3,j}\,\Delta p(J+1) + c_{4,J}\,\Delta W(J+1) = h_j \tag{12.6-45}$$

12.6.2.2 Finite Differencing of the Continuity Equation for a Mesh Segment Which Contains a Bubble Interface

12.6.2.2.1 Adjustment of the Form of the Continuity Equation to Account for Interface Motion

The representation of the partial derivative with respect to time is not as straightforward at an interface as it is at an interior node. Referring to Fig. 12.6-3, in which node boundary *J* is the interface, the partial derivative of the density ρ is still calculated as

$$\frac{\partial \rho}{\partial t}\Big|_{J+1/2} = \frac{1}{2}\left[\frac{\partial \rho}{\partial t}\Big|_J + \frac{\partial \rho}{\partial t}\Big|_{J+1} \right]. \tag{12.6-46}$$

The partial derivatives at *J* and *J*+1 are computed just as they are for an interior node; in particular,

$$\frac{\partial \rho}{\partial t}\Big|_J = \frac{\rho\left(z(J,t), t+\Delta t\right) - \rho\left(z(J,t), t\right)}{\Delta t}, \tag{12.6-47}$$

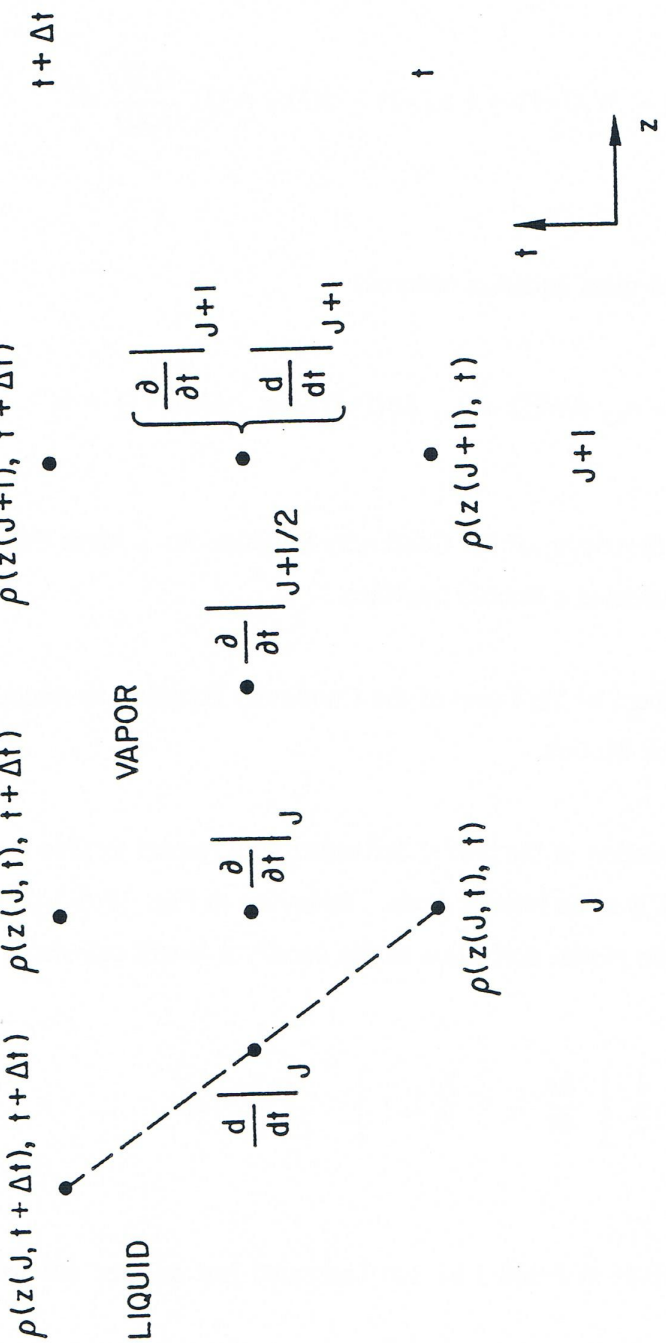

Figure 12.6-3. Evaluation of the total Derivative at a Liquid-Vapor Interface

so the partial derivative at J is differenced as though the interface were stationary at $z(J,t)$. However, the interface is moving at a velocity v^i and moves a distance $v^i\Delta t$ from $z(J,t)$ to $z(J,t+\Delta t)$ during the time step, so the spatial derivative in the continuity equation must be differenced from $z(J+1,t+\Delta t)$ to z$(J,t+\Delta t)$, rather than to z(J,t). Thus, the continuity equation for an interface node will involve advanced time quantities at three spatial points ($z(J,t)$, $z(J,t+\Delta t)$, and $z(J+1,t+\Delta t)$) rather than at two. This difficulty can be resolved if the partial derivative with respect to time is expressed in terms of $\rho(z(J,t+\Delta t),t+\Delta t)$ rather than $\rho(z(J,t),t+\Delta t)$ by introducing the Lagrangian total derivative, $\frac{d\rho}{dt}$.

$$\frac{d\rho}{\partial t} = \frac{\partial \rho}{\partial t} + v\frac{\partial \rho}{\partial z} \tag{12.6-48}$$

or

$$\frac{d\rho}{\partial t} = \frac{d\rho}{dt} - v\frac{\partial \rho}{\partial z} \tag{12.6-49}$$

with

$$\frac{d\rho}{dt} = \frac{\rho\left(z\left(J,t+\Delta t\right),t+\Delta t\right) - \rho\left(z\left(J,t\right),t\right) + \rho\left(z\left(J+1\right),t+\Delta t\right) - \rho\left(z\left(J+1\right),t\right)}{2\ \Delta t}. \tag{12.6-50}$$

$$v = \frac{v^i}{2}, \tag{12.6-51}$$

and

$$\frac{\partial \rho}{\partial z} = \frac{\rho\left(z\left(J,t+\Delta t\right),t+\Delta t\right) - \rho\left(z\left(J+1\right),t+\Delta t\right)}{z\left(J,t+\Delta t\right) - z\left(J+1\right)} \tag{12.6-52}$$

The factor of ½ appears in the velocity term to represent the average of the velocity of the interface point J (which is v^i) an that of the point J+1 (which is zero). This formulation is equivalent to expressing $\rho(z(J,t),t+\Delta t)$ as an interpolated value between $\rho(z(J,t+\Delta t)$ and $\rho(z(J+1),t+\Delta t)$. The continuity equation now takes the form

$$\frac{\partial W}{\partial z} + A_c\frac{d\rho}{dt} - v\frac{\partial \rho}{\partial z} = A_c\frac{Q}{\lambda} \tag{12.6-53}$$

Let a node boundary quantity *x* be represented at the lower interface by $x_j^i(J1)$ and at the upper interface by $x_j^i(J2)$ where *j*=1 or 2 to designate the beginning or end of the time step. A node midpoint quantity *y* is represented at the lower interface by $y_j(J1)$ (since it is contained in node *J*1) and at the upper interface by $y_j(J2\text{-}1)$ (since it is located in node *J*2-1). As shown in Fig. 12.6-4, *J*1 is the number of the fixed mesh node boundary below the lower interface, while *J*2 is the fixed node boundary number above the upper interface. Looking first at the lower interface, the total time derivative of the density is then

$$\frac{d\rho}{dt} = \frac{\rho_2(J1+1) - \rho_1(J1+1) + \rho_2^i(J1) - \rho_1^i(J1)}{2\Delta t} \tag{12.6-54}$$

or, using Eqs. 12.6-22 and 12.6-37 to express $\frac{d\rho}{dt}$ in terms of the change in vapor pressure,

$$\frac{d\rho}{dt} = \frac{1}{2\Delta t}\left(\Delta\rho(J1+1)\frac{d\rho}{dp_{J1+1}} + \Delta\rho^i(J1)\frac{d\rho^i}{dp_{J1}}\right) \tag{12.6-55}$$

The spatial derivative term becomes

$$v\frac{\partial\rho}{\partial z} = \frac{v_2^i(J1)}{2}\frac{(\rho_2(J1+1) - \rho_2^i(J1))}{(z(J1+1) - z_2^i(J1))} \tag{12.6-56}$$

The advanced time velocity is expressed in the linearized form of Eq. 12.6-21 as

$$v_2^i(J1) = v_1^i(J1) + \Delta v^i(J1) \tag{12.6-57}$$

It is apparent from Eqs. 12.6-56 and 12.6-57 that the added complication of treating the bubble interface introduces two extra unknowns beyond those described n Section 12.6.2.1, namely, the change in interface velocity Δv^i, is assumed known). As will be shown in Subsections 12.6.2.2.2 and 12.6.2.2.3, both of these quantities can be expressed as functions of Δp and of known terms, so that their effect on the final differenced equation is to add terms to the coefficients $c_{1,J}$ and $c_{3,J}$ and to the source term h_J in Eq. 12.6-45.

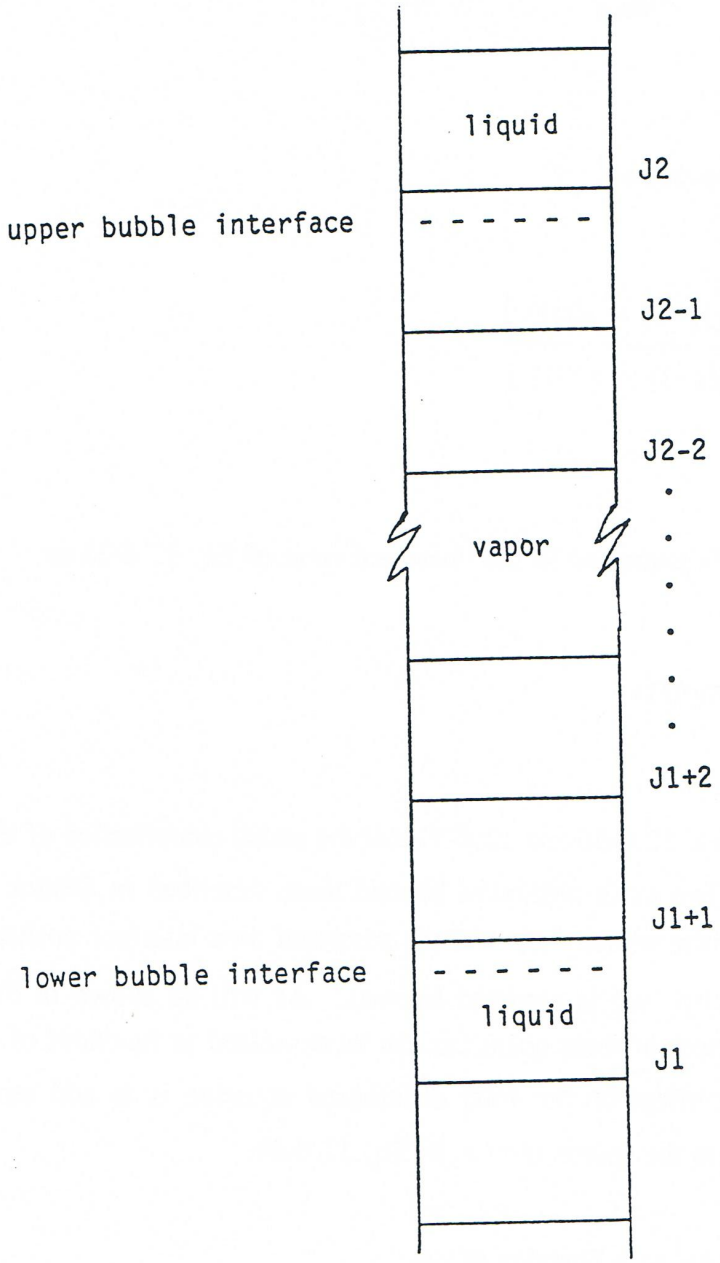

Figure 12.6-4. Placement of a Bubble in the SASSYS-1 Axial Coolant Mesh

12.6.2.2.2 Formulation of Δv^j as a Function of Δp

If the bubble under consideration is labeled bubble *K*, the change in interface velocity is calculated from the change in mass flow rate $\Delta W_\ell(K)$ in liquid slug *K*, which is the slug below bubble *K*:

$$\Delta v^i(J1) = \frac{\Delta W_\ell(K)}{\rho_\ell^i(J1) A_c(J1)} f_{rwt}(K) \tag{12.6-58}$$

where $f_{rwt}(K)$ is the liquid film rewetting factor at the top of slug *K* and $\rho_\ell^i(J1)$ is the liquid sodium density at the interface. The film rewetting factor accounts for the effect of liquid film on the cladding and structure on the interface velocity; this has already been discussed in Section 12.3. From Eq. 12.3-6 of Section 12.3, the liquid film rewetting factor is

$$f_{rwt} = \frac{v^i}{v_l} = \frac{1 - P_e\left(w_{fe} v_{fe} + \gamma_2 w_{fs} v_{fs}\right)/(v_l A_c)}{1 - P_e\left(w_{fe} + \gamma_2 w_{fs}\right)/A_c} \tag{12.6-59}$$

The change in mass flow rate is computed from the liquid slug momentum equation given in Eq. 12.2-34:

$$\Delta W_\ell(K) = \frac{\left(AA_0(K) + \theta_2\left(\Delta p_b(K) - \Delta p_t(K)\right)\right)\Delta t}{I_1(K) + \theta_2 \Delta I_1(K) + BB_0(K)\theta_2 \Delta t} \tag{12.6-60}$$

with $\theta_1 = \theta_2 = 1/2$ for the semi-implicit method and $\theta_1 = 0$, $\theta_2 = 1$ for the fully implicit formulation. The pressure changes are defined as

$\Delta p_b(K)$= change in pressure at lower end of liquid slug K.

$\Delta p_t(K)$= change in pressure at upper end of liquid slug K.

Since $\Delta p_t(K)$ is the pressure change at the bubble interface,

$$\Delta p_t(K) = \Delta p^i(J1) \tag{12.6-61}$$

Therefore, $\Delta v^i(J1)$ can be split into two parts as

$$\Delta v^i(J1) = \Delta v_o^i(J1) + \Delta p^i(J1)\frac{dv^i}{dp_{J1}} \tag{12.6-62}$$

with

$$\Delta v_o^i(J1) = \frac{f_{rwt}(K)}{\rho_\ell^i(J1)A(J1)} \frac{\left(AA_o(K) + \theta_2 \Delta p_b(K)\right)\Delta t}{I_1(K) + \theta_2 \Delta I_1(K) + BB_o(K)\theta_2 \Delta t} \tag{12.6-63}$$

being the change in interface velocity with no change in interface pressure and

$$\frac{dv^i}{dp_{J1}} = -\frac{f_{rwt}(K)}{\rho_\ell^i(J1)A(J1)} \frac{\theta_2 \Delta t}{I_1(K) + \theta_2 \Delta I_1(K) + BB_o(K)\theta_2 \Delta t} \tag{12.6-64}$$

being the velocity change with respect to the change in interface pressure. With the change in interface velocity now expressed as a linear function of the change in interface pressure (Eq. 12.6-62), the advanced time interface velocity in the expression for the spatial derivative term $v\frac{\partial \rho}{\partial z}$ (Eq. 12.6-56) can be replaced using Eqs. 12.6-57 and 12.6-62. In addition, the advanced time densities in Eq. 12.6-56 can be linearized through Eq. 12.6-22 and written in terms of pressure changes form Eq. 12.6-37. This gives $v\frac{\partial \rho}{\partial z}$ as

$$v\frac{\partial p}{\partial z} = \frac{1}{2}\left(v_1^i(J1) + \Delta v_o^i(J1) + \Delta p_i(J1)\frac{dv^i}{dp_{J1}}\right) \cdot \frac{\rho_i(J1+1) + \Delta p(J1+1)\frac{d\rho}{dp_{J1+1}} - \rho_1^i(J1) - \Delta p^i(J1)\frac{d\rho^i}{dp_{J1}}}{z\left(J1+1-z_2^i(J1)\right)} \tag{12.6-65}$$

Now, all that remains is to express the interface position z_2^i as a function of the change in pressure; this will be done in the next subsection.

12.6.2.2.3 Formulation of z_2^i as a Function of Δp

The function height can be written as

$$z_2^i(J1) = z_1^i(J1) + \frac{\Delta t}{2}\left(v_1^i(J1) + v_2^i(J1)\right) \tag{12.6-66}$$

which, substituting Eqs. 12.6-57 and 12.6-62 for v_2^i, becomes

$$z_2^i(J1) = z_1^i(J1) + \frac{\Delta t}{2} v_1^i(J1) + \left(v_1^i(J1) + \Delta v_o^i(J) + \Delta p^i(J1) \frac{dv^i}{dp_{J1}} \right)$$
$$= z_1^i(J1) + v_1^i(J1)\Delta t + \frac{\Delta t}{2} v_o^i(J1) + \Delta p^i(J1) \frac{\Delta t}{2} \frac{dv^i}{dp_{(J1)}} \quad (12.6\text{-}67)$$

Define

$$z_o^i(J1) = z_1^i(J1) + v_1^i(J1)\Delta t + \frac{\Delta t}{2} \Delta v_o^i(J1) \quad (12.6\text{-}68)$$

as the interface height with no pressure change at the interface and

$$\frac{dz^i}{dp_{J1}} = \frac{1}{2} \Delta t \frac{dv^i}{dp_{J1}} \quad (12.6\text{-}69)$$

as the change in interface height with respect to the change in interface pressure. Then z_2^i is the linear function

$$z_2^i(J1) = z_0^i(J1) + \Delta \mathrm{p}^{\mathrm{i}}(J1) \frac{dz^i}{dp_{J1}} \quad (12.6\text{-}70)$$

Using Eq. 12.6-70 in Eq. 12.6-65, $v\frac{d\rho}{dz}$ can be expressed as a function of only Δp,

$$v\frac{\partial p}{\partial z} = \frac{1}{2} \left(v_1^i(J1) + \Delta v_o^i(J1) + \Delta p^i(J1) \frac{dv^i}{dp_{J1}} \right)$$
$$\cdot \frac{\rho_1(J1+1) + \Delta p(J1+1) \frac{d\rho}{dp_{J1+1}} - \rho_1^i(J1) - \Delta p^i(J1) \frac{d\rho^i}{dp_{J1}}}{z\left(J1+1-z_0^i(J1)\right) - \Delta p^i(J1) \frac{dz^i}{dp_{J1}}} \quad (12.6\text{-}71)$$

12.6.2.2.4 Final Differenced Form of the Continuity Equation at the Lower Interface as a Function of Only Δp and ΔW

With $\frac{d\rho}{dt}$ in the interface continuity equation, Eq. 12.6-53, written in the form in Eq. 12.6-55 and $v\frac{\partial \rho}{\partial z}$ given by Eq. 12.6-71 and all other terms in Eq. 12.6-53 treated as in Section 12.6.2.1, the differenced form of the continuity equation at the lower interface is, after multiplication by $\left(z(J1+1) - z_2^I(J1)\right)\Delta t$ and substitution of Eq. 12.6-70 for z_2^i,

$$\Delta t\left(W_1(J1+1)-W_1^i(J1)+\Delta W(J1+1)-\Delta W^i(J1)\right)+$$

$$\frac{A_c(J1)}{2}\left(\Delta\rho(J1+1)\frac{d\rho}{dp_{J1+1}}+\Delta\rho^i(J1)\frac{d\rho^i}{dp_{J1}}\right)\left(z(J1+1)-z_0^i(J1)-\right.$$

$$\left.\Delta p^i(J1)\frac{dz^i}{dp_{J1}}\right)-\frac{A_c(J1)\Delta t}{2}\left(v_1^i(J1)+\Delta v_0^i(J1)+\Delta p^i(J1)\frac{dv^i}{dp_{J1}}\right)\cdot$$

$$\left(\rho_1(J1+1)+\Delta p(J1+1)\frac{d\rho}{dp_{J1+1}}-\rho_1^i(J1)-\Delta p^i(J1)\frac{d\rho^i}{dp_{J1}}\right)= \qquad (12.6\text{-}72)$$

$$A_c(J1)\Delta t\frac{Q_0(J1)}{\lambda_1(J1)}\left[1+\left(\Delta\mathrm{p}^{\mathrm{i}}(J1)\frac{dT^i}{dp_{J1}}+\Delta\mathrm{p}(J1+1)\frac{d\mathrm{T}}{dp_{J1+1}}\right)\frac{1}{2Q_0(J1)}\frac{dQ_0}{dT_{J1}}-\right.$$

$$\left.\left(\Delta\mathrm{p}^{\mathrm{i}}(J1)+\Delta\mathrm{p}(J1+1)\frac{1}{2\lambda_1(J1)}\frac{d\lambda}{dp_{J1}}\right)\right]\left(\mathrm{z}(J1+1)-z_0^i(J1)+\right.$$

$$\left.\Delta\mathrm{p}^{\mathrm{i}}(J1)\frac{dz^i}{dp_{J1}}\right)$$

Setting $\Delta z_0(J1)=z(J1+1)-z_0^i(J1)$ and eliminating second-order terms gives a differenced interface continuity equation which is linear in the pressure and mass flow rate changes:

$$\begin{aligned}
&\Delta t\left(W_1(J+1)-W_1^i(J1)+\Delta W(J1+1)-\Delta W^i(J1)\right)\\
&+\frac{A_c(J1)}{2}\Delta z_o(J1)\left(\Delta p(J1+1)\frac{d\rho}{dp_{J1+1}}+\Delta p^i(J1)\frac{d\rho^i}{dp_{J1}}\right)\\
&-\frac{A_c(J1)\Delta t}{2}\left(\left[v_1^i(J1)+\Delta v_o^i(J1)\right]\left[\rho_1(J1+1)-\rho_1^i(J1)\right]+\left[v_1^i(J1)\right]\right)\\
&+\Delta v_o^i(J1)\left[\Delta p(J1+1)\frac{d\rho}{dp_{J1+1}}-\Delta p^i(J1)\frac{d\rho^i}{dp_{J1}}\right]\\
&+\Delta p^i(J1)\frac{dv^i}{dp_{J1}}\left[\rho_1(J1+1)-\rho_1^i(J1)\right]-A_c(J1)\Delta t\frac{Q_o(J1)}{\lambda_1(J1)}\left\{\Delta z_o(J1)\right.\\
&-\Delta p^i(J1)\frac{dz^i}{dp_{J1}}+\Delta z_o(J)\left[\Delta p^i(J1)\frac{dT^i}{dp_{J1}}+\Delta p(J1+1)\frac{dT}{dp_{J1+1}}\right]\frac{1}{2Q_o(J1)}\frac{dQ_o}{dT_{J1}}\\
&\left.-\Delta z_o(J1)\frac{1}{2\lambda_1(J1)}\left[\Delta p^i(J1)+\Delta p(J1+1)\right]\frac{d\lambda}{dp_{J1}}\right\}=0.
\end{aligned} \qquad (12.6\text{-}73)$$

Equation 12.6-73 can be simplified by defining the coefficients

$$c_{1,J1} = \frac{A_c(J1)}{2}\Bigg\{\Delta z_o(J1)\frac{d\rho^i}{dp_{J1}} + \Delta t\Bigg[\left(v_1^i(J1) + \Delta v_0^i(J1)\right)\frac{d\rho^i}{dp_{J1}} - \left(\rho_1(J1+1) - \rho_1^i(J1)\right)\frac{dv^i}{dp_J}\Bigg] + \Delta t\Bigg[\frac{2Q_o(J1)}{\lambda_1(J1)}\frac{dz^i}{dp_{J1}} - \frac{\Delta z_o(J1)}{\lambda_1(J1)}\frac{dQ_o}{dT_{J1}}\frac{dT^i}{dp_{J1}} + \frac{Q_o(J1)\Delta z_o(J1)}{\lambda_1^2(J1)}\frac{d\lambda}{dp_{J1}}\Bigg\}\Bigg] \tag{12.6-74}$$

$$c_{2,J1} = -\Delta t, \tag{12.6-75}$$

$$c_{3,J1} = \frac{A_c(J1)}{2}\Bigg\{\Delta z_o(J1)\frac{d\rho}{dp_{J1+1}} - \Delta t\Bigg[\left(v_1^i(J1) + \Delta v_o^i(J1)\right)\frac{d\rho}{dp_{J1+1}} - \Delta t\frac{\Delta z_o(J1)}{\lambda_1(J1)}\left[\frac{dQ_o}{dT_{J1}}\frac{dT}{dp_{J1+1}} - \frac{Q_o(J1)}{\lambda_1(J1)}\frac{d\lambda}{dp_{J1}}\right]\Bigg\} \tag{12.6-76}$$

$$c_{4,J1} = \Delta t \tag{12.6-77}$$

and the source term

$$h_{J1} = \Delta t\ \Big\{W_1^i(J1) - W_1(J1+1) + A_c(J1)\Big[1/2\left(v_1^i(J1) + \Delta v_o^i(J1)\right)\left(\rho_1(J1+1) - \rho_1^i(J1)\right) + \frac{Q_o(J1)\Delta z_o(J1)}{\lambda_1(J1)}\Big]\Big\} \tag{12.6-78}$$

Then the differenced continuity equation at the lower interface can be written as

$$c_{1,J1}\Delta p^i(J1) + c_{2,J1}\Delta W^i(J1) + c_{3,J1}\Delta p(J1+1) + c_{4,J1}\Delta W(J1+1) = h_{J1} \tag{12.6-79}$$

Note that with $v_1^i, \Delta v_o^i, \frac{dv^i}{dp}$, and $\frac{dz^i}{dp}$ set to zero, the expressions for the coefficients $c_{1,J1}$ and the source term h_{J1} reduce to the forms given at the end of Section 12.6.2.1 for the continuity equation for a mesh segment which lies entirely within the bubble.

12.6.2.2.5 Differenced Form of the Continuity Equation at the Upper Interface

The derivation of the differenced continuity equation at the upper interface is nearly identical to that for the lower interface, and so just a brief explanation will be given

here. The terms in the interface continuity equation of Eq. 12.6-53 are now expressed as follows:

The time derivative is

$$\frac{d\rho}{dt} = \frac{\rho_2^i(J2) - \rho_1^i(J2) + \rho_2(J2-1) - \rho_1(J2-1)}{2\Delta t} = \frac{1}{2\Delta t}\left(\Delta p^i(J2)\frac{d\rho^i}{dp_{J2}} + \Delta p(J2-1)\frac{d\rho}{dp_{J2-1}}\right) \tag{12.6-80}$$

The $v\frac{\partial\rho}{\partial z}$ term is

$$v\frac{\partial\rho}{\partial z} = \frac{v_1^i(J2) + \Delta v^i(J2)}{2}\frac{\rho_2^i(J2) - \rho_2(J2-1)}{z_2^i(J2) - z(J2-1)} \tag{12.6-81}$$

where

$$\Delta v^i(J2) = \frac{\Delta W_\ell(K+1)}{\rho_\ell^i(J2)\,A_c(J2-1)} f_{rwb}(K+1) \tag{12.6-82}$$

and

$$\Delta W_\ell(K+1) = \frac{\left(AA_0(K+1) + \theta_2\left(\Delta p^i(J2) - \Delta p_t(K+1)\right)\right)\Delta t}{I_1(K+1) + \theta_2\,\Delta I_1(K+1) + BB_0(K+1)\theta_2\Delta t} \tag{12.6-83}$$

The rewetting factor at the bottom of liquid slug K+1, f_{rwb} (K+1), is computed as in Eq. 12.6-59. The expression for $\Delta v_i(J2)$ then reduces to

$$\Delta v^i(J2) = \Delta v_0^i(J2) + \Delta p^i(J2)\frac{dv^i}{dp_{J2}} \tag{12.6-84}$$

with the definitions of $\Delta v_o^i(J2)$ and $\frac{dv^i}{dp_{J2}}$ being set as were those for $\Delta v_o^i(J1)$ and $\frac{dv^i}{dp_{J1}}$.

Also,

$$z_2^i(J2) = z_o^i(J2) + \Delta p^i(J2)\frac{dz^i}{dp_{J2}} \tag{12.6-85}$$

can be derived in exactly the same fashion as was Eq. 12.6-70. Therefore,

$$v\frac{\partial\rho}{\partial z}=\frac{1}{2}\left(v_1^i(J2)+\Delta v_o^i(J2)+\Delta p^i(J2)\frac{dv^i}{dp_{J2}}\right)$$
$$\cdot\left(\frac{\rho_1^i(J2)+\Delta p^i(J2)\dfrac{d\rho^i}{dp_{J2}}-\rho_1^i(J2-1)-\Delta p(J2-1)\dfrac{d\rho}{dp_{J2-1}}}{z_o^i(J2)+\Delta p^i(J2)\dfrac{dz^i}{dp_{J2}}-z(J2-1)}\right) \tag{12.6-86}$$

Substituting Eqs. 12.6-80 and 12.6-86 into Eq. 12.6-53 and expressing $\frac{\partial W}{\partial z}$ and $A_c\frac{Q}{\lambda}$ as in Section 12.6.2.1 gives the differenced upper interface continuity equation

$$c_{1,J2-1}\Delta p(J2-1)+c_{2,J2-1}\Delta W(J2-1)+c_{3,J2-1}\Delta p^i(J2)$$
$$+c_{4,J2-1}\Delta W^i(J2)=h_{J2-1} \tag{12.6-87}$$

where

$$c_{1,J2-1}=\frac{A_c(J2-1)}{2}\left\{\Delta z_o(J2-1)\frac{d\rho}{dp_{J2-1}}+\Delta t\left[\left(v_1^i(J2)+\Delta v_o^i(J2)\right)\frac{d\rho}{dp_{J2-1}}\right.\right.$$
$$\left.\left.+\frac{\Delta z_o(J2-1)}{\lambda_1(J2-1)}\left(\frac{dQ_o}{dT_{J2-1}}\frac{dT}{dp_{J2-1}}-\frac{Q_o(J2-1)}{\lambda(J2-1)}\frac{d\lambda}{dp_{J2}}\right)\right]\right\} \tag{12.6-88}$$

$$c_{2,J2-1}=-\Delta t, \tag{12.6-89}$$

$$c_{3,J2-1}=\frac{A_c(J2-1)}{2}\left\{\Delta z_o(J2-1)\frac{d\rho^i}{dp_{J2}}-\Delta t\left[\left(v_1^i(J2)+\Delta v_o^i(J2)\right)\frac{d\rho^i}{dp_{J2}}\right.\right.$$
$$\left.+\left[\rho_1^i(J2)-\rho_1(J2-1)\right]\frac{dv^i}{dp_{J2}}\right]-\left[\Delta t\,\frac{2Q_o(J2-1)}{\lambda_1(J2-1)}\frac{dz^i}{dp_{J2}}\right. \tag{12.6-90}$$
$$\left.\left.+\frac{\Delta z_o(J2-1)}{\lambda_1(J2-1)}\left(\frac{dQ_o}{dT_{J2-1}}\frac{dT^i}{dp_{J2}}-\frac{Q_o(J2-1)}{\lambda_1(J2-1)}\frac{d\lambda}{dp_{J2}}\right)\right]\right\}$$

$$c_{4,J2-1}=\Delta t, \tag{12.6-91}$$

$$h_{h2-1} = \Delta t \left\{ W_1(J2-1) - W_1^i(J2) + A_c(J2-1)\left[1/2\left(v_1^i(J2) + \Delta v_o^i(J2)\right)\left(\rho_1^i(J2) - \rho_1(J2-1)\right) + \frac{Q_o(J2-1)\Delta z_o(J2-1)}{\lambda_1(J2-1)} \right] \right\} \quad (12.6\text{-}92)$$

$$\text{and } \Delta z_o(J2-1) = z_1^i(J2) - z(J2-1). \quad (12.6\text{-}93)$$

12.6.2.3 Finite Differencing of the Momentum Equation for a Mesh Segment Contained Entirely in One Bubble

Now that differenced forms of the continuity equation both within the bubble and at liquid-vapor interfaces have been derived, a similar process must be applied in the momentum equation. The differencing of the momentum equation is accomplished in essentially the same way as that of the continuity equation. Once again, bubble interface will be ignored for the sake of simplicity until the equations for an interior node have been developed.

12.6.2.3.1 Differencing of the Momentum Equation

The differenced forms of the terms in the momentum equation, Eq. 12.6-2, are a follows. The channel pressure drop is given by

$$\frac{\partial p}{\partial z}\Big|_{J+\frac{1}{2}} = \frac{p_2(J+1) - p_2(J)}{z(J+1) - z(J)} \quad (12.6\text{-}94)$$

The momentum convection takes the form

$$\frac{1}{A_c}\frac{\partial}{\partial z}\left(\frac{W^2}{\rho A_c}\right)\Bigg|_{J+1/2} = \frac{1}{A_c^2(J)\left(z(J+1) - z(J)\right)}\left(\frac{W_2^2(J+1)}{\rho_2(J+1)} - \frac{W_2^2(J)}{\rho_2(J)}\right). \quad (12.6\text{-}95)$$

The condensation term is expressed in terms of the contributions from cladding and structure as

$$F_c(J) = F_{ce}(J) + F_{cs}(J), \quad (12.6\text{-}96)$$

where the functions for F_{ce} and F_{cs} are linearly approximated as follows:

$$\text{If } Q_{e_2}(J) \geq 0,\ F_{ce}(J) = 0, \quad (12.6\text{-}97a)$$

$$\text{if } Q_{e_2}(J) < 0,\ F_{ce}(J) = \frac{Q_{e_2}(J)}{2\lambda_2(J)A_c(J)}\left(\frac{W_2(J)}{\rho_2(J)} + \frac{W_2(J+1)}{\rho_2(J+1)}\right), \tag{12.6-97b}$$

and

$$\text{if } Q_{s_2}(J) \geq 0,\ F_{cs}(J) = 0. \tag{12.6-98a}$$

$$\text{if } Q_{s_2}(J) \leq 0,\ F_{cs}(J) = \frac{Q_{s_2}(J)}{2\lambda_2(J)A_c(J)}\left(\frac{W_2(J)}{\rho_2(J)} + \frac{W_2(J+1)}{\rho_2(J+1)}\right). \tag{12.6-98b}$$

$Q_{e2}(J)$ and $Q_{s2}(J)$ are defined in Eq. 12.6-19. Now, linearize Q_{e2} and Q_{s2} by defining

$$Q_{oe}(J) = \gamma(J)\frac{T_{e_2}(J) - \bar{T}_1(J)}{R_{ec_2}(J)} \tag{12.6-99}$$

$$\frac{dQ_{oe}}{dT_J} = -\frac{\gamma(J)}{R_{ec_2}(J)} \tag{12.6-100}$$

$$Q_{os}(J) = \gamma(J)\gamma_2(J)\frac{T_{s_2}(J) - \bar{T}_1(J)}{R_{sc_2}(J)} \tag{12.6-101}$$

$$\frac{dQ_{os}}{dT_J} = -\frac{\gamma(J)\gamma_2(J)}{R_{sc_2}(J)} \tag{12.6-102}$$

These expressions are related to $Q_o(J)$, defined in Subsection 12.6.2.1.2, by

$$Q_o(J) = Q_{oe}(J) + Q_{os}(J) \tag{12.6-103}$$

and

$$\frac{dQ_o}{dT_J} = \frac{dQ_{oe}}{dT_J} + \frac{dQ_{os}}{dT_J} \tag{12.6-104}$$

Substituting these functions into the above formulations of F_{ce} and F_{cs} gives

$$\text{if } Q_{e_2}(J) \geq 0,\ F_{ce}(J) = 0 \tag{12.6-105a}$$

$$\text{if } Q_{e_2}(J) < 0,\ F_{ce}(J) = \frac{1}{2\lambda_2(J)A_c(J)}\left(\frac{W_2(J)}{\rho_2(J)} + \frac{W_2(J+1)}{\rho_2(J+1)}\right)\left(Q_{oe}(J) + \frac{1}{2}\frac{dQ_{oe}}{dT_J}\left(\Delta T(J) + \Delta T(J+1)\right)\right) \tag{12.6-105b}$$

$$\text{if } Q_{s_2}(J) \geq 0,\ F_{cs}(J) = 0 \tag{12.6-106a}$$

$$\text{if } Q_{s_2}(J) < 0,\ F_{cs}(J) = \frac{1}{2\lambda_2(J)A_c(J)}\left(\frac{W_2(J)}{\rho_2(J)} + \frac{W_2(J+1)}{\rho_2(J+1)}\right)\cdot \left(Q_{os}(J) + \frac{1}{2}\frac{dQ_{os}}{dT_J}\left[\Delta T(j) + \Delta T(J+1)\right]\right) \tag{12.6-106b}$$

If the definitions

$$F_{oe}(J) = \begin{cases} 0, & Q_{e_2} \geq 0, \\ Q_{oe}(J), & Q_{e_2}(J) < 0, \end{cases} \tag{12.6-107a-b}$$

$$F_{os}(J) = \begin{cases} 0, & Q_{s_2} \geq 0, \\ Q_{os}(J), & Q_{s_2}(J) < 0, \end{cases} \tag{12.6-108a-b}$$

$$F_o(J) = F_{oe}(J) + F_{os}(J) \tag{12.6-109}$$

are used in the expressions for F_{ce} and F_{cs}, the condensation term becomes

$$F_c(J) = \frac{F_o(J)}{2A_c(J)\lambda_2(J)}\left[1 + \left(\frac{F_{oc}(J)}{2Q_{oe}(J)\,F_o(J)}\frac{dQ_{oe}}{dT_J} + \frac{F_{os}(J)}{2Q_{os}(J)\,F_o(J)}\frac{dQ_{os}}{dT_J}\right)\cdot\left(\Delta T(J) + \Delta T(J+1)\right)\right]\left(\frac{W_2(J)}{\rho_2(J)} + \frac{W_2(J+1)}{\rho_2(J+1)}\right) \tag{12.6-110}$$

This expression can be simplified by setting

$$\frac{dF_{oe}}{dT_J} = \begin{cases} 0, Q_{e_2}(J) \geq 0, \\ \dfrac{dQ_{oe}}{dT_J}, Q_{e_2}(J) < 0, \end{cases} \tag{12.6-111a-b}$$

which can be stated more compactly as

$$\frac{dF_{oe}}{dT_j} = \frac{F_{oe}(J)}{Q_{oe}(J)} \frac{dQ_{oe}}{dT_J} \tag{12.6-112}$$

Similarly,

$$\frac{dF_{os}}{dT_J} = \frac{F_{os}(J)}{Q_{os}(J)} \frac{dQ_{os}}{dT_J} \tag{12.6-113}$$

so that the definition

$$\frac{dF_o}{dT_J} = \frac{dF_{oe}}{dT_J} + \frac{dF_{os}}{dT_J} \tag{12.6-114}$$

can be made. This gives

$$F_c(J) = \frac{F_o(J)}{2A_c(J)\lambda_2(J)} \left[1 + \frac{dF_o}{2F_o(J)} \frac{dF_o}{dT_J} \left(\Delta T(J) + \Delta T(J+1) \right) \right] \cdot \left(\frac{W_2(J)}{\rho_2(J)} + \frac{W_2(J+1)}{\rho_2(J+1)} \right) \tag{12.6-115}$$

as the differenced form of the condensation term.

The change in mass flow rate with time is

$$\frac{\partial W}{\partial t} = \frac{W_2(J) + W_2(J+1) - W_1(J) - W_1(J+1)}{2\Delta t} \tag{12.6-116}$$

The orifice pressure drop becomes

$$\frac{W|W|}{2\rho_v A_c^2}\frac{\partial k_{or}}{\partial z} = \frac{1}{4A_c^2(J)}\left(\frac{W_2(J)|W_2(J)|}{\rho_2(J)} + \frac{W_2(J+1)|W_2(J+1)|}{\rho_2(J+1)}\right) \cdot \frac{k_{or}(J)}{z(J+1)-z(J)} \tag{12.6-117}$$

Finally, if the friction factor

$$f_v = A_{fr}\left(\frac{D_h W}{\mu A_c}\right)^{b_{fr}} \tag{12.6-118}$$

is considered in the differencing, the friction term may be written as

$$\frac{f_v W|W|}{2\rho A_c^2 D_h} = \frac{A_{fr} W|W|^{1+b_{fr}}}{2\rho\mu^{b_{fr}} D_h^{1-b_{fr}} A_c^{2+b_{fr}}} = \frac{A_{fr}}{4D_h^{1-b_{fr}}(J)A_c^{2+b_{fr}}(J)}\left[\frac{W_2(J+1)|W_2(J+1)|^{1+b_{fr}}}{\rho_2(J+1)\mu_2^{b_{fr}}(J+1)} + \frac{W_2(J)|W_2(J)|^{1+b_{fr}}}{\rho_2(J)\mu_2^{b_{fr}}(J)}\right] \tag{12.6-119}$$

Using Eqs. 12.6-94, 12.6-95, 12.6-115, 12.6-116, 12.6-117, and 12.6-119 results in a differenced momentum equation as follows:

$$\begin{aligned}
&\frac{p_2(J+1)-p_2(J)}{z(J+1)-z(J)} + \frac{1}{A_c^2(J)(z(J+1)-z(J))}\left(\frac{W_2^2(J+1)}{\rho_2(J+1)} - \frac{W_2^2(J)}{\rho_2(J)}\right) \\
&+ \frac{A_{fr}}{4D_h^{1-b_{fr}}(J)A_c^{2+b_{fr}}(J)}\left[\frac{W_2(J+1)|W_2(J+1)|^{1+b_{fr}}}{\rho_2(J+1)\mu_2^{b_{fr}}(J+1)} + \frac{W_2(J)|W_2(J)|^{1+b_{fr}}}{\rho_2(J)\mu_2^{b_{fr}}(J)}\right] \\
&- \frac{F_o(J)}{2A_c(J)\lambda_2(J)}\left[1 + \frac{1}{2F_o(J)}\frac{dF_o}{dT_J}(\Delta T(J) + \Delta T(J+1))\right]\left(\frac{W_2(J)}{\rho_2(J)} + \frac{W_2(J+1)}{\rho_2(J+1)}\right) \\
&+ \frac{W_2(J)+W_2(J+1)-W_1(J)-W_1(J+1)}{2A_c(J)\Delta t} + \frac{1}{4A_c^2(J)}\left(\frac{W_2(J)|W_2(J)|}{\rho_2(J)}\right. \\
&\left. + \frac{W_2(J+1)|W_2(J+1)|}{\rho_2(J+1)}\right)\frac{k_{or}(J)}{z(J+1)-z(J)} = 0.
\end{aligned} \tag{12.6-120}$$

The equation must now be linearized and reduced to a linear function of Δp and ΔW; this procedure will be discussed in the next subsection.

12.6.2.3.2 Linearization of Advanced Time Quantities and Introduction of Saturation Conditions

Equation 12.6-120 is made linear by expressing the advanced time variables in linearized form as in Eq. 12.6-21. This means that, in addition to using the expressions in Eqs. 12.6-22 through 12.6-25 for density, heat of vaporization, mass flow rate, and temperature, the linearized form of Eq. 12.6-120 must include the following representations of pressure and viscosity:

$$p_2(J) = p_1(J) + \Delta p(J), \tag{12.6-121}$$

$$\mu_2(J) = \mu_1(J) + \Delta\mu(J), \tag{12.6-122}$$

The differenced momentum equation therefore becomes

$$\begin{aligned}
&\frac{p_1(J+1)+\Delta p(J+1)-p_1(J)-\Delta p(J)}{z(J+1)-z(J)} + \frac{1}{A_c^2(J)\left(z(J+1)-z(J)\right)} \\
&\quad\cdot\left(\frac{\left(W_1(J+1)+\Delta W(J+1)\right)^2}{\rho_1(J+1)+\Delta\rho(J+1)} - \frac{\left(W_1(J)+\Delta W(J)\right)^2}{\rho_1\left(J+\Delta\rho(J)\right)}\right) \\
&+\frac{A_{fr}}{4D_h^{1-b_{fr}}(J)A_c^{2+b_{fr}}(J)}\left(\frac{\left(W_1(J+1)+\Delta W(J+1)\right)\left|W_1(J+1)+\Delta W(J+1)\right|^{1+b_{fr}}}{\left(\rho_1(J+1)+\Delta\rho(J+1)\right)\left(\mu_1(J+1)+\Delta\mu(J+1)\right)^{b_{fr}}}\right. \\
&\quad\left.+\frac{\left(W_1(J)+\Delta W(J)\left|W_1(J)+\Delta W(J)\right|\right)^{1+b_{fr}}}{\left(\rho_1(J)+\Delta\rho(J)\right)\left(\mu_1(J)+\Delta\mu(J)\right)^{b_{fr}}}\right) - \frac{F_o(J)}{2A_c(J)\left(\lambda_1(J)+\Delta\lambda(J)\right)} \\
&\cdot\left(1+\frac{1}{2F_o(J)}\frac{dF_o}{dT_J}\left(\Delta T(J)+\Delta T(J+1)\right)\right)\left(\frac{W_1(J)+\Delta W(J)}{\rho_1(J)+\Delta\rho(J)} + \frac{W_1(J+1)+\Delta W(J+1)}{\rho_1(J+1)+\Delta\rho(J+1)}\right) \\
&\quad+\frac{\Delta W(J)+\Delta W(J+1)}{2A_c(J)\Delta t} + \frac{1}{4A_c^2(J)}\left(\frac{W_1(J)+\Delta W(J)\left|W_1(J)+\Delta W(J)\right|}{\rho_1(J)+\Delta\rho(J)}\right. \\
&\quad\left.+\frac{\left(W_1(J+1)+\Delta W(J+1)\right)\left|W_1(J+1)+\Delta W(J+1)\right|}{\rho_1(J+1)+\Delta\rho(J+1)}\right)\frac{k_{or}(J)}{z(J+1)-z(J)} = 0
\end{aligned} \tag{12.6-123}$$

Note that the orifice coefficient k_{or} and the hydraulic diameter D_h are, like the channel area A_c, considered to be constant over the time step. Now, Eq. 12.6-123 can be expressed in terms of only two independent variables, Δp and ΔW, by imposing the restriction that ρ, T, λ, and μ be functions of p only, i.e., by imposing saturation conditions. This is accomplished by substituting Eqs. 12.6-36 through 12.6-38, as well as the expression

$$\Delta\mu(J) = \Delta p(J)\frac{d\mu}{dp_J} \tag{12.6-124}$$

into Eq. 12.6-123. The resulting equation, after multiplying by Δt(z(J+1) – z(J)) and letting Δz(J)=z(J+1) – z(J), is the very long expression

$$\begin{aligned}
&\left(p_1(J+1)-p_1(J)\right)\Delta t+\Delta t\Delta p(J+1)-\Delta t\Delta p(J)\\
&+\frac{\Delta t}{A_c^2(J)}\left[\frac{W_1^2(J+1)+2W_1(J+1)\Delta W(J+1)+\left(\Delta W(J+1)\right)^2}{\rho_1(J+1)}\left(1-\frac{\Delta p(J+1)}{\rho_1(J+1)}\frac{d\rho}{dp_{J+1}}\right)\right.\\
&\left.-\frac{W_1^2(J)+2W_1(J)\Delta W(J)+\left(\Delta W(J)\right)^2}{\rho_1(J)}\left(1-\frac{\Delta p(J)}{\rho_1(J)}\frac{d\rho}{dp_J}\right)\right]\\
&+\frac{A_{fr}\Delta t\Delta z(J)}{4D_h^{1-b_{fr}}(J)A_c^{2+b_{fr}}(J)}\left[\frac{W_1(J+1)\left|W_1(J+1)\right|^{1+b_{fr}}\left(1+\left(2+b_{fr}\right)\Delta W(J+1)/W_1(J+1)\right)}{\rho_1(J+1)\mu_1^{b_{fr}}(J+1)}\right.\\
&\qquad\left(1-\frac{\Delta p(J+1)}{\rho_1(J+1)}\frac{d\rho}{dp_{J+1}}-b_{fr}\frac{\Delta p(J+1)}{\mu_1(J+1)}\frac{d\mu}{dp_{J+1}}\right)\\
&\left.+\frac{W_1(J)\left|W_1(J)\right|^{1+b_{fr}}\left(1+\left(2+b_{fr}\right)\Delta W(J)/W_1(J)\right)}{\rho_1(J)\mu_1^{b_{fr}}(J)}\left(1-\frac{\Delta p(J)}{\rho_1(J)}\frac{d\rho}{dp_J}-b_{fr}\frac{\Delta p(J)}{\mu_1(J)}\frac{d\mu}{dp_J}\right)\right]\\
&\qquad-\frac{F_o(J)\Delta t\Delta z(J)}{2A_c(J)\lambda_1(J)}\left(1-\frac{\Delta p(J)+\Delta p(J+1)}{2\lambda_1(J)}\frac{d\lambda}{dp_J}\right)\\
&\qquad\cdot\left[1+\frac{1}{2F_o(J)}\frac{dF_o}{dT_J}\left(\Delta p(J)\frac{dT}{dp_J}+\Delta p(J+1)\frac{dT}{dp_{J+1}}\right)\right]\\
&\qquad\cdot\left[\frac{W_1(J+1)}{\rho_1(J)}\left(1+\frac{\Delta W(J)}{W_1(J)}\right)\left(1-\frac{\Delta p(J)}{\rho_1(J)}\frac{d\rho}{dp_J}\right)\right.\\
&\qquad\left.+\frac{W_1(J+1)}{\rho_1(J+1)}\left(1+\frac{\Delta W(J+1)}{W_1(J+1)}\right)\left(1-\frac{\Delta p(J+1)}{\rho_1(J+1)}\frac{d\rho}{dp_{J+1}}\right)\right]\\
&\qquad+\frac{\Delta z(J)}{2A_c(J)}\Delta W(J)+\frac{\Delta z(J)}{2A_c(J)}\Delta W(J+1)\\
&\qquad+\frac{\Delta t}{4A_c^2(J)}\left[\frac{W_1(J)\left|W_1(J)\right|\left(1+2\Delta W(J)/W_1(J)\right)}{\rho_1(J)}\left(1-\frac{\Delta p(J)}{\rho_1(J)}\frac{d\rho}{dp_J}\right)\right.\\
&\qquad\left.+\frac{W_1(J+1)\left|W_1(J+1)\right|\left(1+2\Delta W(J+1)/W_1(J+1)\right)}{\rho_1(J+1)}\left(1-\frac{\Delta p(J+1)}{\rho_1(J+1)}\frac{d\rho}{dp_{J+1}}\right)\right]\\
&\qquad k_{or}(J)=0,
\end{aligned} \tag{12.6-125}$$

where it is assumed that $\Delta\mu << \mu_1$ and $\Delta\rho << \rho_1 <$, so that

$$\frac{1}{\rho_1(J)+\Delta\rho(J)} = \frac{1}{\rho_1(J)}\left(1-\frac{\Delta\rho(J)}{\rho_1(J)}\right) \tag{12.6-126}$$

and

$$\frac{1}{\left(\mu_1(J)+\Delta\mu(J)\right)^{b_{fr}}} = \frac{1}{\mu_1^{b_{fr}}(J)}\left(1-b_{fr}\frac{\Delta\mu(J)}{\mu_1(J)}\right). \tag{12.6-127}$$

Eliminating second-order terms produces the final linearized form of the differenced momentum equation:

$$b_{1,J}\,\Delta p(J)+b_{2,J}\,\Delta W(J)+b_{3,J}\,\Delta p(J+1)+b_{4,j}\,\Delta W(J+1)=g_J. \tag{12.6-128}$$

with

$$\begin{aligned} b_{1,J} = &-\Delta t+\frac{\Delta t}{A_c^2(J)}\frac{W_1^2(J)}{\rho_1^2(J)}\frac{d\rho}{dp_J}-\frac{A_{fr}\Delta t\Delta z(J)}{4D_h^{1-b_{fr}}(J)A_c^{2+b_{fr}}(J)}\frac{W_1(J)\left|W_1(J)\right|^{1+b_{fr}}}{\rho_1(J)\mu_1^{b_{fr}}(J)} \\ &\cdot\left(\frac{1}{\rho_1(J)}\frac{d\rho}{dp_J}+\frac{b_{fr}}{\mu_1(J)}\frac{d\mu}{dp_J}\right) \\ &+\frac{F_o(J)\Delta t\Delta z(J)}{4A_c(J)\lambda_1(J)}\left[\frac{1}{\lambda_1(J)}\frac{d\lambda}{dp_J}\left(\frac{W_1(J)}{\rho_1(J)}+\frac{W_1(J+1)}{\rho_1(J+1)}\right)\right. \\ &\left.-\frac{1}{F_o(J)}\frac{dF_o}{dT_J}\frac{dT}{dp_J}\left(\frac{W_1(J)}{\rho_1(J)}+\frac{W_1(J+1)}{\rho_1(J+1)}\right)+\frac{2W_1(J)}{\rho_1^2(J)}\frac{d\rho}{d\rho_J}\right] \\ &-\frac{W_1(J)\left|W_1(J)\right|\Delta t}{4A_c^2(J)\rho_1^2(J)}\frac{d\rho}{dp_J}k_{or}(J), \end{aligned} \tag{12.6-129}$$

$$b_{2,J} = -\frac{2W_1(J)\Delta t}{\rho_1(J)A_c^2(J)} + \frac{A_{fr}\Delta t\Delta z(J)}{4D_h^{1-b_{fr}}(J)A_c^{2+b_{fr}}(J)}\frac{(2+b_{fr})|W_1(J)|^{1+b_{fr}}}{\rho_1(J)\mu_1^{b_{fr}}(J)} - \frac{F_o(J)\Delta t\Delta z(J)}{2A_c(J)\lambda_1(J)\rho_1(J)} + \frac{\Delta z(J)}{2A_c(J)} + \frac{\Delta t|W_1(J)|}{2A_c^2(J)\rho_1(J)}k_{or}(J), \quad (12.6\text{-}130)$$

$$b_{3,J} = \Delta t - \frac{\Delta t}{A_c^2(J)}\frac{W_1^2(J+1)}{\rho_1^2(J+1)}\frac{d\rho}{dp_{J+1}} - \frac{A_{fr}\Delta t\Delta z(J)}{4D_h^{1-b_{fr}}(J)A_c^{2+b_{fr}}(J)}\frac{W_1(J+1)|W_1(J+1)|^{1+b_{fr}}}{\rho_1(J+1)\mu_1^{b_{fr}}(J+1)} \cdot\left(\frac{1}{\rho_1(J+1)}\frac{d\rho}{dp_{j+1}} + \frac{b_{fr}}{\mu_1(J+1)}\right)\frac{d\mu}{dp_{J+1}} + \frac{F_o(J)\Delta t\Delta z(J)}{4A_c(J)\lambda_1(J)} \cdot\left[\frac{1}{\lambda_1(J)}\frac{d\lambda}{dp_J}\left(\frac{W_1(J)}{\rho_1(J)} + \frac{W_1(J+1)}{\rho_1(J+1)}\right) - \frac{1}{F_o(J)}\frac{dF_o}{dT_J}\frac{dT}{dp_{J+1}}\left(\frac{W_1(J)}{\rho_1(J)} + \frac{W_1(J+1)}{\rho_1(J+1)}\right) + \frac{2W_1(J+1)}{\rho_1^2(J+1)}\frac{d\rho}{dp_{J+1}}\right] - \frac{W_1(J+1)|W_1(J+1)|\Delta t}{4A_c^2(J)\rho_1^2(J+1)}\frac{d\rho}{dp_{J+1}}k_{or}(J), \quad (12.6\text{-}131)$$

$$b_{4,J} = -\frac{2W_1(J+1)\Delta t}{\rho_1(J+1)A_c^2(J)} + \frac{A_{fr}\Delta t\Delta z(J)}{4D_h^{1-b_{fr}}(J)A_c^{2+b_{fr}}(J)}\frac{(2+b_{fr})|W_1(J+1)|^{1+b_{fr}}}{\rho_1(J+1)\mu_1^{b_{fr}}(J+1)} - \frac{F_o(J)\Delta t\Delta z(J)}{2A_c(J)\lambda_1(J)\rho_1(J+1)} + \frac{\Delta z(J)}{2A_c(J)} + \frac{\Delta t|W_1(J+1)|}{2A_c^2(J)\rho_1(J+1)}k_{or}(J), \quad (12.6\text{-}132)$$

$$g_J = \left(p_1(J) - p_1(J+1)\right)\Delta t - \frac{\Delta t}{A_c^2(J)}\left(\frac{W_1^2(J+1)}{\rho_1(J+1)} - \frac{W_1^2(J)}{\rho_1(J)}\right)$$
$$- \frac{A_{fr}\Delta t \Delta z(J)}{4D_h^{1-b_{fr}}(J)A_c^{2+b_{fr}}(J)}\left(\frac{W_1(J+1)\left|W_1(J+1)\right|^{1+b_{fr}}}{\rho_1(J+1)\mu_1^{b_{fr}}(J+1)} + \frac{W_1(J)\left|W_1(J)\right|^{1+b_{fr}}}{\rho_1(J1)\mu_1^{b_{fr}}(J1)}\right)$$
$$+ \frac{F_o(J)\Delta t \Delta z(J)}{2A_c(J)\lambda_1(J)}\left(\frac{W_1(J)}{\rho_1(J)} + \frac{W_1(J+1)}{\rho_1(J+1)}\right) \qquad (12.6\text{-}133)$$
$$- \frac{\Delta t\, k_{or}(J)}{4A_c^2(J)}\left(\frac{W_1(J)\left|W_1(J)\right|}{\rho_1(J)} + \frac{W_1(J+1)\left|W_1(J+1)\right|}{\rho_1(J+1)}\right).$$

12.6.2.4 Finite Differencing of the Momentum Equation for a Mesh Segment Which Contains a Bubble Interface

The inclusion of a bubble interface in node J introduces the Lagrangian total derivative, as described in Section 12.6.2.2.1. The momentum equation then becomes

$$\frac{\partial p}{\partial z} + \frac{1}{A_c^2}\frac{\partial}{\partial z}\frac{W^2}{\rho_v} + \frac{f_v W|W|}{2\rho_v D_h A_c^2} - F_c + \frac{1}{A_c}\frac{dW}{dt} - v\frac{\partial W}{\partial z} + \frac{W|W|}{2\rho_v A_c^2}\frac{\partial k_{or}}{\partial z} = 0. \qquad (12.6\text{-}134)$$

As in the case of the continuity equation, the impact of the bubble interface on the differenced equation is transmitted via the interface velocity v^i and the interface position z^i. Therefore, only those terms in Eq. 12.6-134 which include either v^i or z^i will alter the coefficient b_i or the source term g in Eq. 12.6-128.

12.6.2.4.1 Differenced Form of the Momentum equation at the Lower Interface

The terms of Eq. 12.6-134 can be differenced as in Section 12.6.2.3; in addition, the term v $\frac{\partial W}{\partial z}$ can be expressed as

$$v\frac{\partial W}{\partial z} = \frac{v_2^i(J1)}{2}\frac{W_2(J1+1) - W_2^i(J1)}{\Delta z^i(J1)} \qquad (12.6\text{-}135)$$

where $\Delta z^i(J1) = z(J1+1) - z_2^i(J)$ Therefore, the differenced form of Eq. 12.6-134 is

$$\frac{p_2(J1+1)-p_2^i(J1)}{\Delta z^i(J1)}+\frac{1}{A_c^2(J1)\Delta z^i(J1)}\left(\frac{W_2^2(J1+1)}{\rho_2(J1+1)}-\frac{W_2^2(J1)}{\rho_2(J1)}\right)$$
$$+\frac{A_{fr}}{4D_h^{1-b_{fr}}(J1)A_c^{2+b_{fr}}(J1)}\left(\frac{W_2(J1+1)\left|W_2(J1+1)\right|^{1+b_{fr}}}{\rho_2(J1+1)\mu_2^{b_{fr}}(J1+1)}+\frac{W_2^i(J1)\left|W_2^i(J1)\right|^{1+b_{fr}}}{\rho_2(J1)\mu_2^{b_{fr}}(J1)}\right)-F_e(J$$
$$+\frac{W_2(J1+1)+W_2^i(J1)-W_1(J1+1)-W_2^i(J1)}{2A_c(J1)\Delta t}\Bigg)-\frac{v_2^i(J1)}{2A_c(J1)}\frac{W_2^i(J1+1)-W_2^i(J1)}{\Delta z^i(J1)} \quad (12.6\text{-}136$$
$$+\frac{1}{4A_c^2(J1)}\left(\frac{W_2^i(J1)\left|W_2^i(J1)\right|}{\rho_2(J1)}+\frac{W_2(J1+1)\left|W_2(J1+1)\right|}{\rho_2(J1+1)}\right)\frac{k_{or}^i(J1)}{\Delta z(J1)}=0$$

Multiplying Eq. 12.6-136 by $\Delta t\Delta z^i(J1)$ eliminates $z_2^i(J1)$ from all but the third, fourth, and fifth terms. The sixth term is the only one which includes $v_2^i(J1)$. Thus, only these four terms need to be examined to determine the contribution of the bubble interface to the final differenced momentum equation.

12.6.2.4.2 Specification of Bubble Interface Terms

Of the four terms, all but the one involving $v_2^i(J1)$are present in the momentum equation as derived in Section 12.6.2.3. They affect the interface contribution only because they involve the factor $\Delta z^i(J1)$. For example, consider the condensation term:

$$\Delta t\,\Delta z^i(J1)F_c(J1)=\Delta tF_c(J1)\Delta z_0^i(J1)-\Delta p^i(J1)\frac{dz^i}{dp_{J1}}\Delta t\;F_c(J1) \quad (12.6\text{-}137)$$

The first term on the right-hand side is identical to the condensation term as expressed in the differenced momentum equation, Eq. 12.6-128. Therefore, the condensation term contribution to the momentum equation is modified to account for the bubble interface simply by adding the second term on the right-hand side of Eq. 12.6-136 to Eq. 12.6-128. Written out in full, this term is, after linearization of advanced time quantities and substitution of the saturation condition relations,

$$\Delta p^i(J1)\frac{dz^i}{dp_{J1}}\Delta t F_c(J1)=\Delta p^i(J1)\frac{dz^i}{dp_{J1}}\frac{F_o(J1)\Delta t}{2A_c(J1)\lambda_1(J1)}$$
$$\cdot\left(1-\frac{\Delta p^i(J1)+\Delta p(J1+1)}{2\lambda_1(J1)}\frac{d\lambda}{dp_{J1}}\right)$$
$$\cdot\left(1+\frac{1}{2F_o(J1)}\frac{dF_o}{dT_{J1}}\left(\Delta p(J1)\frac{dT^i}{dp_{J1}}+\Delta p(J1+1)\frac{dT}{dp_{J1+1}}\right)\right) \quad (12.6\text{-}138)$$
$$\cdot\left(\frac{W_1^i(J1)}{\rho_1(J1)}\left(1+\frac{\Delta W^i(J1)}{W_1^i(J1)}\right)\left(1-\frac{\Delta p^i(J1)}{\rho_1(J1)}\frac{d\rho^i}{dp_{J1}}\right)\right.$$
$$\left.+\frac{W_1(J1+1)}{\rho_1(J1+1)}\left(1+\frac{\Delta W(J1+1)}{W_1(J1+1)}\right)\left(1-\frac{\Delta p(J1+1)}{\rho_1(J1+1)}\frac{dp}{dp_{J1+1}}\right)\right.$$

Neglecting second-order terms, this reduces to

$$\Delta p^i(J1)\frac{dz^i}{dp_{J1}}\Delta t F_c(J1)=\Delta p^i(J1)\frac{dz^i}{dp_{J1}}\frac{F_o(J1)\Delta t}{2A_c(J1)\lambda_1(J1)}\left(\frac{W_1^i(J1)}{\rho_1(J1)}+\frac{W_1(J1+1)}{\rho_1(J1+1)}\right) \quad (12.6\text{-}139)$$

Similarly, the friction term contribution comes from

$$\Delta p^i(J1)\frac{dz^i}{dp_{J1}}\Delta t\ \frac{A_{fr}}{4D_h^{1-b_{fr}}(J1)A_c^{2+b_{fr}}(J1)}\left(\frac{W_2(J1+1)\left|W_2(J1+1)\right|^{1+b_{fr}}}{\rho_2(J1+1)\mu_2^{b_{fr}}(J1+1)}\right.$$
$$\left.+\frac{W_2^i(J1)\left|W_2^i(J1)\right|^{1+b_{fr}}}{\rho_1(J1)\mu_2^{b_{fr}}(J1)}\right)=\Delta p^i(J1)\frac{dz^i}{dp_{J1}}\frac{A_{fr}\Delta t}{4D_h^{1-b_{fr}}(J1)A_c^{2+b_{fr}}(J1)}\cdot \quad (12.6\text{-}140)$$
$$\left(\frac{W_1(J1+1)\left|W_1(J1+1)\right|^{1+b_{fr}}}{\rho_1(J1+1)\mu_2^{b_{fr}}(J1+1)}+\frac{W_1^i(J1)\left|W_1^i(J1)\right|^{1+b_{fr}}}{\rho_1(J1)\mu_1^{b_{fr}}(J1)}\right)$$

if second-order terms are dropped. The time derivative of the mass flow rate is

$$\begin{aligned}
&\Delta t \Delta z^i(J1)\frac{\Delta W(J1+1)-\Delta W^i(J1)}{2A_c(J1)\Delta t} \\
&\quad=\left(\Delta z_o^i(J1)-\Delta p^i(J1)\frac{dz^i}{dp_{J1}}\right)\frac{\Delta W(J1+1)+\Delta W^i(J1)}{2A_c(J1)} \\
&\quad=\frac{\Delta z_o^i(J1)}{2A_c(J1)}\left(\Delta W(J1+1)+\Delta W^i(J1)\right)
\end{aligned} \tag{12.6-141}$$

if second-order terms are dropped. This is identical to the differenced form of $\frac{1}{A_c}\frac{\partial W}{\partial t}$ for mesh segments which are contained within the bubble and so this term actually makes no contribution with respect to the bubble interface.

The last term to analyze is $v\,\frac{\partial W}{\partial z}$. This reduces to

$$\begin{aligned}
&\frac{v_2^i(J1)\Delta t}{2A_c(J1)}\left(W_2^i(J1+1)-W_2^i(J1)\right) \\
&\quad=\frac{\Delta t}{2A_c(J1)}\left(v_1^i(J1)+\Delta v_o^i+\Delta p^i(J1)\frac{dv_i}{dp_{J1}}\right) \\
&\qquad\cdot\left(W_1(J1+1)+\Delta W(J1+1)-W_1^i(J1)-\Delta W^i(J1)\right) \\
&\quad=\frac{\Delta t}{2A_c(J1)}\left(v_1^i(J1)+\Delta v_o^i(J1)\right)\left(W_1(J1+1)-W_1^i(J1)\right) \\
&\qquad+\left(v_1^i(J1)+\Delta v_o^i(J1)\right)\Delta W(J1+1)-\left(v_1^i(J1)+\Delta v_o^i(J1)\right)\Delta W^i(J1) \\
&\qquad+\Delta p^i(J1)\frac{dv^i}{dp_{J1}}\left(W_1(J1+1)-W_1^i(J1)\right)
\end{aligned} \tag{12.6-142}$$

Adding Eqs. 12.6-139, 12.6-140 and 12.6-142 to Eqs. 12.6-128 produces the final differenced momentum equation at the lower interface:

$$\tilde{b}_{1,J1}\,\Delta p^i(J1)+\tilde{b}_{2,J1}\,\Delta W^i(J1)+\tilde{b}_{3,J1}\,\Delta p(J1+1)+\tilde{b}_{4,J1}\,\Delta W(J1+1)=\tilde{g}_{J1}, \tag{12.6-143}$$

where

$$\tilde{b}_{1,J1} = b_{1,J1} + \frac{dz^i}{dp_{J1}}\left[\frac{F_o(J1)\Delta t}{2A_c(J1)\lambda_1(J1)}\left(\frac{W_1^i(J1)}{\rho_1(J1)} + \frac{W_1(J1+1)}{\rho_1(J1+1)}\right)\right.$$
$$- \frac{A_{fr}\Delta t}{4D_h^{1-b_{fr}}(J1)A_c^{2+b_{fr}}(J1)}\left[\frac{W_1(J1+1)\left|W_1(J1+1)\right|^{1+b_{fr}}}{\rho_1(J1+1)\mu_1^{b_{fr}}(J1+1)}\right.$$
$$\left.\left. + \frac{W_1^i(J1)\left|W_1^i(J1)\right|^{1+b_{fr}}}{\rho_1(J1)\mu_1^{b_{fr}}(J1)}\right)\right] \qquad (12.6\text{-}144)$$
$$- \frac{dv^i}{dp_{J1}}\frac{\Delta t}{2A_c(J1)}\left(W_1\left(J1+1-W_1^i(J1)\right)\right)$$

$$\tilde{b}_{2,J1} = b_{2,J1} + \frac{\Delta t}{2A_c(J1)}\left(v_1^i(J1) + \Delta v_o^i(J1)\right) \qquad (12.6\text{-}145)$$

$$\tilde{b}_{3,J1} = b_{3,J1} \qquad (12.6\text{-}146)$$

$$\tilde{b}_{4,J1} = b_{4,J1} - \frac{\Delta t}{2A_c(J1)}\left(v_1^i(J1) + \Delta v_o^i(J1)\right) \qquad (12.6\text{-}147)$$

$$\tilde{g}_{J1} = g_{J1} + \frac{\Delta t}{2A_c(J1)}\left(v_1^i(J1) + \Delta v_o^i(J1)\right)\left(W_1(J1+1) - W_1^i(J1)\right) \qquad (12.6\text{-}148)$$

with $b_{1,J1}$, $b_{2,J1}$, $b_{3,J1}$, $b_{4,J1}$,and g_{J1} being defined as in Eq. 12.6-128.

12.6.2.4.3 Differenced Form of the Momentum Equation at the Upper Interface

The development of the momentum equation at the upper interface is identical to that explained in Subsections 12.6.2.4.1 and 12.6.2.4.2 for the lower interface, and so only the final equation will be given here:

$$\tilde{b}_{1,J2-1}\Delta p(J2-1) + \tilde{b}_{2,J2-1}\Delta W(J2-1) + \tilde{b}_{3,J2-1}\Delta p^i(J2)$$
$$+ \tilde{b}_{4,J2-1}\Delta W^i(J2) = \tilde{g}_{J2-1} \qquad (12.6\text{-}149)$$

with

$$\tilde{b}_{1,J2-1} = b_{1,J2-1} \tag{12.6-150}$$

$$\tilde{b}_{2,J2-1} = b_{2,J2-1} + \frac{\Delta t}{2A_c(J2-1)}\left(v_1^i(J2) + \Delta v_o^i(J2)\right) \tag{12.6-151}$$

$$\begin{aligned}\tilde{b}_{3,J2-1} = {} & b_{3,J2-1} - \frac{\Delta t}{2A_c(J2-1)}\frac{dv^i}{dp_{J2}}\left(W_1^i(J2) - W_1(J2-1)\right) \\ & + \frac{A_{fr}\Delta t}{4D_h^{1-b_{fr}}(J2-1)A_c^{2+b_{fr}}(J2-1)}\frac{dz^i}{dp_{J2}}\left(\frac{W_1^i(J2)\left|W_1^i(J2)\right|^{1+b_{fr}}}{\rho_1(J2)\mu_1^{b_{fr}}(J2)}\right. \\ & \left. + \frac{W_1(J2-1)\left|W_1(J2-1)\right|^{1+b_{fr}}}{\rho_1(J2)\mu_1^{b_{fr}}(J2)}\right) \\ & - \frac{\Delta t}{2A_c(J2-1)}\frac{dz^i}{dp_{J2}}\frac{F_o(J2-1)}{\lambda_1(J2-1)}\left(\frac{W_1^i(J2)}{\rho_1(J2)} + \frac{W_1(J2-1)}{\rho_1(J2-1)}\right)\end{aligned} \tag{12.6-152}$$

$$\tilde{b}_{4,J2-1} = b_{4,J2-1} - \frac{\Delta t}{2A_c(J2-1)}v_1^i(J2) + \Delta v_o^i(J2), \tag{12.6-153}$$

$$\tilde{g}_{J2-1} = g_{J2-1} + \frac{\Delta t}{2A_c(J2-1)}\left(v_1^i(J2) + \Delta v_o^i(J2)\right)\left(W_1^i(J2) - W_1^i(J-2)\right) \tag{12.6-154}$$

12.6.2.5 Additional Details Concerning Interface Nodes

Because at least one of the boundaries of an interface mesh segment is not usually aligned with the fixed segment boundaries of the axial mesh, variables defined at the interface segment midpoint must be handled somewhat differently from what they are for a segment located in the interior of a bubble. Midpoint quantities such as A_c and D_h, which are considered to be piecewise constant over the fixed mesh segments, are assigned the values of the fixes mesh segment in which the bubble interface lies. Thus, for example, the flow area at the upper interface is taken as $A_c(J2\text{-}1)$ because the upper interface lies in axial mesh segment $J2$-1. This convention has been used throughout the equations in Sections 12.6.2.2 and 12.6.2.4. However, three midpoint variables are exceptions to this rule: the cladding temperature T_e, the structure temperature T_s, and the average coolant temperature $\overline{T}$. T_e and T_s are calculated outside the two-phase flow model once every heat-transfer time step. As used in the boiling calculation, both temperatures are extrapolated values calculated using the temperatures at the beginning and the end of the last heat-transfer time step and extrapolated to the end of

the current coolant time step. All three temperatures are taken to be located at the midpoints of the Eulerian grid intervals, whereas the boiling calculation needs them at the midpoints of the interface vapor mesh segments (for example, T_e, T_s, and $\overline{T}$ are needed at a point halfway between $z(J2\text{-}1)$ and the upper interface). Therefore, T_e and T_s are interpolated in space to the center of the interface segments using the values in the interface fixed mesh segments and the adjacent vapor segments, while $\overline{T}$ is interpolated to the points using the temperatures at the interfaces and at the nearest fixed mesh boundaries contained in the bubble.

Special considerations must be given to any mesh boundary that is crossed by a liquid-vapor interface during a time step. When setting up the interior segments for the pressure-drop calculation, any segment which is outside the bubble at either the beginning or the end of the time step is bypassed and treated as part of the interface segment. Also, if at the end of the step the interface is within ϵ of a segment boundary (ϵ = .002 meters) then the segment is also bypassed. These tests are all made on the basis of $z_1^i(J)$ and $z_o^i(J)$ as given by Eq. 12.6-68. therefore, a segment JC is included as an interior segment only if

$$z_1^i(J1) < z(JC),$$

$$z_o^i(J1) < z(JC) - \varepsilon,$$

$$z_1^i(J2) > z(JC+1),$$

and

$$z_o^i(J2) > z(JC+1) + \varepsilon.$$

After the calculations of Δ_p and ΔW for segments inside the bubble are completed, p_2 and W_2 for bypassed segments are obtained by linear interpolation between the interface and the first segment inside the interface.

If an interface segment, JT = J1 or JT = $J2$, represents parts of more than one fixed Eulerian mesh segment, then $A_c(JT)$ and $D_h(JT)$ for the interface segment are obtained as weighted averages over the Eulerian segment values. The weighting factors are proportional to the Δz within the bubble. Also, $1/D_h$ is averaged:

$$\frac{1}{D_h(JT)} = \frac{\sum_{JC} \frac{\Delta z(JC)}{D_h(JC)}}{\sum_{JC} \Delta z(JC)} \qquad (12.6\text{-}155)$$

The Δ(JC)'s are based on $z_o^i(JT)$.

12.6.3 Simultaneous Solution of the Differenced, Linearized Mass and Momentum Equations

If the discretized mass and momentum equations derived in Section 12.6.2 (Eqs. 12.6-45 and 12.6-128) are applied to each axial segment in the bubble, the result is a set of simultaneous linear equations which have as independent variables only the changes in vapor pressure and in mass flow rate. To this set must be added the equations at the upper and lower bubble interfaces (Eqs. 12.6-79, 12.6-87, 12.6-143, and 12.6-149), giving a set of 2(J2-J1) equations in 2(J2-J1+1) unknowns. To complete the set, a boundary condition must be imposed at both interfaces. This requirement is satisfied by expressing the interface mass flow rate as

$$W_1^i(JT) = v_1^i(JT)\rho_1^i(JT)A_c(JX) \tag{12.6-156}$$

which can be differenced to give

$$\Delta W^i(JT) = \left(v_1^i(JT)\Delta\rho^i(JT) + \rho_1^i(JT)\Delta v^i(JT)\right)A_c(JX) \tag{12.6-157}$$

The index JT is J1 for the lower interface and J2 for the upper interface, while JX is J1 for the lower interface and J2-1 at the upper one. Using the expressions derived earlier for $\Delta\rho^i$(JT) and Δv^i(JT) (Eqs. 12.6-37 and 12.6-62) produces

$$\begin{aligned}\Delta w^i(JT) = &\left(v_1^i(JT)\frac{d\rho^i}{dp_{JT}} + \rho_1^i(JT)\frac{dv^i}{dp_{JT}}\right)A_c(JX)\Delta p^i(JT)\\ &+ \Delta v_o^i(JT)A_c(JX)\rho_1^i(JT)\end{aligned} \tag{12.6-158}$$

which can be rearranged to give

$$\begin{aligned}&-\left(v_1^i(JT)\frac{d\rho^i}{dp_{JT}} + \rho_1^i(JT)\frac{dv^i}{dp_{JT}}\right)A_c(JX)\Delta p^i(JT) + \Delta W^i(JT)\\ &= \rho_1^i(JT)\Delta v_o^i(JT)A_c(JX)\end{aligned} \tag{12.6-159}$$

Define

$$a_{1,JX} = -\left(v_1^i(JT)\frac{d\rho^i}{dp_{JT}} + \rho_1^i(JT)\frac{dv^i}{dp_{JT}}\right)A_c(JX), \tag{12.6-160}$$

$$a_{2,JX} = 1.0, \tag{12.6-161}$$

and

$$d_{JX} = \rho_1^i(JT)\Delta v_o^i(JT)A_c(JX). \tag{12.6-162}$$

Then Eq. 12.6-159 becomes

$$a_{1,JX}\Delta p^i(JT) + a_{2,JX}\Delta W^i(JT) = d_{JX}\,. \tag{12.6-163}$$

If Eq. 12.6-163 is applied to both upper and lower interfaces and the resulting two equations are added to the set of mass and momentum equations, a set of 2(J2-J1+1) equations in 2(J2-J1+1) unknowns will result. This set can be written in matrix form as

$$AX = B, \tag{12.6-164a}$$

where the form of the matrix A is shown in Eq. 12.6-164b of Fig. 12.6-5 and the X and B vectors are given by

$$A = \begin{bmatrix}
a_{1,J1} & a_{2,J1} & 0 & 0 & 0 & 0\ldots\ldots & 0 & 0 & 0 & 0 \\
\tilde{b}_{1,J1} & \tilde{b}_{2,J1} & \tilde{b}_{34,J1} & \tilde{b}_{4,J1} & 0 & 0\ldots\ldots & 0 & 0 & 0 & 0 \\
c_{1,J1} & c_{2,J1} & c_{3,J1} & c_{4,J1} & 0 & 0\ldots\ldots & 0 & 0 & 0 & 0 \\
0 & 0 & b_{1,J1+1} & b_{2,J1+1} & b_{3,J1+1} & b_{4,J1+1}\cdots & 0 & 0 & 0 & 0 \\
0 & 0 & c_{1,J1+1} & c_{2,J1+1} & b_{3,J1+1} & c_{4,J1+1}\cdots & 0 & 0 & 0 & 0 \\
 & & & & & & . & & & \\
 & & & & & & . & & & \\
 & & & & & & . & & & \\
0 & 0 & 0 & 0 & 0 & 0\ldots\ldots & \tilde{b}_{1,J2-1} & \tilde{b}_{2,J1-1} & \tilde{b}_{3,J2-1} & \tilde{b}_{4,J2-1} \\
0 & 0 & 0 & 0 & 0 & 0\ldots\ldots & c_{1,J2-1} & c_{2,J2-1} & c_{3,J2-1} & c_{4,J2-1} \\
0 & 0 & 0 & 0 & 0 & 0\ldots\ldots & 0 & 0 & a_{1,J2-1} & a_{2,J2-1}
\end{bmatrix}$$

Figure 12.6-5. Coefficient Matrix for the Differenced, Linearized Mass and Momentum Equation in the Vapor Pressure Gradient Voiding Model (12.6-164b)

$$X = \begin{bmatrix} \Delta p^i(J1) \\ \Delta W^i(J1) \\ \Delta p(J1+1) \\ \Delta W(J1+1) \\ . \\ . \\ . \\ \Delta p(J2-1) \\ \Delta W(J2-1) \\ \Delta p^i(J2) \\ \Delta W^i(J2) \end{bmatrix}, \qquad \text{(12.6-164c)}$$

and

$$B = \begin{bmatrix} d_{J1} \\ \widetilde{g}_{J1} \\ h_{J1} \\ g_{J1+1} \\ h_{J1+1} \\ . \\ . \\ . \\ \widetilde{g}_{J2-1} \\ h_{J2-1} \\ d_{J2-1} \end{bmatrix}. \qquad \text{(12.6-164d)}$$

This matrix equation can be solved using Gaussian elimination to give the changes in vapor pressure and mass flow rate at all nodes in the bubble. Appendix 12.2 presents a step-by-step description of how Eq. 12.6-164 is solved using Gaussian elimination. Once the new vapor pressures are known, the vapor temperatures and all thermodynamic sodium properties can be calculated.

12.7 Voiding Due to Gas Release from Failed Fuel Pins

The boiling model in SASSYS-1 and SAS4A has been modified to account for voiding due to release of plenum gas from failed fuel pins. The main purpose of this modification is to address the question of whether pin failure in a transient that would otherwise not lead to boiling recovery would be prevented. Another case that can be addressed with this model is one in which pin failure occurs after the onset of boiling and increases the severity of the voiding. DEFORM-5 predicts the time and location of pin failure, or the user can specify the time and location of the pin failure. The gas release then provides a fictitious source of noncondensing vapor for the boiling model. An adjustable rip area and orifice coefficient determine the rate at which gas is released from the pins. Reduction in the plenum pressure is calculated as the gas flows out the rip. The gas fraction in each bubble in the coolant channel is calculated. The presence of gas in a bubble has two effects: it reduces the condensation coefficient and it increases the vapor friction factor. As the gas bubbles out the top of the subassembly a smooth transition is made to normal boiling. Three pin failure groups are used to account for incoherence. Each group represents a fraction of the pins. A separate life fraction is used by DEFORM-5 to predict failure for each pin group. Each pin group has a separate plenum gas pressure and temperature and a separate flow rate out the rupture.

For this model the rate of gas flow from the plenums to the coolant channel is calculated as

$$w_g = \sum_m f_m A* \sqrt{\frac{2\left(p_{pm} - p_c\right)\overline{\rho}_{gm}}{K_g}} \tag{12.7-1}$$

where

m = pin group number

p_{pm} = plenum pressure for pin group m

p_c = pressure in the coolant channel

A^* = rip area

K_g = rip orifice coefficient

$$\overline{\rho}_{gm} = \frac{\rho_{gm} + \rho_{gc}}{2} \tag{12.7-2}$$

f_m = fraction of the pins in group m

ρ_{pm} = gas density in the plenum

ρ_{gc} = gas density in the coolant channel

Note that for $p_{pm} > > p_c$ and $K_g \sim 2$, Eq. 12.7-1 reduces to the expression for choked flow through as orifice, whereas for small pressure differences the equation reduces to the ordinary orifice flow expression.

Also, for a perfect gas:

$$p_{pm} V_p = m_{pm} R_g T_{pm} \tag{12.7-3}$$

or

$$p_{pm} = \rho_{pm} R_g T_{pm} \tag{12.7-4}$$

and

$$\rho_{gc} = \frac{p_c}{R_g T_{gc}} \tag{12.7-5}$$

where

p_c = pressure in the coolant channel near the rip

T_{gc} = gas temperature as it enters the coolant channel

p_{pm} = plenum gas pressure

R_g = gas constant

T_{pm} = gas temperature in the plenum

The gas flow at the end of the time step is calculated as

$$w_g(t+\Delta t) = \sum_m f_m \left(w_{gm1} + \Delta p_v \, w_{gm3} \right) \tag{12.7-6}$$

where

t = time at beginning of step

Δt = step size

Δp_v = change in coolant channel pressure during the step

$$w_{gm1} = A * \sqrt{\frac{\left[p_{pm}(t) - p_c(t) \right] 2 \bar{\rho}_{gm}(t)}{K_g}} \tag{12.7-7}$$

$$w_{gm3} = \frac{A * \bar{\rho}_{gm}}{k_g \sqrt{\frac{\left[p_{pm}(t) - p_c(t)\right] 2\,\bar{\rho}_{gm}(t)}{k_g}}} \tag{12.7-8}$$

The gas that comes into the coolant channel is converted into enough vapor to have the same pressure-volume product. Thus

$$p_g = \frac{w_g}{\rho_{gc}} = p_v \frac{w_v}{\rho_v} \tag{12.7-9}$$

where

w_v = vapor source

p_v = vapor pressure

ρ_v = vapor density

A conversion factor, γ_g between gas and vapor is defined as

$$w_g = \gamma_g\, w_v \tag{12.7-10}$$

Then

$$\gamma_g = \frac{p_v / \rho_v}{p_g / \rho_g} = \frac{p_v / \rho_v}{R_g / T_{gc}} \tag{12.7-11}$$

The temperature used for T_{gc}, the temperature of the gas entering the coolant channel, is the fuel surface temperature at the rupture node.

The treatment of the gas after it enters the coolant channel depends on whether it is entering a small, nonpressure gradient bubble on a larger, pressure gradient bubble. In a small, nonpressure gradient bubble the gas adds to the heat flow, Q_{es}, from cladding and structure to the vapor:

$$\begin{aligned} Q_{es}(t + \Delta t) = {} & I_{e1} + \delta I_{e1g} + \Delta T_v \left(I_{e2} + \delta I_{e2g}\right) \\ & + I_{c3} \Delta Z'(K,2) + I_{e4}\, \Delta Z'(K,1) \end{aligned} \tag{12.7-12}$$

where

ΔT_v = change in vapor temperature for the time

$\Delta Z'(K,2)$ = change in lower bubble interface position due to change in bubble pressure

$\Delta Z'(K,1)$=change in lower bubble interface position due to change in bubble pressure

K =bubble number

$I_{e1}, I_{e2}, I_{e3}, I_{e4}$=contribution from normal vapor sources

δI_{e1g}, δI_{e2g}=gas source contributions

$$\delta I_{e1g} = \frac{\lambda_v}{\gamma_g} A \cdot \sum_m f_m \sqrt{\frac{\left[p_{pm}(t) - p_c(t)\right] 2\,\bar{\rho}_{gm}(t)}{K_g}} \tag{12.7-13}$$

$$\delta I_{e2g} = \frac{\lambda_v}{\delta_g} A \cdot \frac{\partial p_v}{\partial T_v} \sum_m f_m \frac{\bar{\rho}_{gm}(t)}{K_g} \sqrt{\frac{K_g}{2\bar{\rho}_{pm}(t)\left[p_{pm}(t) - p_c(t)\right]}} \tag{12.7-14}$$

λ = heat of vaporization

For a larger, pressure gradient bubble Eq. 12.6-45 gives a mass equation of the form

$$C_{1,J}\,\Delta p(J) + C_{2,J}\Delta W(J) + C_{3,J}\Delta p(J+1) + C_{4,J}\Delta W(J+1) = h_J \tag{12.7-15}$$

For the mode J at which the pin rupture occurs the gas adds contributions to C_{1J}, C_{3J}, and h_J:

$$h_J \rightarrow h_J + \sum_m \frac{\Delta t\, f_m}{\lambda_g}\, w_{gm1} \tag{12.7-16}$$

$$C_{1,J} \rightarrow C_{1,J} + d_2 \tag{12.7-17}$$

$$C_{3,J} \rightarrow C_{3,J} + d_2 \tag{12.7-18}$$

$$d_2 = \sum_m \frac{\Delta t}{2\gamma_g} f_m\, w_{gm3} \tag{12.7-19}$$

The gas plenum calculations for a time step are done in two parts. First the effects of gas release are calculated. Then the heat flow from the cladding to the gas is accounted for as before.

The gas mass lost from the plenum in pin group in during a time step is calculated using

$$m_{pgm}(t+\Delta t) = m_{pgm}(t) - \Delta t\left(w_{gm1} + \frac{\Delta p_v}{2} w_{gm3} \right) \tag{12.7-20}$$

where

m_{pgm} = gas mass in plenum for group m

Then the remaining gas in the plenum is expanded adiabatically:

$$p_{pm}(t+\Delta t) = p_{pm}(t)\left(\frac{m_{pgm}(t+\Delta t)}{m_{pgm}(t)} \right)^{\gamma} \tag{12.7-21}$$

where

γ = gas specific heat at constant pressure/specific heat at constant volume

The gas temperature, T_{pgm}, for the first part of the step is calculated as:

$$T_{pgm}(t+\Delta t) = \frac{p_{pm}(t+\Delta t)\, V_p}{m_{pgm}(t+\Delta t) R_g} \tag{12.7-22}$$

where

V_p = gas plenum volume

Then heat flow from the cladding is used to recalculate T_{pgm} (t+Δt) and p_{pm}(t+Δt).

The amount of gas in each bubble is kept track of, and the gas fraction in a bubble affects the condensation heat transfer coefficient and the friction factor. The mass of gas, m_{gbk}, in bubble k is calculated using

$$m_{gbk}(t+\Delta t) = m_{gbk}(t) + \frac{\Delta t}{\gamma_g} \sum_m \left(w_{gm1} + \frac{\Delta p_v}{2} w_{gm3} \right) \tag{12.7-23}$$

The total mass, m_{tk}, in each bubble is calculated as

$$m_{tk} = \int \rho_v(z) A_c(z) dz \tag{12.7-24}$$

where

A_c = coolant flow area

The gas fraction, f_{gk}, in bubble k is then defined as

$$f_{gk} = m_{gbk} / m_{tk} \tag{12.7-25}$$

Gas stays in bubble until it blows out the top of the subassembly. When a vapor bubble extends far enough out the top of the subassembly, part of the bubble is assumed to break away and go up into the outlet plenum. If the bubble upper position, z_{iuk}, exceeds the top of subassembly, z_{tsa}, by an amount Δ_{zbu} (if $z_{iuk} \geq z_{tsa} + \Delta_{zbu}$) then the part of the bubble above $z_{tsa} + \Delta z_{b1}$ is broken off from the bubble. When this happens m_{gbk} is decreased by the amount of gas in the part broken off:

$$m_{gbk} \rightarrow m_{gbk} - \Delta m_g \tag{12.7-26}$$

where

$$\Delta m_g = f_{gk} A_c \rho_v \left(z_{iuk} - z_{tsa} - \Delta z_{b1} \right) \tag{12.7-27}$$

Then the upper interface of the bubble is moved down to $z_{tsa} + \Delta z_{b1}$:

$$z_{iuk} \rightarrow z_{tsa} + \Delta z_{b1} \tag{12.7-28}$$

Also, each time that the top part of a bubble is broken off, the velocity of the upper interface is cut in half. The condensation coefficient, h_c, in a bubble containing gas is calculated as

$$h_c = \frac{h_{co}}{1 + 100{,}000\ f_{gk}} \tag{12.7-29}$$

where

h_{co} = normal vapor condensation coefficient.

Gas streaming in a bubble will have a different friction pressure drop than sodium vapor moving at the same velocity, so in this model the vapor friction factor is adjusted when gas is present in a bubble. The friction pressure drop, Δp_f, due to vapor streaming in the coolant channel is

$$\Delta p_f = \frac{L}{D_h} f \rho_v v^2 \tag{12.7-30}$$

where

f = friction factor

v = vapor velocity

L = length

D_h = hydraulic diameter

When gas is turned into fictitious vapor in the coolant channel, its pressure-volume product is conserved; so its velocity should be approximately correct. On the other hand, fission product gas has a higher density than sodium vapor, so the friction pressure drop will not be correct unless the density ratio is accounted for. In this model, the friction factor is adjusted to account for the density ratio:

$$f = f_o \left(\frac{M_{wg}}{M_{wNa}} f_{gk} + 1 - f_{gk} \right) \tag{12.7-31}$$

where

f_o = normal friction factor

M_{wg} = molecular weight of the gas

M_{wNa} = molecular weight of sodium, taken to be 46

12.8 Time Step Controls

In order to operate the voiding model as efficiently and accurately as possible, provision is made for varying the coolant time-step size. This allows a large step size to be used in portions of the transient when no rapid changes are taking place, with a transfer to small time steps when changes occur more rapidly. The size of the step is bounded from below by a user-input minimum value (variable TPDMIN, block 64, number 177) and is limited above by the user-input maximum heat-transfer, primary-loop, and main time step sizes. Within this rather broad range, the actual step size is determined as the largest value which will satisfy several limiting criteria on other quantities involved in the calculation. These criteria require the time-step size to be small enough so that all of the following are satisfied:

1. No bubble which is decreasing in size will shrink to less than half its size from the start to the end of the time step. This prevents collapsing bubbles from disappearing in the middle of the time step and allows them to be removed by the bubble-size criterion at a point in the coding at which the loss of the bubble may be properly accounted for.
2. Neither the highest not the lowest liquid slug is ejected from the subassembly over the span of the time step. As in item 1, such an event must be recorded at the end of a time step in a specific section of the coding.
3. Neither the liquid-sodium nor sodium-vapor temperature anywhere in the channel changes by more than a user-input amount over the time step.
4. The liquid-slug mass flow rate in any slug does not change by more than thirty percent over the time step.

5. Neither the highest nor the lowest vapor bubble is ejected from the subassembly over the span of the time step.
6. No vapor-liquid interface travels more than a user-supplied distance over the time step.
7. No vapor-liquid interface crosses more than one axial mesh segment boundary during the time step.
8. No liquid slug shrinks to less than a minimum length over the time step.

In addition to satisfying these criteria, the time-step selection must obey the following rules:

1. No time step can be less than 10^{-7} seconds.
2. The new time step cannot be more than four times as large as the old step, even if it satisfies the eight criteria listed above.
3. The coolant time step cannot extend past the end of the heat-transfer or primary-loop time steps.

Not that it is possible that the time step which satisfied the eight limiting criteria may be less than 10^{-7} seconds long, which violates the first rule shown above. In this case, the time step is simply set to 10^{-7} seconds, even though one or ore of the criteria may not be satisfied.

The size of the new time step is set in subroutine TSC9 at the end of the voiding calculation over the old time step. This subroutine determines the time step which will satisfy the rules and criteria just discussed. In addition, checks are made on several of the criteria during the course of the calculation; if the time step fails to meet any of these checks, it is reset at the point at which the check was made and the calculation for that step is started over again.

A special case exists when boiling is initiated in any channel. In this instance, the coding will iterate to try to determine the exact time of voiding onset, and so the time step must be adjusted repeatedly so as to locate the beginning of boiling exactly. The time-step adjustment is made from a linear extrapolation based on the amount of liquid superheat.

12.9 Interaction with Other SASSYS-1 Models

As mentioned in the introduction to this chapter, the voiding model interacts directly with several other major modules in SASSYS-1. This section will provide a more detailed discussion of these interactions.

The voiding model first makes use of information from another module by accessing initialization data from the prevoiding calculation. Quantities such as liquid sodium temperatures, pressures, and mass flow rates are computed in the prevoiding module and passed to the voiding model coding, once the prevoiding calculation has predicted that initiation of voiding is imminent. The voiding model then begins interacting with the transient heat-transfer module at the end of each heat-transfer time step. The heat-transfer calculation provides the cladding and structure axial temperature profiles

required by the voiding model (T_e and T_s, respectively). The voiding model estimates these temperatures at the end of the new heat-transfer time step by extrapolating the cladding and structure temperatures form the ends of the previous two heat-transfer time steps. It then computes the advanced time cladding and structure temperatures for each coolant time step by interpolating between the temperatures at the beginning and the end of the heat-transfer time step. During the course of the heat-transfer time step, the voiding model computes the time-integrated heat fluxes from the cladding (E_{ec}) and the structure (E_{es}) and supplies them to the transient heat-transfer calculation at the end of the heat-transfer time step.

Reactivity feedback due to coolant voiding is provided by the voiding model through calculation of a spatially smeared liquid sodium density for each axial mesh segment. This density is passed to the point kinetics module, where it is used to compute the sodium void fraction in each segment. The reactivity change due to voiding is then computed from

$$\rho_c = \sum_i \sum_j (\rho_c)_{jI} \alpha_{jI} \qquad (12.9\text{-}1)$$

where

$(\rho_c)_{jI}$ = reactivity worth of sodium in axial segment j of channel I (input through variable VOIDRA, Block 62, 112)

and

α_{jI} = average sodium void fraction in segment j.

Although the point kinetics module does not feed any information back directly to the voiding model, it does supply the transient heat-transfer module with information about the change in power, which in turn affects the computation of the cladding temperatures, and so the point kinetics model does indirectly influence the voiding model.

12.10 Detailed Flow Description

The logic of the voiding model coding is displayed in the flow diagrams of Fig. 12.10-1. The flowchart is broken up into several sections: the main flow diagram, which outlines the structure of the driver subroutine TSBOIL, and several auxiliary diagrams which give more detail about larger subroutines called by TSBOIL. A brief description of the function of each subroutine used in the voiding model is provided in Table 12.10-1 immediately following Fig. 12.10-1.

The flowchart may be easier to follow if it is studied in conjunction with a more detailed description of the coding logic. The driver subroutine TSBOIL is first called by TSTHRM once the prevoiding model has predicted that initiation of voiding in the channel is imminent. On this first call, TSBOIL uses subroutines CHIN and TSILLB to initialize variables needed in the voiding model calculation from information generated in the prevoiding model. Subroutine TSCSET is then called to update voiding-related

variables to the current coolant time step. Temperatures and liquid-sodium material properties are extrapolated to the end of the time step in subroutine TSC2, which, together with MOMEN and TSC21, also solves the liquid slug momentum equation for a preliminary value of the liquid mass flow rate in the channel at the end of the time step. The code then branches to subroutine TSOV45. This subroutine completes the liquid slug calculations by calling TSC5 to compute the final value of the mass flow rate, TSC6 to determine the liquid sodium temperatures along the channel, and TSC7 to find the axial pressure distribution and saturation temperatures and to determine whether the exact time of voiding initiation has been calculated or whether it is necessary to iterate on the start of voiding. If iteration is necessary, the program adjusts the time step for a new estimate of the time of voiding initiation and returns to TSC2. This process is repeated until the time of the start of boiling has been found. At this point, TSOV45 calls TSC8, which uses TSCBUB, TSC85, and TSC86 to initialize the variables necessary to account properly in the voiding calculation for the presence of the newly formed bubble. Next, the increments in the heat fluxes and the heat-transfer coefficients and the temperatures of the structure, reflectors, plenum gas, and plenum cladding are computed through TSCA, TSCA1, and TSCA2. The new time-step size is set in TSC9, and the updated heat fluxes and heat-transfer coefficients are determined in TSCA. Before returning control to TSBOIL, TSOV45 checks to see if cladding motion has started, and, if it has, it calls TSCLD2. The coding then returns to TSBOIL. A check is made to see if the end of the primary-loop time step has been reached, and if it has, the PRIMAR-4 model is called through PRIMUP and the inlet and outlet temperatures are updated from TSCMP1. Tests are then made on error flogs and on whether the heat-transfer time step has been completed; if it has, a new heat-transfer time step is calculated in TSHTRV. If the appropriate debug flag is set, a printout of some of the voiding model variables is created by NODEPR; otherwise, the coolant time step is over, and control is returned to TSTHRM.

On subsequent calls to TSBOIL, the code branches immediately to TSCSET to update the appropriate variables. Subroutine TSC2 is then called, and then the film thicknesses on the cladding and structure in any voided regions, as well as some heat-transfer coefficient and heat-flux information, are computed using TSC3 and TSC31. The subroutine T4A3D is then called to perform the voiding model calculation. This subroutine first checks for any bubbles that are small enough to used the uniform-vapor-pressure model and calls TSC43A to compute the vapor temperatures and pressures in these bubbles. The pressure-gradient mode is applied by T4A3D to any remaining bubbles, with subroutine T41A3D used to set up the matrix Eq. 12.6-164 and T42A3D responsible for applying the Gaussian elimination procedure to solve the equation. Once the voiding calculation is completed, TSOV45 is called. This subroutine and the subroutines it calls perform the operations described above; in addition, TSC5 computes the liquid-vapor interface positions and TSC8, with the help of TSC82, TSC83, TSC84, TSC85, and TSC86, takes care of all liquid-slug and vapor-bubble accounting. Phenomena such as bubble formation and collapse; liquid-slug disappearance, expulsion, and reentry; and vapor-bubble combination are treated in these subroutines. Subroutine TSC9 not only computes a new time step but also performs a series of checks to see if the current time step should be cut back and the calculation redone; if

this is the case, the step size is cut, the coding branches back to the middle of TSCSET for extrapolation to the end of the revised time step of the required variables, and the calculation is repeated. Otherwise, TSOV45 returns control to TSBOI, and the remainder of the computation proceeds as above.

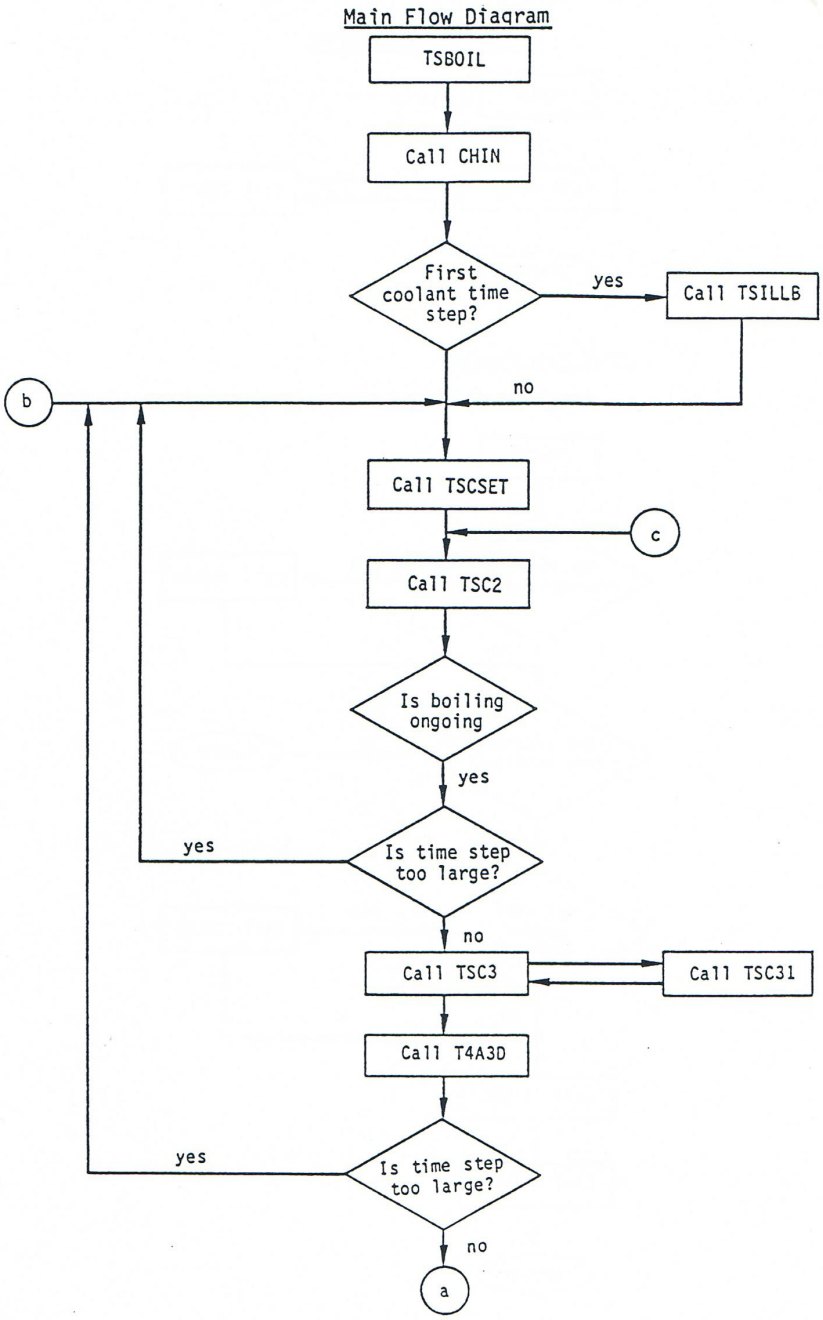

Figure 12.10-1. Flow Chart of the Voiding Model Coding

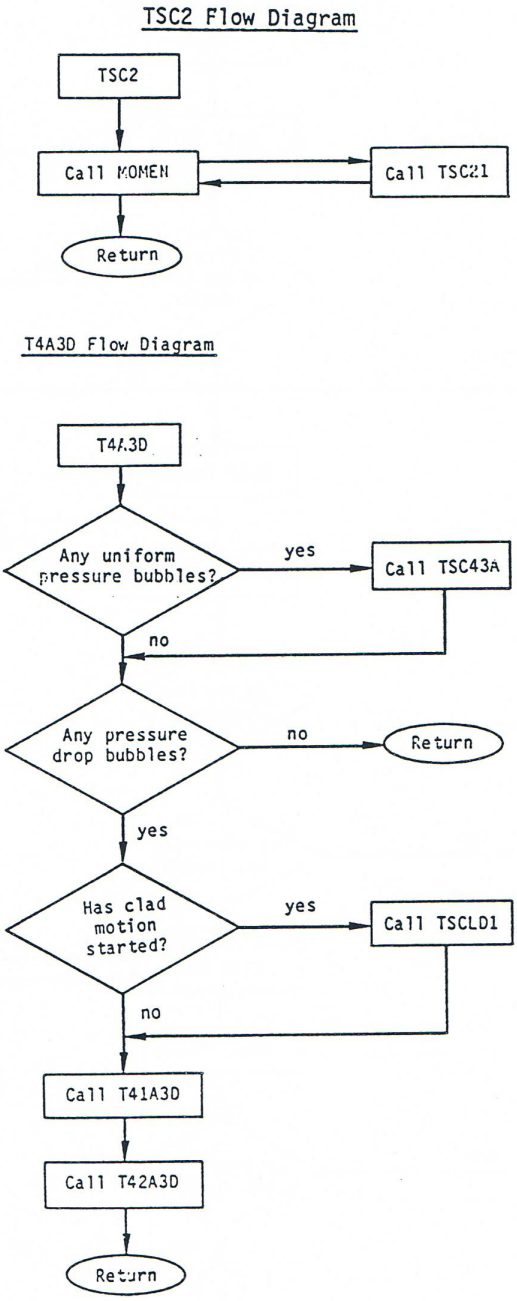

Figure 12.10-2. Flow Chart of the Voiding Model Coding (Cont'd)

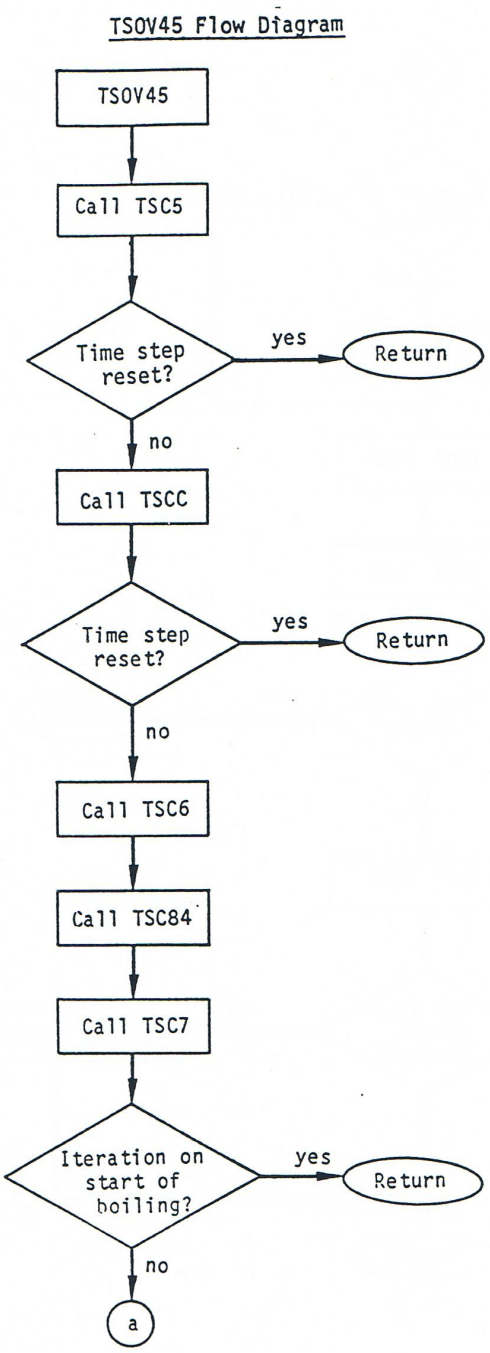

Figure 12.10-3. Flow Chart of the Voiding Model Coding (Cont'd)

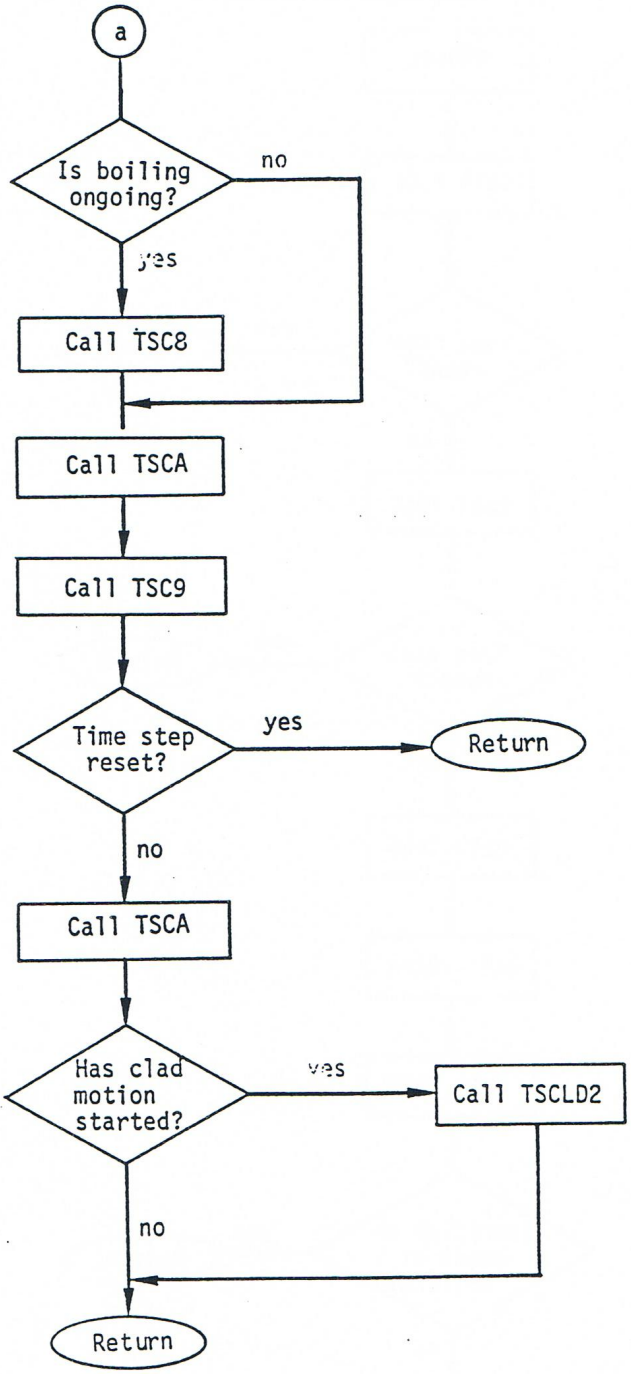

Figure 12.10-4. Flow Chart of the Voiding Model Coding (Cont'd)

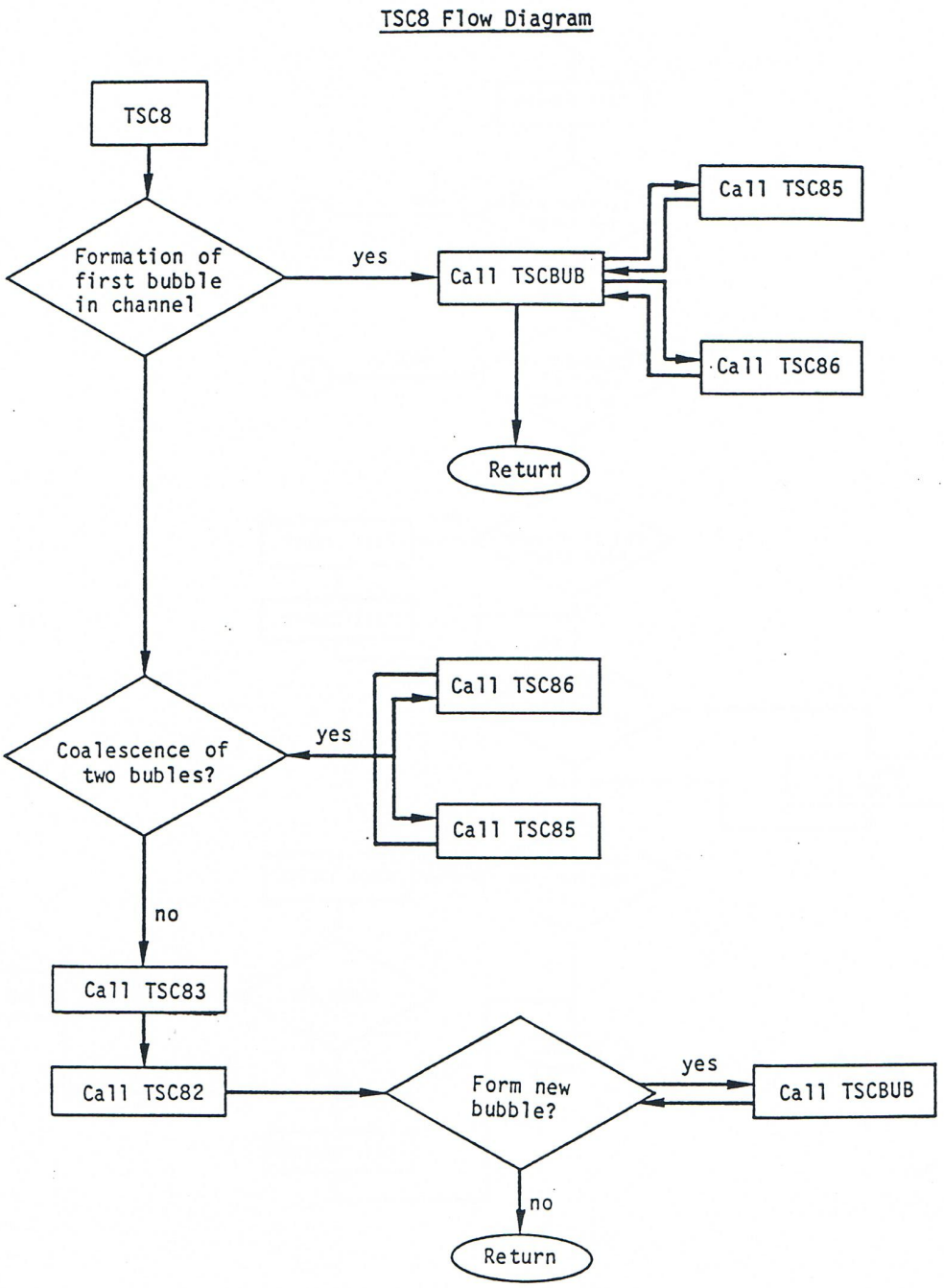

Figure 12.10-5. Flow Chart of the Voiding Model Coding (Cont'd)

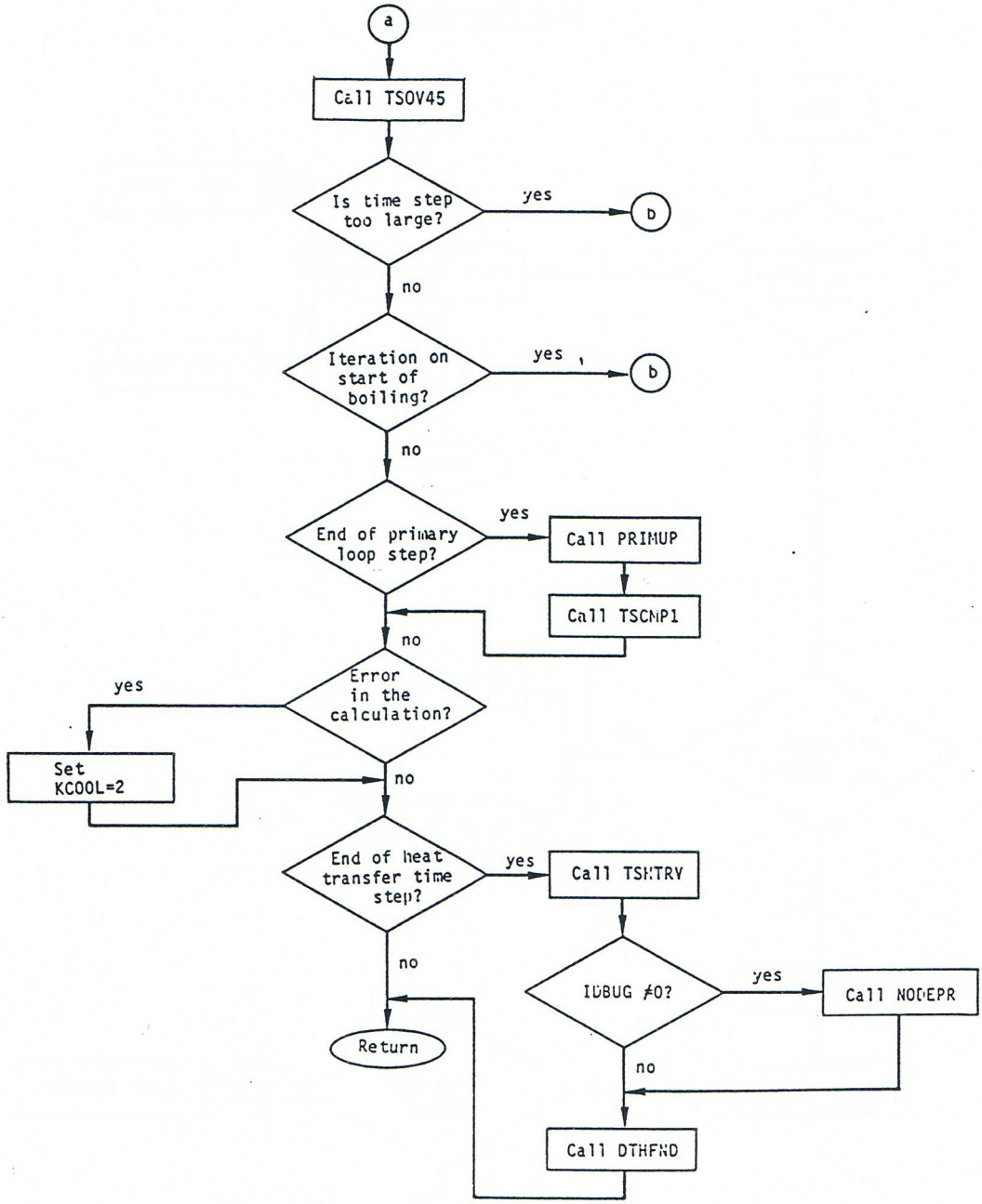

Figure 12.10-6. Flow chart of the Voiding Model Coding

Table 12.10-1. Alphabetical Listing of Voiding Model Subroutines with Description

Subroutine	Description
CHIN	Calculates the ratio of the fuel pin outer perimeter to the coolant area. Called by TSBOIL.
DTHFND	Calculates new heat-transfer time step. Called by TSBOIL.
MOMEN	Computes the terms in the momentum equation for each segment of each liquid slug. Called by TSC2.
NODEPR	Gives printout of all temperatures. Called by TSBOIL.
ORUNYO	Updates data for PRIMAR-4. Called TSBOIL.
TSBOIL	Drives the two-phase calculation. Also, forms a new gas bubble, if necessary, when pin rupture occurs, and reduces the time step when approaching rupture. Called for TSTHRM each coolant time step.
TSCA	Comprises two independent sections. First section calls TSCA1 and TSCA2. Second section computes film heat-transfer coefficients and heat fluxes and sets cladding temperatures in the fuel pin for the next time step. Reduces the gas mass in a bubble when part of the bubble is cut off after blowing out the top of the subassembly. Called by TSOV45.
TSCA1	Calculates increments to the integrated heat fluxes from the cladding to the coolant and from the structure to the coolant. Also calculates increments to the film heat-transfer coefficients and the average sodium density. Called by TSCA.
TSCA2	Calculates temperatures of structure, reflectors, cladding in the plenum, and gas in the plenum. Also, calculates mass of gas in the plenum and in a bubble. Called by TSCA.
TSCBUB	Creates a new vapor bubble. Also, sets the initial gas mass in a bubble to zero. Called by TSC8 and TSC82.
TSCC	Calculates film motion (not currently used). Called by TSOV45.
TSCLD1	Driver subroutine for cladding motion. Called by T4A3D.
TSCLD2	Performs moving cladding velocity calculation. Called by TSO45.
TSCMP1	Updates inlet and outlet pressures. Called by TSBOIL.
TSCSET	Initializes coolant variables and gas release variables each coolant time step. Called by TSBOIL.
TSC2	Extrapolates coolant, cladding, and structure temperatures; computes density, thermal conductivity, heat capacity, and viscosity at the extrapolated time; and computes the change in coolant flow rate, neglecting the pressure change with time at the interfaces. Called by TSBOIL.
TSC21	Computes the terms in the momentum equation for each fully liquid segment of each coolant slug. Called by MOMEN.

Subroutine	Description
TSC3	Computes coolant heat transfer coefficient and film thicknesses. Also calculates heat flow and gas source to uniform pressure bubbles. Adjusts condensation coefficient when gas is present. Called by TSBOIL.
TSC31	Function used by TSC3 to calculate liquid film heat transfer coefficients in voided regions.
TSC43A	Calculates vapor temperatures and pressures in uniform pressure bubbles. Called by T4A3D.
TSC5	Calculates liquid slug flow rates and liquid-vapor interface positions after the first bubble is formed. Called by TSOV45.
TSC6	Calculates temperatures in liquid slugs. Called by TSOV45.
TSC7	Computes pressure and saturation temperatures in liquid slugs and performs the iteration to specify the time at which boiling starts. Called by TSOV45.
TSC8	Performs accounting for bubble collapse, bubble formation, liquid slug expulsion and reentry, and combination of bubbles upon disappearance of a liquid slug. Called by TSOV45.
TSC82	Checks for formation of a new bubble (other than the first bubble formed in the subassembly). Called by TSC8.
TSC83	Calculates liquid slug expulsion and reentry. Called by TSC8.
TSC84	Calculates bubble collapse. Called by TSOV45.
TSC85	Performs vapor bubble accounting. Called by TSC8, TSCBUB, and TSC84.
TSC86	Performs liquid slug accounting. Called by TSC8, TSCBUB, and TSC84.
TSC87	Keeps track of which bubble is in contact with the rupture if gas is being released. Called from TSC8.
TSC9	Computes next coolant time step size. Also evaluates and resets the current time step if the step size is too large. Called by TSOV45.
TSHTRV	Transient state heat transfer. Called by TSBOIL.
TSILLB	Initializes cladding temperatures, velocities at interfaces, and interface positions. Called by TSBOIL only for the first coolant time step.
TSOV45	Drives the calculation of the pressure, temperature, and flow rates in the liquid slugs and the bubble accounting. Also calculates the gas fraction in each bubble. Called by TSBOIL.
T4A3D	Separates pressure drop and uniform-pressure bubble calculations and initializes variables for calculation of vapor pressures and mass flow rates. Called by TSBOIL.

Subroutine	Description
T41A3D	Sets up matrix for pressure-drop bubble calculations. Also, for the gas release model, calculates the gas source into pressure gradient bubbles and adjusts friction factors. Called by T4A3D.
T42A3D	Calculates solution of simultaneous equations by Gaussian elimination to solve for changes in pressures and mass flow rates in pressure-drop bubbles. Called by T4A3D.

12.11 Input Description

Table 12.11-1 lists the input information that is needed in order to run the voiding model section of the SASSYS-1 and SAS4A Codes. This information is of two types: that used directly in the voiding calculation and that used by models which provide necessary input to the voiding model. This listing is a subset of the full input listing given in Appendix 2.2. To simplify the discussion of the information displayed in Table 12.11-1, the input variables will not be examined in the order presented in the table, but rather, they will be presented in groups of data by category, i.e., all variables pertaining to materials properties will be discussed together, all which give problem geometry information will be grouped together, etc. This discussion should be helpful to users trying to assemble input decks for running their own problems.

The variables which provide information on materials properties will be described first. Most materials-property information, other than that for sodium, is provided through input rather than being fixed within the code in order to allow greater flexibility in the use of SASSYS-1. In most cases, this information is input in the form of tables; however, in the case of the solid fuel density and fuel thermal conductivity, either tables or coefficients for functional relationships can be entered. The choice between these two options is made on a channel-by-channel basis and is flagged by the variable IRHOK (Block 51, 3); a positive value of IRHOK indicates that the functional form has been selected, and a non-positive value means that the tabular format has been chosen. The variable COEFDS (Block 13, 1-3) contains the coefficients for the fuel density relationship as a function of temperature, while RHOTAB (Block 13,91-250) contains a table of fuel density as a function of temperature RHOTEM (Block 13, 251-410). Similarly, the coefficient for the thermal conductivity function can be read into COEFK (Block 13, 4-10), while a table of thermal conductivity values can be used in XKTAB (Block 13, 420-570) together with a table of temperatures in XKTEM (Block 13, 580-599). In addition, the specific heat of the fuel is read into the table CPFTAB (Block 13, 606-765) as a function of temperature CPFTEM (Block 13, 766-785).

Table 12.11-1. List of Input Variables Needed by the Voiding Model

Equation Variable	Reference Equation Number	Input Variable	Input Location	Suggested Value	External Reference
-	-	NCHAN	Block 1, #1	-	-
-	-	IFUEL1	Block 1, #3	-	-
-	-	ICLAD1	Block 1, #4	-	-
-	-	IPLUP	Block 1, #5	-	-
-	-	ITKEL	Block 1, #7	-	-
-	-	IPOWER	Block 1, #8	-	-
-	-	IPOWOP	Block 1, #9	-	-
-	-	MAXSTP	Block 1, #11	-	-
-	-	IPO	Block 1, #12	-	-
-	-	IPOBOI	Block 1, #13	-	-
-	-	IBLPRT	Block 1, #14	-	-
-	-	NPREAT	Block 1, #18	-	-
-	-	NPRES	Block 1, #19	-	-
-	-	IFLOW	Block 1, #20	-	-
-	-	NTOTAB	Block 1, #22	-	-
-	-	DTO	Block 11, #5	-	-
-	-	DTMXB	Block 11, #6	-	-
-	-	TIMAX	Block 11, #7	-	-
-	-	DTFUEL	Block 11, #10	-	-
-	-	DTCLAD	Block 11, #11	-	-
-	-	DTMMXB	Block 11, #21	-	-
-	-	DPWMAX	Block 11, #22	-	-
	-	POW	Block 12, #1	-	-
	-	PREATB	Block 12, #29-48	-	-
	-	PREATM	Block 12 #49-68	-	-
	-	FRPR	Block 12 #69	-	-
	-	FRFLOW	Block 12 #70	-	-
ρ_f	-	COEFDS	Block 13, #1-3	11.08×10^3, 2.04×10^{-5},	-

				8.7×10^{-9}	
k_f	-	COEFK	Block 13, #4-10	2.1, 2.88×10^{-3}, 2.52×10^{-5}, 5.83×10^{-10}, 5.75×10^{-2}, 5.03×10^{-4}, 2.91×10^{-11}	-
k_c	-	EXKTB	Block 13, #11-70	-	-
-	-	EXKTM	Block 13, #71-90	-	-
ρ_f	-	RHOTAB	Block 13, #91-250	-	-
-	-	RHOTEM	Block 13, #251-410	-	-
-	-	TR	Block 13, #419	300	-
k_f	-	XKTAB	Block 13, #420579	-	-
-	-	XKTEM	Block 13, #580-599	-	-
C_f	-	CPFTAB	Block 13, #606-765	-	-
-	-	CPFTEM	Block 13, #766-785	-	-
-	-	TFSOL	Block 13, #786-793	-	-
-	-	TFLIQ	Block 13, #794-801	-	-
-	-	UFMELT	Block 13, #802-809	-	-
-	-	TESOL	Block 13, #810-812	-	-
-	-	TELIQ	Block 13, #813-815	-	-
-	-	UEMELT	Block 13, #816-818	-	-
-	-	CPCTAB	Block 13, #819-878	-	-
-	-	CPCTEM	Block 13, #879-898	-	-
$(C\rho)_e$	-	CROETB	Block 13, #990-1049	-	-
-	-	CROETM	Block 13, #1050-1069	-	-
C_e	-	CE	Block 13, #1070-1072	690	-
γ	12.7-21	GAMGAS	Block 14, #1299	1.3-1.6	-
P_x	-	PX	Block 13, #1	-	-
-	-	PDEC	Block 13, #2	-	-
-	-	PDEC1	Block 13, #3	-	-
-	-	PDEC2	Block 13, #4	-	-
-	-	PRETAB	Block 14, #5-24	-	-
-	-	PRETME	Block 14, #25-44	-	-
T_O	-	TOTAB	Block 14, #45-64	-	-

-	-	TOTME	Block 14, #65-84	-	-
-	-	ZPLENL	Block 14, #87	-	-
-	-	ZPLENU	Block 14, #88	-	-
ΔZ_{bl}	12.7-28	DZBCGL	Block 14, #90	.1	-
ΔZ_{bu}	-	DZBCGU	Block 14, #91	.25	-
-	-	IDBUGV	Block 51, #1	-	-
-	-	IERSTP	Block 51, #2	-	-
-	-	IRHOK	Block 51, #3	-	-
-	-	NPLN	Block 51, #4	-	-
-	-	NREFB	Block 51, #5	-	-
-	-	NREFT	Block 51, #6	-	-
-	-	NZNODE	Block 51, #7-13	-	-
-	-	NT	Block 51, #14	-	-
-	-	IFUELV	Block 51, #15	-	-
-	-	IFUELB	Block 51, #16	-	-
-	-	ICLADV	Block 51, #17	-	-
-	-	IHGAP	Block 51, #24	-	-
-	-	NPIN	Block 51, #25	-	-
-	-	NSUBAS	Block 51, #26	-	-
-	-	MZUB	Block 51, #27	-	-
-	-	MZLB	Block 51, #28	-	-
-	-	IHEX	Block 51, #29	-	-
-	-	ISSFUE	Block 51, #32	-	-
-	-	ILAG	Block 51, #34	-	-
-	-	ICLADB	Block 51, #85	-	-
-	-	MFAIL	Block 51, #86	-	-
-	-	IFAIL	Block 51, #87	-	-
-	-	JFAIL	Block 51, #88	-	-
-	-	IDBFLG	Block 51, #98-107	-	-
-	-	IDBSTP	Block 51, #108-117	-	-
-	-	IEQMAS	Block 51, #118	-	-
-	-	IBLPRN	Block 51, #119	-	-
-	-	IDBGBL	Block 51, #120	-	-
-	-	IDBLST	Block 51, #121	-	-
-	-	ISSFU2	Block 51, #122	-	-

-	-	IFILM	Block 51, #128	-	-
-	-	NZONF	Block 51, #129-131	-	-
-	-	IFUELI	Block 51, #132-155	-	-
-	-	NODNUM	Block 51, #156-179	-	-
-	-	IGASRL	Block 51, #278	0 or 1	-
-	-	IGRLTM	Block 51, 279	0 or 1	-
A_c	12.2-1	ACCZ	Block 61, #1-7	-	-
Δz	12.2-4	AXHI	Block 61, #8-31	-	-
D_h	12.2-7	DHZ	Block 61, #32-38	-	-
-	-	DSTIZ	Block 61, #39-45	-	-
-	-	DSTOZ	Block 61, #46-52	-	-
-	-	PLENL	Block 61, #53	-	-
-	-	RBR	Block 61, #54-77	-	-
-	-	RER	Block 61, #78-101	-	-
-	-	RBRPL	Block 61, #102	-	-
-	-	RERPL	Block 61, #103	-	-
-	-	RINFP	Block 61, #104-127	-	-
-	-	ROUTFP	Block 61, #118-151	-	-
-	-	ZONEL	Block 61, #152-158	-	-
-	-	SRFSTZ	Block 61, #159-165	-	-
-	-	AREAPC	Block 61, #166	-	-
-	-	DRFO	Block 61, #169-175	-	-
-	-	RBRO	Block 61, #180	-	-
-	-	RERO	Block 61, #181	-	-
p_e	12.3-2	SER	Block 61, #182-188	-	-
-	-	DRFI	Block 61, #189-195	-	-
-	-	VFC	Block 61, #196	-	-
γ_s	-	GAMSS	Block 62, #2	-	-
γ_c	-	GAMTNC	Block 62, #4	-	-
γ_e	-	GAMTNE	Block 62, #5	-	-
-	-	PSHAPE	Block 62, #6-29	-	-
-	-	PSHAPR	Block 62, #30-44	-	-
-	-	AHBPAR	Block 63, #2	-	-
-	-	BHBPAR	Block 63, #3	-	-

-	-	CHBPAR	Block 63, #4	-	-
-	-	HBMAX	Block 63, #5	-	-
-	-	HBMIN	Block 63, #6	-	-
-	-	HBPAR	Block 63, #7	-	-
k_s	-	XKSTIZ	Block 63, #11-17	-	-
k_s	-	XKSTOZ	Block 63, #18-24	-	-
-	-	DEL	Block 63, #25	-	-
-	-	POGAS	Block 63, #27	-	-
k_f	-	XKRF	Block 63, #28-34	-	-
ρ_c	-	DENSS	Block 63, #35	-	-
$(\rho c)_s$	-	RHOCSI	Block 63, #37-43	-	-
$(\rho c)_s$	-	RHOCSO	Block 63, #44-50	-	-
$(\rho c)_r$	-	RHOCR	Block 63, #51-57	-	-
$(\rho c)_g$	-	RHOCG	Block 63, #58	-	-
R_g	-	RG	Block 63, #59	-	-
A_{fr}	12.2-2	AFR	Block 64, #1	0.1875	5-22
b_{fr}	12.2-2	BFR	Block 64, #2	-0.2	5-22
-	-	C1	Block 64, #3	-	5-22
-	-	C2	Block 64, #4	-	5-22
-	-	C3	Block 64, #5	-	5-22
-	-	DWMAX	Block 64, #6	0.2	-
w	-	WO	Block 64, #47	-	-
K_{or}	12.2-9	XKORV	Block 64, #48-63	-	5-23
$(\Delta z_i/A)_b$	12.8-6	DZIAB	Block 64, #65	$(D_h/2\ A_c)$	-
$(\Delta z_i/A)_t$	12.8-6	DZIAT	Block 64, #66	$(D_h/2\ A_c)$	-
$\theta 1$	12.2-15	THETA1	Block 64, #67	-	-
$\theta 2$	12.2-15	THETA2	Block 64, #68	-	-
-	-	DTLMAX	Block 64, #69	-15	-
-	-	DTVMAX	Block 64, #70	50	-
-	-	DZIMAX	Block 64, #71	0.1	-
h_{cond}	-	HCOND	Block 64, #72	-	-
-	-	SLMIN	Block 64, #73	0.02	-
-	-	TUPL	Block 64, #74	-	-
-	-	WFMIN	Block 64, #75	0.667 x	-

				WFO	
-	-	WFMINS	Block 64, #76	WFMIN	-
w_{fs}	12.5-12	WFSOO	Block 64, #77	WFO	-
f_m	12.7-1	FRACP	Block 64, #78-80	-	-
-	-	FRUPT	Block 64, #81-83	-	-
w_{fe}	12.5-8	WFO	Block 64, #84	-	-
-	-	DTSI	Block 64, #164	3	-
-	-	DTS	Block 64, #165	10	-
A_{fr}	12.6-9	AFRV	Block 64, #168	0.316	5-22
b_{fr}	12.6-9	BFRV	Block 64, #169	-0.25	5-22
-	-	XMINL	Block 64, #170	0.05	-
-	-	DTCMIN	Block 64, #171	-	-
-	-	WFMIND	Block 64, #172	-	-
-	-	WFMNSD	Block 64, #173	-	-
$f_{2\phi}$	12.6-10	FVAPM	Block 64, #174	0	5-7
A_{fr}	-	AFRF	Block 64, #175	0.316	5-22
b_{fr}	-	BFRF	Block 64, #176	-0.25	5.7
-	-	TPDMIN	Block 64, #177	1.0×10^{-5}	5-22
A^*	12.7.1	AGSRLS	Block 64, #181	-	-
k_g	12.7.1	GASKOR	Block 64, #182	1.5-2	-
		PGRMIN	Block 64, #183	-	-
M_{wg}	12.7-31	GASMW	Block 64, #184	100-130	-
		TMFAIL	Block 64, #186-188	-	-

Since the SASSYS-1 or SAS4A calculation can accommodate up to eight different types of fuel material, the number of fuel types used in a given data deck must be specified. This is done through the variable IFULE1 (Block 1, 3). The fuel types must then each be designated as belonging to the core or the blankets. If, in a given channel, the blankets are of one homogeneous material and the core is of another, the quantity IFUELV (Block 51, 15) specifies which of the IFULE1 fuel types is assigned to the core, while IFULEB (Bloc 51, 16) indicates which is assigned to the radial blankets. If, on the other hand, the core and/or blankets each consist of radial bands of different types of fuel, the variable IFUEL1 (Block 51, 132-155) is used to match up each radial zone with the appropriate fuel type in both the core and the blankets.

The cladding properties are used only in tabular form by the code. Although only one type of cladding material is used in any one channel, different types may be used in

different channels. The total number of types (maximum of three) for a particular run is designated in ICLAD1 (Block 1, 4), and the type assigned to each channel is specified in ICLADV (Block 51, 17). The cladding thermal conductivity values are input to EXKTB (Block 13, 11-70) as a function of temperature EXKTM (Block 13, 71-90). The specific heats are entered in CPCTAB (Block 13, 819-878) with the corresponding temperatures CPCTEM (Block 13, 879-898). The product of the cladding specific heat and the density is entered as a variable in CROETB (Block 13, 990-1049) as a function of temperature CROETM (Block 13, 1050-1069). In addition, the specific heat of the cladding at the solidus temperature is specified in CE (Block 13, 1070-1072). Finally, the density of the solid cladding at an input reference temperature is given for each channel in DENSS (Block 63, 35).

The material properties for the structure and reflector regions are also input in tabular form. In the case of the structure, the code allows different sets of properties to be used for the inner and outer structure nodes. However, the properties are constant for each node within a particular zone and are independent of temperature. The thermal conductivity for the inner structure node is stored in XKSTIZ (Block 63, 11-17), and that for the outer node is input to XKSTOZ (Block 63, 18-24). Similarly, the product of the density and the heat capacity for the inner node is read into RHOCSI (Block 63, 37-43), and for the outer node, this quantity is stored in RHOCSO (Block 63, 44-50). Of course, the structure properties can vary from channel to channel.

The materials properties for the reflectors are also considered to be constant within a given zone and independent of temperature. However, unlike the case of the structure, the reflector variables are not allowed to differ between the inner and outer segments. The thermal conductivity is given in XKRF (Block 63, 28-34), and the product of density and heat capacity is input to RHOCR (Block 63, 51-57). These, too, may be different in different channels.

A couple of properties are input for the gas plenum. The product of density and heat capacity for the plenum gas is found in RHOCG (Block 63, 58), and the thermal resistance of the gas is given in RG (Block 63, 59). These are both independent of temperature and variable form channel to channel.

As indicated earlier in the text, several fluid heat-transfer coefficients are required in order to model the heat transfer to the sodium. For the bond which exists between the fuel and the cladding, the heat-transfer coefficient is given by a correlation for which the coefficients are read into AHPAR, BHBPAR, CHBPAR (Block 63, 2-4), and HBPAR (Block 63, 7). The limits on the bond heat-transfer coefficient are set in HBMAX and HBMIN (Block 63, 5-6). Also, the option exists for calculating the coefficient by the method used in the SAS3D code; this option is invoked by setting the variable IHGAP (Block 51, 24) to zero. The convective heat-transfer coefficient of the sodium is given by the Dittus-Boettler correlation, for which the coefficients C1, C2, and C3 (Block 64, 3-5) must be input. If condensation of sodium vapor onto the cladding or structure is occurring, the user-supplied condensation heat-transfer coefficient HCOND (Block 64, 72) must be employed.

Much of the input to the voiding model is concerned with the geometry of the problem. Most of this information can be varied from channel to channel, but a few geometry-related features are consistent throughout the system. First, of course, the number of channels must be specified in NCHAN (Block 1, 1). The location of the gas plenum must also be set through the variable IPLUP (Block 1, 5); IPLUP=0 fixes the plenum above the core, while IPLUP=1 designates that it does below the core. The heights of the lower coolant plenum inlet and the upper coolant plenum outlet (ZPLENL and ZPLENU, Block 14, 87-88) must be input. Finally, because modeling exists in SASSYS-1 to allow material expansion with temperature, the temperature at which the input geometry information is measured must be known; this is specified in TR (Block 13, 419).

Much of the geometric information is initially assumed constant within each axial zone and therefore is read in zone by zone. This requires specification of the number of zones. The pin section always constitutes ne axial zone, and each reflector contains from one to five zones. The number of zones in the lower axial reflector is read into NREFB (Block 51, 5), while that for the upper reflector is given in NREFT (Block 51, 6). The data which are input on a zonal basis are the coolant flow area per fuel pin ACCZ (Block 61, 1-7), the hydraulic diameter DHZ (Block 61, 32-38), and the length of each zone ZONEL (Block 61, 152-158). The structure variables designating the thickness of the inner node (DSTIZ, Block 61, 39-45) and the outer node (DSTOX, Block 61, 46-52) are read in by zone, as is the structure perimeter SRFSTZ (Block 61, 159-165). Finally, the thicknesses of the outer and inner reflector segments (DRFO, Block 61, 169-175), and DRFI, block 61, 189-195, respectively) and the reflector perimeter SER (Block 61, 182-188) are all input by zone.

Some of the remaining geometric information is read in by axial mesh segment. The input information required about the axial mesh structure includes the number of mesh segments in the gas plenum NPLN (Block 51, 4), the number of segments in the upper and lower blankets (MZUB and MZLB, respectively, Block 51, 27-28), and the total number of segments in each axial zone (NZNODE, Block 51, 7-13). Quantities for which a value must be entered for each axial mesh segment in the pin region include AXHI, the length of each axial segment (Block 61, 8-31); RBR, the inner radius of the cladding (Block 61, 54-77); RER, the outer radius of the cladding (Block 61, 78-101); RINFP, the fuel inner radius (Block 61, 104-127); and ROUTFP, the fuel outer radius (Block 61, 128-151).

Some geometric variables define the radial composition of the problem. These include data such as the number of radial temperature segments in the fuel (NT, Block 51, 14), the number of concentric rings of different types of fuel in the core and blankets (NZONF, Block 51, 129-131), the radial mesh boundaries of the fuel rings (NODNUM, Block 51, 156-179), and a flag to specify whether the radial mesh is set up on an equal radius or equal mass basis (EQMAS, Block 51, 118).

A few additional pieces of information on the problem geometry must be input. The cladding inner and outer radii in the gas plenum (RBRPL and RERPL, Block 61, 102-103) must be specified separately from the values in the pin region (RBR and RER, mentioned above), as must values for the nominal cladding inner and outer radii (RBRO

and RERO, Block 61, 180-181). The nominal radii simply represent average values in the pin region; usually the cladding radii in the pin are all equal at the beginning of a run, and the nominal radii are just set to these values. The length of the fission-gas plenum is given in PLENL (Block 61, 53), the area of the coolant channel plus the pin is set in AREAPC (Block 61, 166), and the volume fraction fo the coolant in the channel is represented in VFC (Block 61, 196). The inertial terms below and above the subassembly are read into DZIAB and DZIAT (Block 64, 65-66), and the orifice coefficients at the entrance and exit of each axial zone are store in XKORV (Block 64, 48-63). The number of pins per subassembly is given in NPIN (Block 51, 25), and the number of subassemblies represented by the channel is designated in NSUBAS (Block 51, 26).

Another category of input data is that of temperature initialization. The inlet temperature TOTAB (Block 14, 45-64) must be specified as a function of time TOTME (Block 14, 65-84), with NTOTAB (Block 1, 22) being the number of entries in the inlet temperature table. The temperature of any liquid sodium which reenters the subassembly from the top is fixed at TUPL (Block 64, 74). The solidus and liquidus temperatures of the fuel are given in TFSOL and TFLIQ, respectively (Block 13, 786-793 and 794-801), while those for the cladding are defined in TESOL and TELIQ (block 13, 810-812 and 813-815). The flag which directs whether an Eulerian or a Lagrangian liquid temperature calculation is performed prior to flow reversal is set in ILAG (Block 51, 34), and the amount of superheat required before boiling can begin is fixed in DTS (Block 64, 165). The superheat required for formation of new bubbles after voiding has begun is given by DTSI (Block 64, 164).

Several pieces of information concerning reactor power must be input. The code contains an option for specifying either the power or the external reactivity as a function of time, and the flag IPOWR (Block 1, 8) indicates which quantity is chosen. A total of NPREAT (Block 1, 18) values of the power are read into the array PREATB (Block 12, 29-48), with the corresponding times read into array PREATM (Block 12. 49-68). The flag IPOWOP (Block 1, 9) determines whether the total steady-state reactor power is computed form the power in the peak axial segment, or vice versa, and the power in the peak axial segment is entered in POW (Block 12, 1). The fraction of the total reactor power represented by all the SASSYS-1 channels must be given, since some possible channel configurations omit a few low power channels which must be given, since some possible channel configurations omit a few low channels which have a minimal impact on the calculation, and this number is input to FRPR (block 12, 69).

The remaining power-related data must be inserted channel by channel. The fraction of the total power due to direct gamma heating must be specified for the structure (GAMSS), coolant (GAMTNC), and cladding (GAMTNE) (block 62, 2, 4, and 5). In addition, the axial and radial shapes of the power distribution are read into PSHAPE (Block 62, 6-29) and PSHAPR (Block 62, 30-44), respectively.

Several conditions concerning the coolant pressure must be designated through the input. The coolant exit pressure is held constant throughout the calculation and is read into variable PX (Block 14, 1). The magnitude of the coolant inlet pressure at steady state is computed by the code, but, if the PRIMAR-4 option is not invoked, the variation

of the normalized inlet pressure with time is either read from a table or calculated from a simple equation. The flag NPRES (Block 1, 19) determines whether the table or the equation will be used. If the equation is chosen, the coefficients PDEC, PDEC1, and PDEC2 (Block 14, 2-4) must be entered. If the inlet pressure is to be determined from a table, the values are entered in PRETAB (Block 14, 5-24), with the corresponding times specified in PRETME (Block 14, 25-44). There is also an option to enter the coolant flow rather than the driving pressure in PRETAB. This option is indicated by the flag IFLOW (Block 1, 20). The user specified coolant flow vs. time is only available if the PRIMAR-1 option is used, IPRION (Block, 27) = 1. With this option, the coolant flow rate in channel IFLOW is specified as a function of time. The outlet plenum pressure is also specified as a function of time. The code back-calculates the inlet plenum pressure required to give the specified flow rate, and this inlet plenum pressure drives the coolant flow in all other channels. Currently, this option does not work after the onset of boiling in channel IFLOW. Finally, the initial gas pressure in the gas plenum at the reference temperature TR is input through POGAS (Block 63, 27).

Two other areas for which input data are needed are the expressions for calculation of friction discussed earlier and the determination of sodium film thickness in voided regions. The coefficients A_{fr} and b_{fr} which are used in the friction expressions are user-input rather than fixed within the code to allow greater flexibility. These include coefficients for the liquid slugs (AFR and BFR, Block 64, 1-2), the sodium vapor (AFRV and BFRV, Block 64, 168-169), and the liquid sodium film (AFRF and BFRF, Block 64, 175-176). Also, the fraction of the two-phase friction factor to be used in voided regions is set in FFVAPM (Block 64, 174). The calculation of film thickness requires information about the initial film thickness left on cladding and structure as the voiding front passes by; these numbers are stored in WFO (Block 64, 84) for the cladding and WFS00 (Black 64, 77) for the structure. In addition, the SASSYS-1 model does not try to predict when the sodium films will evaporate completely (zero film thickness); rather, the films are considered to be evaporated when the calculated estimates them to be less than user-input values. In the early part of the calculation, these minimum values are WFMIN for the cladding and WRMINS for the structure (Block 64, 76-76), but after IFILM (Block 51, 128) axial segments have experienced dryout, the values in WFWIND and WFMNSD (Block 64, 172-173) are used instead.

A few additional pieces fo information are needed inorder to run the calculation. The steady-state coolant mass flow rate is input to WO (Block 64, 47) and the fractionof the total reactor flow which is actually represented by core channels is read into FRFLOW (Block 12, 70) (again, to accommodate channel maps which do not include all the subassemblies in the reactor; see the discussion of FRPR given above). The heat of fusion for the fuel is given in UFMELT (Block 13, 802-809), and that for the cladding is read into UEMELT (Block 13, 816-818). Also, the product of the Stefan-Boltzmann constant and the emissivity is assigned to the variable DEL (Block 63, 25).

The options for gas release due to pin failure are determined by IGASRL (Block 51, 278) and IGRLTM (Block 51, 279). If IGASRL=0, this option is not used. The method in which pin failure is determined is specified by IGRLTM. If IGRLTM = 0, then DEFORM-5 triggers pin failure in pin group M when the cladding life fraction exceeds FRUPT(M)

(Block 64, 81-83). If IGRLTM=1, then gas release is pin group M occurs in node IFAIL (Block 51, 88) at time TMFAIL(M) (Block 64, 186-188). In addition, the gas release model requires input values for DZBCGL (Block 14, 90) and DZBCGU (Block 14, 91) for cutting off bubbles after they flow out the top of the subassembly. GAMGAS (Block 14, 1299) and GASMW (Block 64, 184) provide properties of the gas. FRACP(M) (Block 64, 78-80) specifies the fraction of the pins in each group. AGSRLS (Block 64, 181) and GASKOR (Block 64, 182) determine the gas flow rate through the cladding rip, and PGRMIN specifies when gas release will be shut off. The initial plenum gas pressure is determined by POGAS (Block 63, 27) if it is not calculated by DEFORM.

Time-step control involves specification of a number of input variables. The maximum number of main time steps is given in MAXSTP (Block 1, 11), and the maximum problem tie is TIMAX (Block 11, 7). The initial main time-step size is DTO (Block 11, 5), and the maximum size after the initiation of voiding is DTMMXB (Block 11, 21). The maximum heat-transfer time-step length after boiling has begun is DTMXB (Block 11, 6). The minimum coolant time-step size before voiding is DTCMIN (Block 64, 171); after the onset of boiling, it is TPDMIN (Block 64, 177).

The different time-step sizes are limited by several input criteria. The main time step must be small enough so that the power does not make a fractional change greater than that specified in DPWMAX (Block 11, 22) during the step. The heat-transfer time step must be limited so that, over its span, the fuel temperature does not change by more than DTFUEL (Block 11, 10), the cladding temperature by more than DTCLAD (Block 11, 11), and, prior to voiding, the coolant flow rate by DWMAX (Block 64, 6). The coolant time-step size must be small enough so that the liquid temperature does not change by more than DTLMAX, the vapor temperature by more than DTVMAX, and the position of any liquid-vapor interface by more than DZIMAX (Block 64, 69-171).

Printout of results is guided by several input variables. Normally, a standard printout pertaining just to the voiding model is output at the end of designated coolant time steps, and a general standard printout is given at the end of designated main time steps. Boiling printout occurs every IBLPRN coolant time steps (Block 51, 119). General printout is done every IPO main time steps (Block 1, 12) up until main time step IBGLPRT (Block 1, 14); after step IBLPRT, general printout is given every IPOBOI time steps (Block 1, 13). The temperatures in the general printout may be listed in units of degrees Kelvin or degrees centigrade at the discretion of the user through the variable ITKEL (Block 1, 7); however, the user is advised that the labels in the printout will state that temperatures are listed in degrees Kelvin regardless of which option is chosen.

If desired, more detailed output can be obtained through several of the input variables. This is intended primarily for the use of the code developers and outside users who wish to modify the code, but it may on occasion be helpful if problems are encountered in simply running the code. The simplest of this additional output is flagged by the variable IHEX (Block 51, 29). This number will activate a hexadecimal printout of the sum of the coolant temperatures in a channel. The hexadecimal print is an exact representation of the sum (without truncation) and is therefore useful when comparing two different runs of similar data decks to indicate at what point the two

calculations began to diverge. A more extensive output is invoked by the variable IDBUGV (Block 51, 1). As indicated in Table 3.10-1, many different printout options are incorporated into IDBUGV. The print selected will begin at step IERSTP (Block 51, 2). Prints specialized to the voiding model are also available. The variable IDBGBL (Block 51, 120) will trigger the same extensive voiding-related output as the IDBUGV=4 option, but it will begin the output on coolant time step IDBLST (Block 51, 121) rather than on main time step IERSTP. This allows the user to begin a lengthy printout much closer to the time at which the difficulty develops than is possible with IDBUGV. The array IDBFLG (Block 51, 98-107) initiates more specialized voiding points. The coolant time step on which each of these prints starts is stored in array IDBSTP (Block 51, 108, 117).

A few additional input variables remain to be discussed. The remaining quantities include THETA1 and THETA2 (Block 64, 67-68), the coefficients which determine the degree of implicitness of the liquid slug calculation; SLMIN (Block 64, 73), the minimum length of a liquid slug in between two vapor bubbles (minimum slug length is required to stabilize the calculation); and XMINL (Block 64, 170), the bubble length above which the pressure gradient voiding model is used and below which the pressure gradient voiding model is used.

12.12 Sample Output

Samples of the voiding model output are presented in Figs. 12.12-1 and 12.12-2. A brief discussion of the data contained in these figures will be given shortly, but first, an explanation of the categories of information listed will be presented. Beginning with the first line of headings in the output, the items listed are as follows:

bubble number – the row to which this heading belongs gives information about each bubble that is currently in the channel. The bubble number identifies each bubble uniquely and is assigned in the order in which the bubbles are formed.

gas type – in future modeling, bubbles will be allowed to contain fission gas or fission gas/sodium vapor mixtures, as well as pure sodium vapor, and the composition of the bubble will be identified by the gas type number. For now, all bubbles are gas type 1 (pure sodium vapor).

interface position – this gives the axial position, in meters, of the lower and upper vapor-liquid interfaces of each bubble in the channel. Bubbles are listed in this section of the output in increasing order of axial position.

velocity – the velocity with which each interface is moving is given in this column in meters per second.

pressure – the saturation vapor pressure at each interface in pascals.

vapor and liquid temperatures – as discussed in the introduction to the chapter, sharp temperature gradients are sometimes present at liquid-vapor interfaces, so at each interface, the code computes a vapor temperature and a liquid temperature a short distance away from the interface. These two temperatures are listed in the output for each interface in kelvins.

boiling time – This is the time in seconds that has elapsed since the bubble was formed.

cladding film thickness – this is the thickness in meters of the liquid sodium film which is present on the cladding in the vapor region by the liquid-vapor interface.

cladding film velocity – in a later version of the code, the liquid film on the cladding will be allowed to move, and this column will show the speed in meters per second with which the film is moving at the interfaces. At the moment, the film velocity is considered to be zero.

structure film thickness – the thickness in meters of the liquid film on the structure in each interfacial vapor region.

axial node – this heading begins a new section of the printout in which information is presented on a node-by-node basis. The axial node number identifies each axial mesh segment interface.

axial position – this is the height along the channel, in meters, of each axial node.

coolant pressure – this is the saturation pressure, in pascals, at each axial node. If the node is contained in a liquid slug, it is the pressure in the liquid, and if the node is part of a vapor bubble, it is the vapor pressure.

coolant flow rate – this is the mass flow rate, in kilograms per second, of the sodium at each node. In liquid nodes, it is the flow rate of the liquid sodium, while in vapor nodes it is that of the sodium vapor.

cladding film velocity – this is the velocity in meters per second of the liquid sodium film on the cladding at each axial node. As mentioned above in the discussion of film velocity at the interfaces, the film velocity is currently set to zero in the code.

cladding film thickness – the thickness in meters of the liquid film on the cladding. This variable is a constraint over a given axial mesh segment (just as the coolant flow area is), and therefore it should actually be designated by axial segment number rather than by axial node number. Since the segment number is just the node number of the node at the bottom of the segment, this variable is listed in the output by the axial node number for segments 1 through MZC-1, with the entry for axial node MZC to be ignored.

clad temperature – this is the cladding temperature, in kelvins, at the midpoint of each axial mesh segment. The comments just made about the listing of the clad film thickness in the output therefore also apply to the cladding temperature; that is, the axial node numbers should be regarded as axial segment numbers for this variable.

saturation temperature – the saturation temperature in kelvins corresponding to the coolant pressure. This variable is calculated at the axial anodes and is listed in that format in the output.

structure temperature – the temperature in kelvins of the structure material. Like the cladding temperature, it is calculated at the mesh segment midpoints and is listed as such in the output.

structure film thickness – the thickness in meters of the liquid sodium film on the structure. It is constant over a given axial mesh segment and is thus listed by segment number.

TCBAR2 – this is the coolant temperature in kelvins at the midpoint of the mesh segment. The heading is jus the name of the variable used in the coding. It is listed by mesh segment, just as the cladding and structure temperatures are.

reflector temperature – the temperature in kelvins in the reflector regions. It too, is computed at the midpoint of the mesh segment and is given by segment number.

Figures 12.12-1 and 12.12-2 show two examples of data presented in the format just discussed. Both are taken from a run made for the analysis of a loss-of-flow case. Figure 12.12-1 gives information about conditions in the lead channel a short time after voiding initiation. Already, twelve bubbles have formed and the first seven have either collapsed or been swept out of the channel. At this point, all the bubbles are small enough to use the uniform vapor pressure model, as shown by the axially constant pressure and vapor temperature in each bubble. Most of the bubbles are contained in one axial mesh segment, but one, bubble 10, spans a segment interface; this produces the mass flow rate of zero in node 32, since the flow rate is assumed to be zero in the uniform-vapor-pressure model.

Figure 12.12-2 presents data about the same channel at a more advanced stage of voiding. Only one bubble is present in the channel, although more than ninety have been formed since voiding started. The pressure-gradient model is now in operation, and the upper bubble interface is past the top of the channel. A significant region of the cladding has experienced film dryout (i.e., the film thickness calculated by the code has dropped below a user-input minimum value and therefore the thickness has been set to zero), resulting in the high cladding temperatures shown in that region. On the other hand, the structure is cold enough that liquid has condensed on it, increasing the thickness of the film. This has also happened in some areas of the cladding. Note the large temperature difference at the lower void interface between the vapor and liquid temperatures – better than 100 K.

100 STEPS, 0.14657 SECONDS, SINCE BOILING STARTED IN CHANNEL 2 13 BUBBLES FORMED

337 MAIN TIME STEPS HAVE BEEN COMPLETED AT 0.16223D+02 SECONDS, COOLANT TIME STEP IS 0.48092000D-03

BUBBLE NUMBER	GAS TYPE	INTERFACE POSITION	VELOCITY	PRESSURE	TEMPERATURE VAPOR	TEMPERATURE LIQUID	BOILING TIME	* CLAD THICKNESS	FILM * VELOCITY	STRUCTURE THICKNESS	FILM VELOCITY
12	1	1.7739	2.326	0.1679D+06	1218.053	1222.611	0.00365	1.459D-04	0.0	1.460D-04	0.0
		1.7760	3.265	0.1679D+06	1218.053	1222.589		1.459D-04	0.0	1.460D-04	0.0
11	1	1.7961	3.265	0.1657D+06	1216.416	1222.199	0.01048	1.458D-04	0.0	1.461D-04	0.0
		1.8124	5.994	0.1657D+06	1216.416	1221.867		1.458D-04	0.0	1.461D-04	0.0
10	1	1.8325	5.996	0.1535D+06	1211.038	1220.252	0.02234	1.461D-04	0.0	1.462D-04	0.0
		1.8326	5.926	0.1535D+06	1211.038	1217.704		1.463D-04	0.0	1.461D-04	0.0
9	1	1.9008	5.926	0.1753D+06	1223.768	1215.004	0.02548	1.464D-04	0.0	1.461D-04	0.0
		1.9028	2.900	0.1753D+06	1223.768	1214.304		1.464D-04	0.0	1.461D-04	0.0

AXIAL NODE	AXIAL POSITION	COOLANT PRESSURE	COOLANT TEMPERATURE	COOLANT FLOW RATE	CLAD FILM VELOCITY	CLAD FILM THICKNESS	* * TEMPERATURE CLAD	SATURATION	* * STRUCTURE FILM STRUCTURE	FILM THICKNESS	TCBAR2	REFLECTOR TEMPERATURE
38	2.579	1.543D+05	1141.490	4.741D-02	0.0	1.460D-04	0.0	1207.72	0.0	1.460D-04	570.745	0.0
37	2.459	1.581D+05	1152.257	4.741D-02	0.0	1.460D-04	1141.22	1210.70	1145.10	1.460D-04	1146.873	1141.22
36	2.339	1.619D+05	1161.596	4.741D-02	0.0	1.460D-04	1152.11	1213.62	1156.01	1.460D-04	1156.927	1152.11
35	2.219	1.657D+05	1175.037	4.741D-02	0.0	1.460D-04	1162.95	1216.48	1166.93	1.460D-04	1168.342	1162.95
34	2.099	1.696D+05	1184.933	4.741D-02	0.0	1.460D-04	1173.85	1219.29	1177.89	1.460D-04	1180.010	1173.85
33	1.979	1.734D+05	1201.749	4.741D-02	0.0	1.460D-04	1185.53	1222.05	1189.15	1.460D-04	1193.341	1185.53
32	1.859	1.585D+05	1211.038	0.0	0.0	1.460D-04	1198.70	1211.04	1202.83	1.460D-04	1207.453	1198.70
31	1.696	1.691D+05	1222.722	3.547D-02	0.0	1.460D-04	1223.15	1218.93	1214.50	1.460D-04	1217.806	
30	1.614	1.703D+05	1222.610	3.547D-02	0.0	1.460D-04	1223.06	1219.84	1211.55	1.460D-04	1222.666	
29	1.533	1.716D+05	1220.829	3.547D-02	0.0	1.460D-04	1223.03	1220.74	1210.10	1.460D-04	1221.719	
28	1.451	1.728D+05	1217.075	3.547D-02	0.0	1.460D-04	1221.42	1221.65	1207.34	1.460D-04	1218.952	
27	1.399	1.737D+05	1201.438	3.547D-02	0.0	1.460D-04	1222.95	1222.23	1197.71	1.460D-04	1209.256	
26	1.347	1.745D+05	1183.053	3.547D-02	0.0	1.460D-04	1208.07	1222.82	1180.97	1.460D-04	1192.245	
25	1.294	1.753D+05	1161.938	3.547D-02	0.0	1.460D-04	1190.36	1223.40	1161.52	1.460D-04	1172.495	
24	1.189	1.770D+05	1112.190	3.547D-02	0.0	1.460D-04	1157.57	1224.57	1126.61	1.460D-04	1137.064	
23	1.084	1.786D+05	1054.158	3.547D-02	0.0	1.460D-04	1106.19	1225.75	1073.49	1.460D-04	1083.174	
22	0.977	1.803D+05	990.528	3.547D-02	0.0	1.460D-04	1046.64	1226.92	1013.54	1.460D-04	1022.343	
21	0.871	1.820D+05	924.342	3.547D-02	0.0	1.460D-04	982.01	1228.08	949.61	1.460D-04	957.435	
20	0.766	1.837D+05	858.866	3.547D-02	0.0	1.460D-04	915.30	1229.23	884.88	1.460D-04	891.604	
19	0.662	1.853D+05	797.433	3.547D-02	0.0	1.460D-04	849.88	1230.36	822.61	1.460D-04	828.150	
18	0.558	1.870D+05	742.927	3.547D-02	0.0	1.460D-04	789.07	1231.47	765.90	1.460D-04	770.180	
17	0.506	1.878D+05	718.971	3.547D-02	0.0	1.460D-04	747.32	1232.02	727.69	1.460D-04	730.949	
16	0.455	1.886D+05	697.375	3.547D-02	0.0	1.460D-04	722.79	1232.57	705.74	1.460D-04	708.173	
15	0.404	1.894D+05	678.166	3.547D-02	0.0	1.460D-04	700.63	1233.12	686.32	1.460D-04	687.770	
14	0.323	1.907D+05	670.010	3.547D-02	0.0	1.460D-04	677.57	1233.96	673.31	1.460D-04	674.088	
13	0.161	1.932D+05	659.944	3.547D-02	0.0	1.460D-04	667.13	1235.63	664.50	1.460D-04	664.977	
12	0.0	1.958D+05	654.150	3.547D-02	0.0	1.460D-04	658.27	1237.28	656.89	1.460D-04	657.047	
11	-0.086	1.969D+05	654.150	3.547D-02	0.0	1.460D-04	654.15	1238.00	654.15	1.460D-04	654.150	
10	-0.173	1.980D+05	654.150	3.547D-02	0.0	1.460D-04	654.15	1238.72	654.15	1.460D-04	654.150	
9	-0.259	1.991D+05	654.150	3.547D-02	0.0	1.460D-04	654.15	1239.44	654.15	1.460D-04	654.150	
8	-0.346	2.002D+05	654.150	3.547D-02	0.0	1.460D-04	654.15	1240.15	654.15	1.460D-04	654.150	
7	-0.432	2.013D+05	654.150	3.547D-02	0.0	1.460D-04	654.15	1240.86	654.15	1.460D-04	654.150	
6	-0.519	2.024D+05	654.150	3.547D-02	0.0	1.460D-04	654.15	1241.56	654.15	1.460D-04	654.150	
5	-0.637	2.040D+05	654.150	3.547D-02	0.0	1.460D-04	654.15	1242.52	654.15	1.460D-04	654.150	654.15
4	-0.755	2.055D+05	654.150	3.547D-02	0.0	1.460D-04	654.15	1243.47	654.15	1.460D-04	654.150	654.15
3	-0.873	2.070D+05	654.150	3.547D-02	0.0	1.460D-04	654.15	1244.42	654.15	1.460D-04	654.150	654.15
2	-0.991	2.035D+05	654.150	3.547D-02	0.0	1.460D-04	654.15	1245.36	654.15	1.460D-04	654.150	654.15
1	-1.109	2.218D+05	654.150	3.547D-02	0.0	1.460D-04	654.15	1253.37	654.15	1.460D-04	654.150	654.15

Figure 12.12-1. Example of a Printout from the Voiding Model Shortly after Voiding Initiation

CHANNEL 2 SAS4A 0.0 TRANSIENT PIN CALCULATION FOR MAC 9/10/83 12.04.36 PAGE1383
JUNE,1982

1730 STEPS, 1.82099 SECONDS, SINCE BOILING STARTED IN CHANNEL 2 89 BUBBLES FORMED

500 MAIN TIME STEPS HAVE BEEN COMPLETED AT 0.17893D+02 SECONDS, COOLANT TIME STEP IS 0.325285000D-02

BUBBLE NUMBER	GAS TYPE	INTERFACE POSITION	VELOCITY	PRESSURE	TEMPERATURE VAPOR	TEMPERATURE LIQUID	BOILING TIME	* CLAD FILM * THICKNESS	* CLAD FILM * VELOCITY	STRUCTURE FILM THICKNESS	STRUCTURE FILM VELOCITY
87	1	0.3828	0.359	0.2059D+06	1243.733	1150.336	0.88208	3.710D-04	0.0	4.315D-04	0.0
		2.6749	57.632	0.1638D+06	1215.066	1205.610		1.460D-04	0.0	1.460D-04	0.0

AXIAL NODE	AXIAL POSITION	COOLANT PRESSURE	COOLANT TEMPERATURE	COOLANT FLOW RATE	CLAD FILM VELOCITY	CLAD FILM THICKNESS	** TEMPERATURE ** CLAD	SATURATION	STRUCTURE	STRUCTURE FILM THICKNESS	TCBAR2	REFLECTOR TEMPERATURE
38	2.585	1.641D+05	1215.247	8.589D-04	0.0	1.460D-04	0.0	1215.25	0.0	1.460D-04	1215.188	0.0
37	2.465	1.646D+05	1215.613	1.037D-03	0.0	2.920D-04	1210.83	1215.61	1205.65	2.087D-04	1215.430	1210.83
36	2.345	1.655D+05	1216.303	1.147D-03	0.0	2.900D-04	1213.62	1216.30	1198.77	2.441D-04	1215.958	1213.62
35	2.225	1.667D+05	1217.151	1.252D-03	0.0	2.849D-04	1214.57	1217.15	1202.29	2.270D-04	1216.727	1214.57
34	2.105	1.680D+05	1218.172	1.346D-03	0.0	2.569D-04	1215.92	1218.17	1206.60	2.019D-04	1217.661	1215.92
33	1.985	1.697D+05	1219.371	1.425D-03	0.0	2.332D-04	1217.47	1219.37	1211.17	1.783D-04	1218.772	1217.47
32	1.865	1.716D+05	1220.726	1.491D-03	0.0	2.093D-04	1219.09	1220.73	1215.54	1.593D-04	1220.049	1219.09
31	1.702	1.773D+05	1224.847	1.448D-03	0.0	1.367D-04	1223.26	1224.85	1222.04	1.379D-04	1222.786	
30	1.620	1.803D+05	1226.924	1.403D-03	0.0	1.222D-04	1226.83	1226.92	1226.51	1.402D-04	1225.885	
29	1.539	1.834D+05	1229.022	1.329D-03	0.0	1.070D-04	1229.40	1229.02	1229.38	1.420D-04	1227.973	
28	1.457	1.865D+05	1231.120	1.216D-03	0.0	8.643D-05	1232.07	1231.12	1232.48	1.403D-04	1230.071	
27	1.405	1.876D+05	1231.872	1.216D-03	0.0	0.0	1355.97	1231.87	1232.49	1.641D-04	1231.496	
26	1.352	1.887D+05	1232.617	1.216D-03	0.0	0.0	1391.92	1232.62	1230.04	2.015D-04	1232.244	
25	1.300	1.898D+05	1233.355	1.216D-03	0.0	0.0	1425.02	1233.35	1226.38	2.448D-04	1232.986	
24	1.194	1.920D+05	1234.808	1.216D-03	0.0	0.0	1464.02	1234.81	1220.33	2.920D-04	1234.082	
23	1.088	1.941D+05	1236.233	1.216D-03	0.0	0.0	1492.51	1236.23	1207.06	2.920D-04	1235.520	
22	0.981	1.963D+05	1237.625	1.217D-03	0.0	0.0	1462.63	1237.63	1186.89	2.920D-04	1236.929	
21	0.874	1.984D+05	1238.973	1.217D-03	0.0	0.0	1408.65	1238.97	1164.37	2.920D-04	1238.299	
20	0.769	2.004D+05	1240.275	1.217D-03	0.0	0.0	1324.64	1240.28	1136.64	2.920D-04	1239.624	
19	0.663	2.060D+05	1243.834	4.170D-04	0.0	3.806D-05	1250.62	1243.83	1104.17	2.920D-04	1242.055	
18	0.559	2.067D+05	1244.238	-1.389D-04	0.0	1.446D-04	1252.03	1244.24	1068.86	2.920D-04	1244.036	
17	0.507	2.064D+05	1244.049	-3.122D-04	0.0	2.266D-04	1250.22	1244.05	1032.08	2.920D-04	1244.143	
16	0.455	2.061D+05	1243.845	-4.080D-04	0.0	2.735D-04	1247.81	1243.84	1015.05	2.920D-04	1243.947	
15	0.404	2.059D+05	1243.752	-4.165D-04	0.0	2.904D-04	1244.23	1243.75	986.64	2.920D-04	1243.798	
14	0.323	2.062D+05	894.669	4.610D-03	0.0	1.460D-04	1116.97	1243.94	955.46	1.460D-04	943.268	
13	0.161	2.072D+05	713.862	4.610D-03	0.0	1.460D-04	808.45	1244.55	743.25	1.460D-04	804.265	
12	0.0	2.082D+05	674.318	4.610D-03	0.0	1.460D-04	695.05	1245.17	680.60	1.460D-04	694.090	
11	-0.086	2.085D+05	651.927	4.610D-03	0.0	1.460D-04	661.96	1245.51	661.88	1.460D-04	663.123	
10	-0.173	2.093D+05	663.838	4.610D-03	0.0	1.460D-04	659.52	1245.85	653.53	1.460D-04	657.883	
9	-0.259	2.099D+05	659.469	4.610D-03	0.0	1.460D-04	661.16	1246.19	658.58	1.460D-04	661.654	
8	-0.346	2.104D+05	659.146	4.610D-03	0.0	1.460D-04	660.20	1246.53	654.75	1.460D-04	659.307	
7	-0.432	2.109D+05	661.291	4.610D-03	0.0	1.460D-04	660.57	1246.86	657.31	1.460D-04	660.218	
6	-0.519	2.115D+05	660.171	4.610D-03	0.0	1.460D-04	660.72	1247.20	655.67	1.460D-04	660.731	
5	-0.637	2.123D+05	649.506	4.610D-03	0.0	1.460D-04	655.61	1247.66	655.01	1.460D-04	654.839	655.61
4	-0.755	2.130D+05	659.296	4.610D-03	0.0	1.460D-04	653.66	1248.12	653.85	1.460D-04	654.401	653.66
3	-0.873	2.138D+05	647.692	4.610D-03	0.0	1.460D-04	654.32	1248.57	654.28	1.460D-04	653.494	654.32
2	-0.991	2.145D+05	662.482	4.610D-03	0.0	1.460D-04	654.12	1249.03	654.10	1.460D-04	655.087	654.12
1	-1.109	2.155D+05	653.821	4.610D-03	0.0	1.460D-04	657.14	1249.60	655.31	1.460D-04	658.152	657.13

Figure 12.12-2. Example of a Printout from the Voiding Model at an Advanced Stage of Boiling

12.13 Physical Properties of Sodium

The expressions used in SASSYS-1 and SAS4A to model the physical properties of sodium as functions of temperature are derived from data correlations generated by Padilla [12.1] and by Fink and Leibowitz [12-12]. These correlations were developed using the most recent measurements available, namely those of Bhise and Bonilla [12-13] and Da Gupta and Bonilla [12-14]. The experiments described in Refs. [12-13] and [12-14] resulted in the firs measurements of sodium properties in the temperature range from about 1250 K up to the critical point (2503.3 K). Because of this new information, sodium properties can be modeled in SASSYS-1 and SAS4A over a much wider temperature range than was possible in previous versions of the SAS code.

The correlations given in Refs. [12.11] and [12-12] could have been used directly in SASSY-1. However, in order to increase computational efficiency least-squares approximations to these correlations were generated and incorporated in the code. These approximations introduce little additional error into the calculation (they fit the correlations to 1.5% or better in all cases), and they require less central processing time than do the more complex expressions given in the references. In addition, one polynomial fit is made over the temperature range of interest per sodium property. The references often present two or more correlations (each valid over different sections of the temperature range) for a given property. Implementing different correlations over different temperature ranges for a single property would require computationally expensive branching logic in the code; this is avoided by the polynomial fits.

Because most sections of the code do not require properties at temperatures above about 90% of the critical point (2270 K), the polynomial fits do not extend past 2270 K in order to avoid the difficulty of fitting a polynomial to the rapid changes that occur in most properties near the critical point. On the low end, the temperature range goes down to 590 K, well below any temperature needed in fast reactor accident analyses.

The polynomial expressions for each property are listed below, along with a brief explanation of their origin. In all cases, the temperature T is in Kelvins.

Heat of Vaporization (λ in J/g)

$$\lambda = A_1 + A_2 T + A_3 T^2 + A_4 T^3 \qquad (12.13\text{-}1)$$

$A_1 = 5.3139 \times 10^6$

$A_2 = -2.0296 \times 10^3$

$A_3 = 1.0625$

$A_4 = -3.3163 \times 10^{-4}$

The expression for λ is a fit to two equations recommended by Padilla; the first (valid below 1644 K) is from Golden Tokar's [12-15] quasichemical approach, while the

second (for T > 1644 K) is the model of Miller, Cohen, and Dickerman [12-16], as adjusted by Padilla. The polynomial fit approximates both equations to within 1%.

Saturation Vapor Pressure (P_s in Pa)

$$\ln(P_s) = A_5 - \frac{A_6}{T} - \frac{A_7}{T^2} \qquad (12.13\text{-}2)$$

$A_5 = 2.169 \times 10$

$A_6 = 1.14846 \times 10^4$

$A_7 = 3.41769 \times 10^5$

Fink and Leibowitz present the equation

$$\ell n\left(P_s\right) = 3.0345\times10 - 13113/T - 1.09481\,\ell n\left(T\right) + 1.9777\times10^{-4}T \qquad (12.13\text{-}3)$$

However, SASSYS-1 and SAS4A require an expression for temperature as a function of pressure, which must be obtained by inverting the equation, giving pressure as a function of temperature. Since this formula cannot be inverted directly, the least-squares fit shown above was use. The polynomial approximates the reference equation to within 1.2%.

Saturation Temperature (T_s in K)

$$T_s = \frac{A_8}{A_9 + \sqrt{A_{10} + A_{11}\,\ell n\left(P_s\right)}} \qquad (12.13\text{-}4)$$

$A_8 = 2A_7$

$A_9 = -A_6$

$A_{10} = A_6^2 + 4A_5\,A_7$

$A_{11} = -4A_7$

$3.5 \le P_s \le 1.6 \times 10^7$ Pa

Liquid Density (ρ_ℓ in kg/m^3)

$$\rho_\ell = A_{12} + A_{13}T + A_{14}T^2 \qquad (12.13\text{-}5)$$

$A_{12} = 1.00423 \times 10^3$

A_{13} = -0.21390

A_{14} = -11046 x 10^{-5}

This equation fits two empirical equations recommended by fink and Leibowitz to within 9.5%. Below 1644 K, they suggest the equation of Stone, et al. [12-17], while above 1644 K, they use a mode of their own.

Vapor Density (ρ_v in kg/m^3)

$$\rho_v = P_s\left(\frac{A_{15}}{T} + A_{16} + A_{17}T + A_{18}T^2 + A_{19}T^3 + A_{20}T^4\right) \qquad (12.13\text{-}6)$$

A_{15} = 4.1444 x 10^{-3}

A_{16} = -7.4461 x 10^{-6}

A_{17} = 1.3768 x 10^{-8}

A_{18} = -1.0834 x 10^{-11}

A_{19} = 3.8903 x 10^{-15}

A_{20} = -4.922 x 10^{-19}

with P_s in pascals. This equation substitutes for the two correlations presented by Padila, one generated using the quasichemical approach (below 1644 K), the other (above 1644 K) being the Clapeyron equation. The polynomial is accurate to 1.5%.

Liquid Heat Capacity (C_ℓ in J/kg-K)

$$C_\ell = \frac{A_{28}}{(T_c - T)^2} + \frac{A_{29}}{T_c - T} + A_{30} + A_{31}(T_c - T) + A_{32}(T_c - T)^2 \qquad (12.13\text{-}7)$$

A_{28} = 7.3898 x 10^5

A_{29} = 3.154 x 10^5

A_{30} = 1.1340 x 10^3

A_{31} = -2.2153 x 10^{-1}

A_{32} = 1.1156 x 10^{-4}

T_c = 2503.3K = the critical temperature

This equation fits to within 1.5% the data generated by Padilla using a thermodynamic relation from Rowlinson [12-18].

Vapor Heat Capacity (C_g in J/kg-K)

$$c_g = A_{33} + A_{34}\,T + A_{35}T^2 + A_{36}T^3 + A_{37}T^4 + A_{38}T^5 + A_{39}T^6 \qquad (12.13\text{-}8)$$

$A_{33} = 2.1409 \times 10^{3}$

$A_{34} = -2.2401 \times 10$

$A_{35} = 7.9787 \times 10^{-2}$

$A_{36} = -1.0618 \times 10^{-4}$

$A_{37} = 6.7874 \times 10^{-8}$

$_{38} = -2.1127 \times 10^{-11}$

$A_{39} = 2.5834 \times 10^{-15}$

Padilla recommends a quasichemical approach below 1644 k and a relation of Rowlinson's above that point. This polynomial approximates both correlations to better than 1%.

Liquid Adiabatic Compressibility (B_s in Pa^{-1})

$$\beta_s = A_{40} + \frac{A_{41}}{T_c - T} \qquad (12.13\text{-}9)$$

$A_{40} = -5.4415 \times 10^{-11}$

$A_{41} = 4.7663 \times 10^{-7}$

Padilla computed values for this quantity from experimental measurements of sonic velocity below 1773 K and from an empirical correlation due to Grosse [12-19] above that temperature. The polynomial fits these data to better than 0.1%.

Liquid Thermal Expansion Coefficient (α_p in K^{-1})

$$\alpha_p = A_{42} + \frac{A_{43}}{T_c - T} + \frac{A_{44}}{(T_c - T)^2} + \frac{A_{45}}{(T_c - T)^3} + \frac{A_{46}}{(T_c - T)^4} + \frac{A_{47}}{(T_c - T)^5} \qquad (12.13\text{-}10)$$

$A_{42} = 2.5156 \times 10^{-6}$

$A_{43} = 0.79919$

$A_{44} = -6.9716 \times 10^{2}$

$A_{45} = 3.3140 \times 10^{5}$

$A_{46} = -7.0502 \times 10^{7}$

$A_{47} = 5.4920 \times 10^{9}$

Fink and Leibowitz express α_p by applying a thermodynamic relation to the data of Das Gupta and Bonilla. The above expression fits their correlation to better than 0.7%.

Liquid Thermal Conductivity (k_ℓ in W/m-K)

$$k_\ell = A_{48} + A_{49} T + A_{50} T^2 + A_{51} T^3 \qquad (12.13\text{-}11)$$

$A_{48} = 1.1045 \times 10^{2}$

$A_{49} = -6.5112 \times 10^{-2}$

$A_{50} = 1.5430 \times 10^{-5}$

$A_{51} = -2.4617 \times 10^{-9}$

The expression approximates the data given by Fink and Leibowitz to within 0.5%. This information comes from experimental data below 1500 K and extrapolated values above 1500 K generated by a method described by Grosse [12-20].

Liquid Viscosity (μ_ℓ in P_a-s)

$$\mu_\ell = A_{52} + \frac{A_{53}}{T} + \frac{A_{54}}{T^2} + \frac{A_{55}}{T^3} \qquad (12.13\text{-}12)$$

$A_{52} = 3.6522 \times 10^{-5}$

$A_{53} = 0.16626$

$A_{54} = -4.56877 \times 10$

$A_{55} = 2.8733 \times 10^{4}$

Fink and Leibowitz present this variable as a combination of experimental data below 1200 K and extrapolated values based on a method suggested by Grosse [12-21]. Their results are approximated by the above polynomial to within 0.5%.

REFERENCES

NOTICE

Several references in this document refer to unpublished information. For a list of available open-literature citations, please contact the authors.

APPENDIX 12.1
DERIVATION OF THE EXPRESSION FOR THE SPATIAL DERIVATIVE OF THE LIQUID TEMPERATURE AT A LIQUID-VAPOR INTERFACE

The derivation of Eq. 12.5-37, the expression for $\left.\frac{\partial T_\ell}{\partial \xi}\right|_{\xi=0}$, from the general heat conduction equation involves a somewhat lengthy process which will be described in this appendix. The starting point is Eq. 12.5-34, the general heat conduction equation, written as

$$\frac{\partial^2 T(\xi,t')}{\partial \xi^2} + \frac{Q(\xi,t')}{k_\ell} = \frac{1}{\alpha}\frac{\partial T(\xi,t')}{\partial t'} \tag{A12.1-1}$$

where the nomenclature is defined in Section 12.5. As discussed in Section 12.5, the boundary conditions for Eq. A12.1-1 are $T(0, t')$ equal to the vapor temperature and $T(\xi, t')$ finite, while the initial condition is that $T(\infty, 0)$ is known. If the Laplace transform is applied to Eq. A12.1-1, the resulting equation is

$$\frac{\partial^2 \overline{T}(\xi,s)}{\partial \xi^2} + \frac{\overline{Q}(\xi,s)}{k_\ell} = \frac{1}{\alpha}\left(s\overline{T}(\xi,s) - T(\xi,0)\right) \tag{A12.1-2}$$

where $\overline{T}$ and $\overline{Q}$ are the Laplace transforms of T and Q, respectively, and s is the transform variable. Equation A12.1-2 will be somewhat easier to work with if the function $g(\xi, s)$ is defined as

$$g(\xi,s) = -\frac{\overline{Q}(\xi,s)}{k_\ell} - \frac{T(\xi,0)}{\alpha} \tag{A12.1-3}$$

so that the transformed equation becomes

$$\frac{\partial^2 \overline{T}}{\partial \xi^2} - \frac{s}{\alpha}\overline{T} = g \tag{A12.1-4}$$

The arguments ξ and s have been suppressed in Eq. A12.1-4 for simplicity of notation. Equation A12.1-4 is a second-order partial differential equation in ξ, which can be solved in a straightforward manner. First, one additional notational simplification will be introduced by defining the variable q as

$$q = \frac{s}{\alpha} \tag{A12.1-5}$$

which gives

$$\frac{\partial^2 \overline{T}}{\partial \xi^2} - q^2 \overline{T} = g \tag{A12.1-6}$$

The solution to this equation can be divided into a homogeneous solution $\overline{T}_h$ and a particular solution $\overline{T}_p$:

$$\overline{T} = \overline{T}_h + \overline{T}_p \tag{A12.1-7}$$

The homogeneous solution is just the solution to the equation

$$\frac{\partial^2 \overline{T}_h}{\partial \xi^2} - q^2 \overline{T}_h = 0 \tag{A12.1-8}$$

so that $\overline{T}_h$ has the form

$$\overline{T}_h = C_1 \exp(q\xi) - C_2 \exp(-q\xi) \tag{A12.1-9}$$

where C_1 and C_2 are constants to be determined from the boundary conditions.

Finding the functional form of the particular solution is a more complex process than was finding the form of the homogeneous solution. The particular solution satisfies the equation

$$\frac{\partial^2 \overline{T}_p}{\partial \xi^2} - q^2 \overline{T}_p = g \tag{A12.1-10}$$

which can be rewritten as

$$\left(\frac{\partial}{\partial \xi} - q\right)\left(\frac{\partial}{\partial \xi} + q\right)\overline{T}_p = g \tag{A12.1-11}$$

If the function u is defined as

$$u = \frac{\partial \overline{T}_p}{\partial \xi} + q\overline{T}_p \tag{A12.1-12}$$

then Eq. A12.1-11 takes the simpler form

$$\frac{\partial u}{\partial \xi} - qu = g \tag{A12.1-13}$$

Equation A12.1-13 is a simple first-order equation which is easily solved. First, multiply the equation by $e^{-q\xi}$:

$$\frac{\partial u}{\partial \xi} e^{-q\xi} - que^{-q\xi} = ge^{-q\xi} \tag{A12.1-14}$$

which can be written more simply as

$$\frac{\partial}{\partial \xi}\left(ue^{-q\xi}\right) = ge^{-q\xi} \tag{A12.1-15}$$

Equation A12.1-15 can then be solved for u by integrating from 0 to ξ,

$$ue^{-q\xi} = \int_0^{\xi} ge^{-q\xi'} d\xi' \tag{A12.1-16}$$

or

$$u = e^{q\xi} \int_0^{\xi} ge^{-q\xi'} d\xi' \tag{A12.1-17}$$

If this expression is substituted into Eq. A12.1-12, the following equation for the particular solution results:

$$\frac{\partial \overline{T}_p}{\partial \xi} + q\overline{T}_p = e^{q\xi} \int_0^{\xi} ge^{-q\xi'} d\xi' \tag{A12.1-18}$$

Equation A12.1-18 is solved using the same procedure as was employed to solve Eq. A12.1 for u, only this time, the multiplier is $e^{q\xi}$, giving

$$\frac{\partial}{\partial \xi}\left(\overline{T_p} e^{q\xi}\right) = e^{2q\xi} \int_0^{\xi} ge^{-q\xi''} d\xi'' \tag{A12.1-19}$$

which gives the following expression for $\overline{T}_p$:

$$\overline{T_p} = e^{-q\xi} \int_0^{\xi} e^{2q\xi} \left(\int_0^{\xi'} g e^{-q\xi"} d\xi" \right) d\xi' \qquad \text{(A12.1-20)}$$

Using integration by parts, Eq. A12.1-20 can be modified from a double integral to the difference of two integrals, giving

$$\overline{T_p} = e^{q\xi} \int_0^{\xi} \frac{g}{2q} e^{-q\xi'} \, d\xi' - e^{-q\xi} \int_0^{\xi} \frac{g}{2q} e^{q\xi'} \, d\xi' \qquad \text{(A12.1-21)}$$

The Laplace transform of the liquid temperature is then just the sum of the expression for $\overline{T}_h$ from Eq. A12.1-9 and that for $\overline{T}_p$ from Eq. A12.1-21:

$$\begin{aligned} \overline{T} &= \overline{T}_h + \overline{T}_p \\ &= C_1 \exp(q\xi) + C_2 \exp(-q\xi) + \exp(q\xi) \int_0^{\xi} \frac{g}{2q} \exp(-q\xi') d\xi' \\ &\quad - \exp(-q\xi) \int_0^{\xi} \frac{g}{2q} \exp(q\xi') d\xi' \end{aligned} \qquad \text{(A12.1-22)}$$

The constants C_1 and C_2 in Eq. A12.1-22 can be evaluated by imposing the boundary conditions stated at the beginning of the appendix. The condition at $\xi = 0$ gives

$$\overline{T}(0,s) = C_1 + C_2 \qquad \text{(A12.1-23)}$$

while that for $\xi \to \infty$ requires that

$$C_1 + \int_0^{\infty} \frac{g}{2q} \exp(-q\xi') d\xi' = 0 \qquad \text{(A12.1-24)}$$

If these are applied to Eq. A12.1-22, the resulting expression for $\overline{T}$ is

$$\begin{aligned} \overline{T}(\xi,s) &= -\exp(q\xi) \int_0^{\infty} \frac{g}{2q} \exp(-q\xi') d\xi' + \overline{T}(0,s) \exp(-q\xi) \\ &\quad + \exp(-q\xi) \int_0^{\infty} \frac{g}{2q} \exp(-q\xi') d\xi' + \exp(q\xi) \int_0^{\xi} \frac{g}{2q} \exp(-q\xi') d\xi' \\ &\quad - \exp(-q\xi) \int_0^{\xi} \frac{g}{2q} \exp(q\xi') d\xi' \end{aligned} \qquad \text{(A12.1-25)}$$

Taking the derivative of Eq. A12.1-25 with respect to ξ and evaluating the result at $\xi = 0$ gives

$$\begin{aligned}\frac{\partial \bar{T}}{\partial \xi}\Big|_{\xi=0} &= -q\int_0^\infty \frac{g}{2q}\exp\left(-q\xi'\right)d\xi' - q\,\bar{T}\left(0,s\right)\\ &\quad - q\int_0^\infty \frac{g}{2q}\exp\left(-q\xi'\right)d\xi' + \frac{g}{2q} - \frac{g}{2q}\end{aligned} \tag{A12.1-26}$$

which, substituting in the functions represented by q and g, produces

$$\begin{aligned}\frac{\partial \bar{T}}{\partial \xi}\Big|_{\xi=0} &= -\bar{T}\left(0,s\right)\frac{s}{\alpha} + \int_0^\infty \frac{\bar{Q}\left(\xi',s\right)}{k_\ell}\exp\left(-\xi'\frac{s}{\alpha}\right)d\xi'\\ &\quad + \int_0^\infty \frac{T\left(\xi',0\right)}{\alpha}\exp\left(-\xi'\frac{s}{\alpha}\right)d\xi'\end{aligned} \tag{A12.1-27}$$

All that remains now is to take the inverse Laplace transform of Eq. A12.1-27. Representing the inverse transform by L^{-1}, the necessary inverse transforms are

$$L^{-1}\left(\frac{\partial \bar{T}}{\partial \xi}\Big|_{\xi=0}\right) = \frac{\partial T}{\partial \xi}\Big|_{\xi=0} \tag{A12.1-28}$$

$$\begin{aligned}L^{-1}\left(\bar{T}\left(0,s\right)\frac{s}{\alpha}\right) &= L^{-1}\left(\bar{T}\left(0,s\right)\frac{s}{\sqrt{s\alpha}}\right)\\ &= L^{-1}\left[s\bar{T}\left(0,s\right)\frac{1}{\sqrt{\alpha}\sqrt{s}}\right]\\ &= \int_0^{t'} \frac{1}{\sqrt{\pi\alpha}}\frac{1}{\sqrt{t'-\tau}}\left(\frac{\partial \bar{T}\left(0,\tau\right)}{\partial \tau}\right)d\tau \quad \text{by convolution}\end{aligned} \tag{A12.1-29}$$

$$\begin{aligned}L^{-1}\left(T\left(\xi,0\right)\exp\left(-\xi\frac{s}{\alpha}\right)\right) &= T\left(\xi,0\right)L^{-1}\left(\exp\left(-\frac{\xi}{\sqrt{a}}\sqrt{s}\right)\right)\\ &= T\left(\xi,0\right)\frac{\xi}{2\sqrt{\pi\alpha\left(t'\right)^3}}\exp\left(-\frac{\xi^2}{4\alpha t'}\right)\end{aligned} \tag{A12.1-30}$$

$$L^{-1}\left(\bar{Q}(\xi,s)\exp\left(-\xi\frac{s}{\alpha}\right)\right)=\int_0^{t'}Q(\xi,\tau)\frac{\xi}{2\sqrt{\pi\alpha(t'-\tau)^3}}\exp\left(-\frac{\xi^2}{4a(t'-\tau)}\right)d\tau \qquad \text{(A12.1-31)}$$

The above inverse transforms can be found in any good handbook which lists inverse Laplace transforms. Taking the inverse transform of Eq. A12.1-27 and using the above expressions for the individual inverse transforms finally produces Eq. 12.5-37:

$$\begin{aligned}\left.\frac{\partial\bar{T}(t')}{\partial\xi}\right|_{\xi=0} &= -\frac{1}{\sqrt{\pi\alpha}}\int_0^{t'}\frac{\partial T(0,\tau)}{\partial\tau}\frac{1}{\sqrt{t'-\tau}}d\tau \\ &\quad -\frac{T(0,0)}{\sqrt{\alpha\pi t'}}+\int_0^{\infty}d\xi\int_0^{t'}\frac{\xi Q(\xi,\tau)\exp\left[-\dfrac{\xi^2}{4\alpha(t'-\tau)}\right]}{2k_\ell\sqrt{\pi\alpha(t'-\tau)^3}}d\tau \\ &\quad +\int_0^{\infty}\frac{T(\xi,0)\xi\exp\left[-\dfrac{\xi^2}{4\alpha t'}\right]}{2\alpha\sqrt{\pi\alpha(t')^3}}d\xi\end{aligned} \qquad \text{(A12.1-32)}$$

APPENDIX 12.2
GAUSSIAN ELIMINATION SOLUTION OF LINEARIZED VAPOR-PRESSURE-GRADIENT EQUATIONS

The series of equations represented by Eq. 12.6-164 is solved as follows:

1. Divide the second equation by $b_{2,j1}$:

   $b_{i,J1} \rightarrow b_{i,J1} / b_{2,J1},\ i = 1...4;\ g_{j1} \rightarrow g_{J1} / b_{2,J1}.$

2. Divide the third equation by $c_{2,j1}$:

   $c_{i,J1} \rightarrow c_{i,J1} / c_{2,J1},\ i = 1...4;\ h_{j1} \rightarrow h_{J1} / c_{2,J1}.$

3. Subtract the first equation from the second:

   $b_{i,J1} \rightarrow b_{i,J1} - a_{1,J1}, b_{2.j1} \rightarrow 0,\ g_{J1} \rightarrow g_{J1} - d_{J1}.$

4. Subtract the first equation from the third:

   $c_{1,J1} \rightarrow c_{1,J1} - a_{1,J1}, c_{2,J1} \rightarrow 0, h_{J1} \rightarrow h_{J1} - d_{J1}$

5. Divide the second equation by $b_{1,J1}$:

   $b_{i,J1} \rightarrow b_{i,J1} / b_{1,J1},\ i = 1...4;\ g_{J1} \rightarrow g_{J1} / b_{i,J1}.$

6. Divide the third equation by $c_{1,J1}$:

   $c_{i,J1} \rightarrow c_{i,J1} / c_{1,J1},\ i = 1...4;\ h_{J1} \rightarrow h_{J1} / c_{1,J1}.$

7. Subtract the second equation from the third:

   $c_{1,J1} \rightarrow 0, c_{3,J1} \rightarrow c_{3,J1} - \tilde{b}_{3,J1}, c_{4,J1} \rightarrow c_{4,J1} - \tilde{b}_{4,J1}$

   $h_{J1} \rightarrow h_{J1} - \tilde{g}_{J1}$

   If J2-1 equals J1, skip to step 16. Otherwise, do steps 8-15 for j=J1 + 1, J1 + 2, …, J2-1.

8. $c_{4,J-1} \rightarrow c_{4,J-1} / c_{3,J-1},\ c_{3,J-1} \rightarrow 1,\ h_{j-1} \rightarrow h_{j-1} / c_{3,j-1} \left(c_{1,j-1} = 0,\ c_{2,j-1} = 0\right).$

9. $b_{i,j} \rightarrow b_{i,j} / b_{1,j},\ i = 1...4;\ g_j \rightarrow g_j / b_{1,j}.$

10. $c_{i,j} \rightarrow c_{i,j} / c_{1,j},\ i = 1...4;\ h_j \rightarrow h_j / c_{1,j}.$

11. Subtract step 8 from step 9:

    $b_{2,j} \rightarrow b_{2,j} - c_{4,j-1},\ b_{1,j} \rightarrow 0,\ g_j \rightarrow g_j - h_{j-1}.$

12. Subtract step 8 from step 10:

    $c_{2,j} \rightarrow c_{2,j} - c_{4,j-1},\ c_{1,j} \rightarrow 0,\ h_j \rightarrow h_j - h_{j-1}.$

13. $b_{i,j} \rightarrow b_{i,j} / b_{2,j}, i = 3, 4; b_{2,j} \rightarrow 1, g_j \rightarrow g_j / b_{2j}.$

14. $c_{i,j} \rightarrow c_{i,j} / c_{2,j}, i = 3, 4; c_{2,j} \rightarrow 1, h_j \rightarrow h_j / c_{2j}.$

15. Subtract step 13 from step 14:

    $c_{i,j} \rightarrow c_{i,j} - b_{i,j}, i = 3, 4;\ c_{2,j} \rightarrow 0, h_j \rightarrow h_j - g_j$

16. $c_{3,J2-1} \rightarrow c_{3,J2-1} / c_{4,J2-1}, c_{4,J2-1} \rightarrow 1, h_{J2-1} \rightarrow h_{J2-1} / c_{4,J2-1}.$

17. $a_{1,J2-1} \rightarrow a_{1,J2-1} - c_{3,J2-1}, a_{2,J2-1} \rightarrow 0, d_{J2-1} \rightarrow d_{J2-1} - h_{J2-1}.$

    (Note that initially $a_{2,J2-1} = a_{2,J1} = 1.$)

18. $\Delta p^i(J2) = d_{J2-1} / a_{1,J2-1}$

19. $\Delta W^i(J2) = h_{J2-1} - c_{3,J2-1} \Delta p^i(J2).$

20. $\Delta W(J2-1) = \tilde{g}_{J2-1} - \tilde{b}_{3,J2-1} \Delta p^i(J2) - \tilde{b}_{4,J2-1} \Delta W^i(J2).$

21. $\Delta p(J2-1) = h_{J2-1} - c_{4,J2-1} \Delta W(J2-1).$

    Do steps 22 and 23 for $j = J2 - 2, J2 - 3, \ldots, J1 + 1.$

22. $\Delta W(j) = g_j - b_{3,j} \Delta p(j+1) - b_{4,j} \Delta W(j+1).$

23. $\Delta p(j) = h_j - c_{4,j} \Delta W(j).$

24. $\Delta p^i(J1) = \tilde{g}_{J1} - \tilde{b}_{3,J1} \Delta p(J1+1) - \tilde{b}_{4,J1} \Delta W(J1+1).$

25. $\Delta W^i(J1) = d_{J1} - a_{1,J1} \Delta p^i(J1).$